

Novel technique in RGD-functionalisation of unstructured and structured inanimate surfaces

Zur Erlangung des akademischen Grades eines

DOKTORS DER NATURWISSENSCHAFTEN

(Dr. rer. nat.)

der Fakultät für Chemie und Biowissenschaften der
Universität Karlsruhe (TH)
vorgelegte

DISSERTATION

von

Sviatlana Kalinina

aus Minsk

Dekan: Prof. Dr. Stefan Bräse

Referent: Prof. Dr. Doris Wedlich

Korreferent: Prof. Dr. Martin Bastmeyer

Tag der mündlichen Prüfung: 10. -14. Dezember 2007

Der experimentelle Teil der vorliegenden Arbeit wurde im Institut für molekulare Zoologisches Institut II, Entwicklungs- und Zellphysiologie der Universität Karlsruhe in der Zeit von März 2004 bis Oktober 2007 durchgeführt.

Ich versichere, dass ich diese Arbeit selbständig verfasst und keine anderen als die angegebenen Quellen und Hilfsmittel verwendet habe.

This work was performed at the Zoological Institute II, Department of Molecular Development and Cell Physiology from March 2004 to October 2007.

I declare that I have done this work by myself; no other methods, equipment or reagents were used other than those described in this thesis.

Sviatlana Kalinina, 30.10.2007

CORRECTIONS

Please note the term of the use cell line 3T3 Swiss fibroblasts is incorrect and has to be changed to thymidine kinase-negative L-cells (LTK⁻ mouse fibroblasts) (Ozawa et al., 1989)

Ozawa M, Baribault H, Kemler R. The cytoplasmic domain of the cell adhesion molecule uvomorulin associates with three independent proteins structurally related in different species. *Embo J.* 1989; 8: 1711-7.

ACKNOWLEDGEMENTS

Firstly I would like to thank Prof. Dr. Doris Wedlich, who gave me the opportunity to perform this work at the Zoological Institute II (Karlsruhe), being involved in the challenging interdisciplinary project of Centre for Functional Nanostructures. I am grateful for her support on the sometimes stony road.

I would like to thank Prof. Dr. Horst Kessler (Munich); this research would have not been possible without fruitful collaboration with his laboratory. Also I offer my sincere thanks to Dr. Monica Lopez Garcia, who helped me a lot with her excellent work.

I thank Prof. Dr. Thomas Schimmel and Dr. Hartmut Gliemann for support and guidance in his physical laboratory.

I acknowledge Prof. Dr. Martin Bastmeyer, head of Institute of Zoological Institute I (Karlsruhe), for accepting to read my thesis as a co-referee.

My thanks to all members of Zoological Institute II (Karlsruhe) giving me a helpful hand on the way to prepare this thesis.

I am very grateful towards my friends, Victoria and Charlie Page, for their help and encouragement during the writing of this PhD thesis.

Special thanks to my husband Ihar Radziuk, who provided the needed love and patience during my work.

TABLE OF CONTENTS

1	INTRODUCTION	1
1.1	Integrins.....	1
1.1.1	Integrin structure in general	1
1.2	Integrin ligands	2
1.3	Integrin clustering	7
1.4	Focal adhesion formation.....	8
1.4.1	Vinculin, paxillin, and focal adhesion kinase (FAK).....	12
1.5	Integrin signalling.....	12
1.5.1	FAK pathway	13
1.5.2	Integrin regulation of cytoskeleton reorganisation	15
1.6	Biofunctionalised surfaces	17
1.7	RGD and other cell adhesion sequences	18
1.7.1	Methods of RGD functionalisation	19
1.7.1.1	Self-assembled monolayers	20
1.8	Patterning methodologies	21
1.9	Motivation/ Outlook	23
2	MATERIALS	24
2.1	Chemicals.....	24
2.2	Buffers	26
2.3	Solutions.....	26
2.4	Cultured cell lines	27
2.5	Equipment	27
2.6	Materials.....	28
3	METHODS	29
3.1	Functionalisation of surfaces	29
3.1.1	Aminosilanisation	29
3.1.2	Fabrication of metal covered slides	29
3.1.3	Microcontact printing and thiol SAMs formation	30
3.1.4	Biofunctionalisation with RGD-peptides	30
3.1.4.1	RGD peptides	30

3.1.4.2	RGD peptide coupling	31
3.1.4.3	PEG or Pluronic® passivation	31
3.1.5	Coating of the surfaces by absorption.....	31
3.1.5.1	Fibronectin coating	31
3.1.5.2	Absorbed RGD-peptides on the surfaces	32
3.1.6	Fabrication of homogeneous thiol layers on gold	32
3.1.6.1	Fabrication of homogeneous ODT-SAMs	32
3.1.6.2	Fabrication of homogeneous layers of short thiols	32
3.1.7	Alternative patterning: Gold evaporation through the mask.....	32
3.2	Cell biology methods	32
3.2.1	Cell culturing.....	32
3.2.2	Cell adhesion assay	33
3.2.2.1	Phenylmethanesulfonyl fluoride (PMSF) as trypsin inhibitor	33
3.2.2.2	Cell adhesion assay in the presence of Pluronic®.....	34
3.2.3	Cell proliferation assay	34
3.2.4	Competition assays	34
3.2.5	Immunocytochemistry.....	35
3.3	Microscopic methods and surface quality control	35
3.3.1	Microscopy and image analysis	35
3.3.1.1	Statistics	35
3.3.2	Confocal laser scanning microscopy.....	36
3.3.3	Scanning electron microscopy	36
3.3.4	Contact angle measurement.....	36
3.3.5	X-ray photoelectron spectroscopy (XPS) measurement.....	37
3.4	Molecular biology methods	37
3.4.1	Isolation of RNA	37
3.4.2	Quantitative and qualitative determination of total RNA	37
3.4.3	Complementary DNA synthesis	38
3.4.4	Polymerase chain reaction (PCR).....	38
3.4.5	Agarose gel electrophoresis	39
3.4.6	Photometry	40
4	RESULTS	41
4.1	Biofunctionalisation of surfaces.....	41
4.1.1	RGD-peptides absorption vs. coupling.....	41

4.1.2	Development of coupling conditions	42
4.1.2.1	Concentration of GRGDS.....	43
4.1.3	RGD-peptide functionalisation of glass and SIO2 slides	44
4.1.4	Blocking reagents.....	44
4.2	Quality control of biofunctionalisation.....	46
4.2.1	X-ray photoelectron spectroscopy (XPS).....	46
4.2.2	Contact angle measurement.....	46
4.2.3	Rhodamine-GRGDS.....	48
4.3	Cell adhesion assay as readout system for biocompatibility.....	48
4.3.1	Mouse 3T3 Swiss fibroblasts express RGD-binding integrins	48
4.3.2	Fibroblasts adhesion on biofunctionalised surfaces in the presence and absence of FCS.....	49
4.3.3	Trypsin inhibitors	49
4.3.4	Cell adhesion: duration and classification	50
4.4	Comparison of cell adhesion behaviour to different peptides	51
4.4.1	Mouse fibroblasts spread on the RGD-functionalised surfaces	51
4.4.2	Fibroblast FA formation depends on used RGD-peptide.....	51
4.4.3	Counting of FAs allows to estimate cell spreading and the surface biocompatibility	55
4.4.4	The fibroblast FA formation on Nc(-RGDfK-)	55
4.5	Mouse 3T3 Swiss fibroblasts spread on fibronectin coating	56
4.6	Cell spreading behaviour of different cell lines spread on RGD-functionalised surface	57
4.6.1	Xenopus tadpole cells	57
4.6.2	Rat embryonic fibroblasts stably expressing YFP-paxillin	59
4.6.3	B16 beta3-GFPintegrin-expressing melanoma cells.....	59
4.6.4	MC3T3-E1 pre-osteoblasts.....	62
4.7	Control of the surface biocompatibility	63
4.7.1	Control peptides	63
4.7.2	Competition assays	64
4.7.3	Proliferation assays	65
4.8	The RGD-functionalisation of the structured surfaces	66
4.8.1	Surface preparation: structured Au-ODT slides	67
4.8.2	Metal: thickness of gold	68
4.8.3	Adapter metal	69
4.8.4	Thiol stamping	69

4.8.5	Quality control by atomic force microscopy (AFM).....	71
4.8.6	Alternative patterning: Gold evaporation through the mask.....	71
4.9.	Cell behaviour on the structured surfaces.....	72
4.9.1	Mouse fibroblasts spread on structured Au-ODT/RGD surfaces without any preferences	72
4.9.2	Cells on the RGD-functionalised structured Au-through-mask surface.....	73
4.9.3	Cell behaviour on the homogeneous surfaces: Au and on Au/GRGDSP	73
4.9.4	Homogeneous surfaces: Au-ODT/GRGDSP.....	74
4.9.5	Homogeneous surfaces designed with short thiols	75
4.9.6	Passivation of ODT-gold: PEG and Pluronic®	76
4.9.7	“Bridging” of the cells through unfunctionalised regions	77
4.9.8	Cell adhesion on RGD-functionalised structured surfaces	79
4.9.9	Control of the surface biocompatibility	82
4.9.9.1	Control peptides.....	82
4.9.9.2	Proliferation assays.....	84
4.9.9.3	Long-term stability of the structured distribution of cells	85
5	DISCUSSION	86
5.1	Biocompatibility of different compounds required for RGD-surface functionalisation	86
5.2	Cells bind RGD-peptides specifically	88
5.3	Designed Au-ODT/RGD pattern promoted selective cell distribution.....	92
5.4	Cell behaviour on RGD-surfaces is cell type dependent	93
6	SUMMARY	95
7	ZUSAMMENFASSUNG.....	96
8	REFERENCES	97
9	MISCELLENOUS	108
	List of abbreviations	108
	Curriculum vitae.....	109
	List of publications	110

1. Introduction

Cell survival, growth and differentiation depend on the cellular microenvironment. The latter consists of 3-dimensional molecular network of insoluble polymers, the extracellular matrix (ECM), consisting of proteins and proteoglycans, and soluble factors such as growth factors, nutrients, and ions. Cells are embedded in this microenvironment by specific adhesion contacts, which are formed by cell membrane receptors, the integrins, and their ligands, small domains within different ECM molecules like fibronectin, laminin or collagen. A challenge in tissue repair and regeneration is the reconstruction of the cellular microenvironment to control stem cell differentiation. Thereby, the design of topographically and geometrically optimized cell substrate contacts on inanimate material is of high relevance. For biofunctionalisation of surfaces the structure and orientation of the integrin receptors and their ECM ligands as well as their interacting mode has to be known.

1.1 Integrins

Integrins are major metazoan cell adhesion molecules mediating cell-extracellular matrix (ECM) and, in vertebrates, to some extent also (more exception than general role) cell-cell interaction (Hynes, 1992). By binding the actin cytoskeleton through adaptor proteins to ligands of the ECM, integrins play a key role in translation signals to both sides of the cell membrane, the so called outside-in and the inside-out signalling. While outside-in signalling describes the structural rearrangements of integrins in response to ligand binding, inside-out signalling defines the changing of ligand binding ability triggered by cell activation signals (Takagi et al., 2002, Giancotti and Ruoslahti, 1999).

The integrin family in mammalian comprises 18 α and 8 β subunits that are able to assemble into 24 heterodimers (Humphries et al., 2006, Hynes, 2002). In the heterodimer, the extracellular domains of both subunits associate in non-covalent manner, forming an “ovoid-like” head with two “legs” (Fig. 1).

1.1.1 Integrin structure in general

The extracellular domain of the α and β subunit is about of 1000 or 750 amino acids in length while the cytoplasmic tails are relatively short consisting of 20-50 amino acids. $\alpha 1$, $\alpha 2$, $\alpha 10$, $\alpha 11$, and leukocyte integrins αL , αM , αX , αD , αE subunits contain an additional “inserted” I/A domain in their extracellular tail. The I/A domain, called also αI or αA -domain is about 180 amino acids. I/A domain was the first domain to be crystallized and structurally investigated

(Lee et al., 1995b). It comprises the ligand binding sites in the integrins that contain this domain.

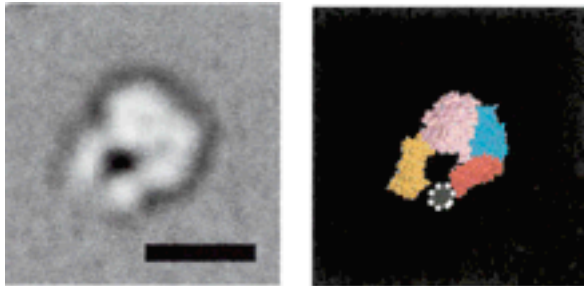


Fig. 1. Structure of the integrins head-group.

Electron microscopic image of an unliganded $\alpha 5 \beta 1$ headpiece (left) and crystal structure of the corresponding region of $\alpha V \beta 3$ (right). Both head groups showed a similar conformation (Takagi, 2004).

First structural information of the extracellular part of the $\alpha V \beta 3$ heterodimer were obtained by X-ray crystal structure analysis (Xiong et al., 2001) (Fig. 2).

Structure analysis revealed that $\alpha V \beta 3$ integrin heterodimer forms an ovoid shaped globular headpiece by association of the seven-bladed β -propeller of αV subunit and βA domain, also called also βI -domain, of the $\beta 3$ subunit. The dimensions of the head are approximately $9 \times 6 \times 4,5$ nm (Beglova et al., 2002, Xiong et al., 2001). The αV subunit is formed by a β -propeller that is followed by three Ig-like “tight” domains and two “calf” domains. Between “thigh” and “calf” domains there is a flexible linker - “knee” - where the Ca^{2+} ion is coordinated. Other 4 metal ions (Ca^{2+} or Mg^{2+}) are coordinated in the β -propeller stabilising the structure of β -hairpin loops.

The $\beta 3$ subunit is composed of a βA domain, a “hybrid” domain, an amino-terminal plexin/semaphorin/integrin (PSI) domain, four epidermal growth factor (EGF) domains, and β -tail domain (βTD). There are three positions in βA domain where metal-ions can bind: the metal ion-dependent adhesion site (MIDAS), the ligand-associated metal binding site (LIMBS), and the adjacent to the MIDAS site (ADMIDAS). The presence of metal ions in these sites changes the conformation of the integrin subunit and regulates ligand binding.

1.2 Integrin ligands

Mediating cell adhesion to ECM, the integrin receptors bind a wide variety of ligands (van der Flier and Sonnenberg, 2001, Plow et al., 2000, Humphries, 1990). However this wide variety could be grouped into four main classes taking into consideration recognizable ligands: receptors of collagens, laminin, RGD, and leukocyte-specific integrins (Humphries et al., 2006, Hynes, 2002) (Fig. 3).

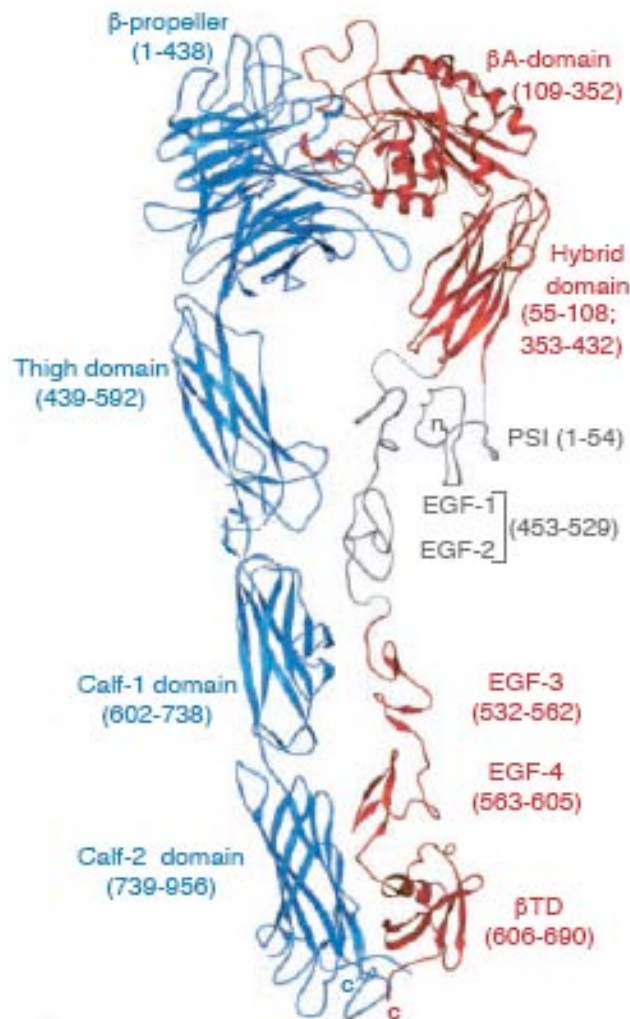


Fig. 2. Model of extracellular segment of $\alpha\text{v}\beta\text{3}$ (Xiong et al., 2001). The αv is shown in blue and β3 is shown in red.

Four α -integrins (α1 , α2 , α10 and α11) containing additional I/A domain combine with β1 and form a group of **collagen receptors**. In all of these integrins, the 180 amino acid I/A domain is responsible for the divalent cation-dependent binding to ligands (Michishita et al., 1993). A metal ion in this case is coordinated at the ligand-binding interface of I/A domain of α subunit through the MIDAS site, and the metal coordination is completed by a glutamate from the ligand (Emsley et al., 2000, Lee et al., 1995b) or, in its absence, by a water molecule (Lee et al., 1995a). These integrins recognise GFOGER motif of collagen (Emsley et al., 2000), but they are also able to bind to other ligands including laminin. Currently, the mechanism of their laminin binding is unknown (Humphries et al., 2006).

Three α integrins that combined with β1 unit (α3 , α6 and α7) compose the group of non-A-domain-containing **laminin-binding integrins**. These highly selective laminin receptors promote adhesion to basement membrane.

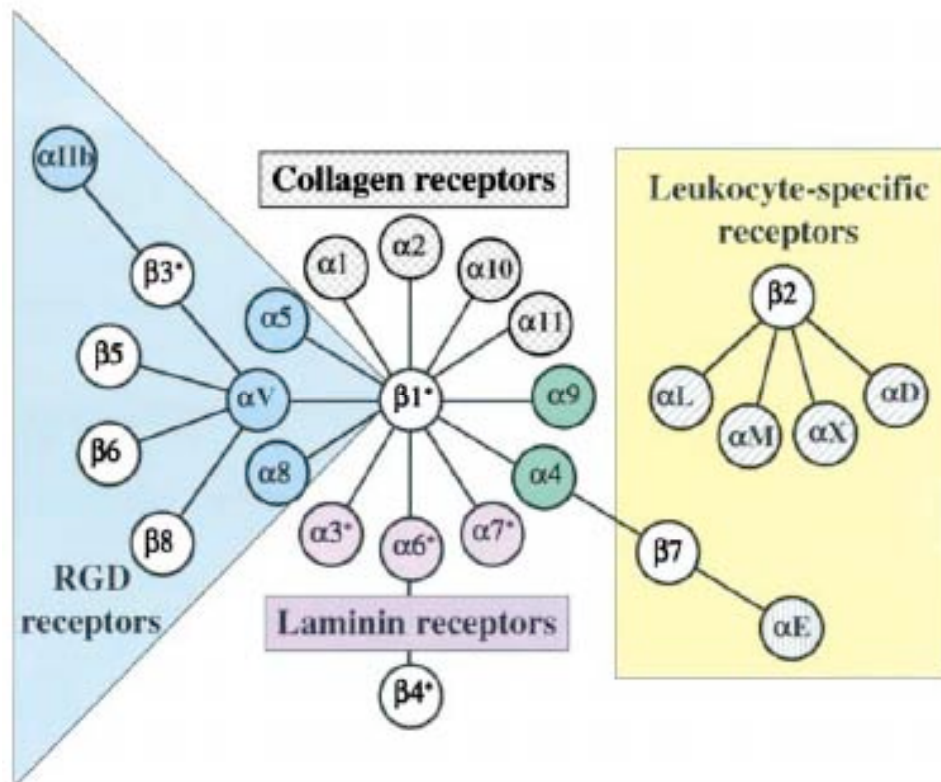


Fig. 3. The complete set of mammalian integrins. 24 possible $\alpha\beta$ associations are depicted. The integrin subfamilies are coloured considering their structure and evolutionary relations. Shown in grey α integrins have “inserted” I/A domain. Asterisks denote alternatively spliced cytoplasmic domains (Hynes, 2002).

Leukocyte-specific integrins $\alpha E\beta 7$, $\alpha 4\beta 7$, four members of $\beta 2$ subfamily (αL , αM , αX and αD), as well as $\alpha 4\beta 1$ and $\alpha 9\beta 1$ recognise Leu-Asp-Val (LDV) motif or related sequences in their ligands. These integrins mediate leukocyte adhesion to various cells during immune response. $\alpha 4\beta 1$, $\alpha 9\beta 1$ and $\alpha 4\beta 7$ presumably bind LDV motif at the junction between the α and β subunits, whereas integrins αL , αM , αX and αD employ an inserted A-domain to bind sequences that are structurally similar to the LDV (Shimaoka et al., 2003). Both groups of leukocyte-specific integrins and collagen receptors contain the additional I/A domain in their α subunits and are restricted to chordates.

The topic in my work are the ancient **RGD-receptors** $\alpha 5\beta 1$, $\alpha V\beta 1$, $\alpha V\beta 3$, $\alpha V\beta 5$, $\alpha V\beta 6$, $\alpha V\beta 8$, $\alpha 8\beta 1$, and $\alpha 11\beta 3$. They bind the tripeptide sequence Arg-Gly-Asp (RGD) within their ligands. I/A domain lacking molecules of these ancient group of integrin receptors bind their ligands at the interface between the β -propeller of the α subunit and βA domain of the β subunit.

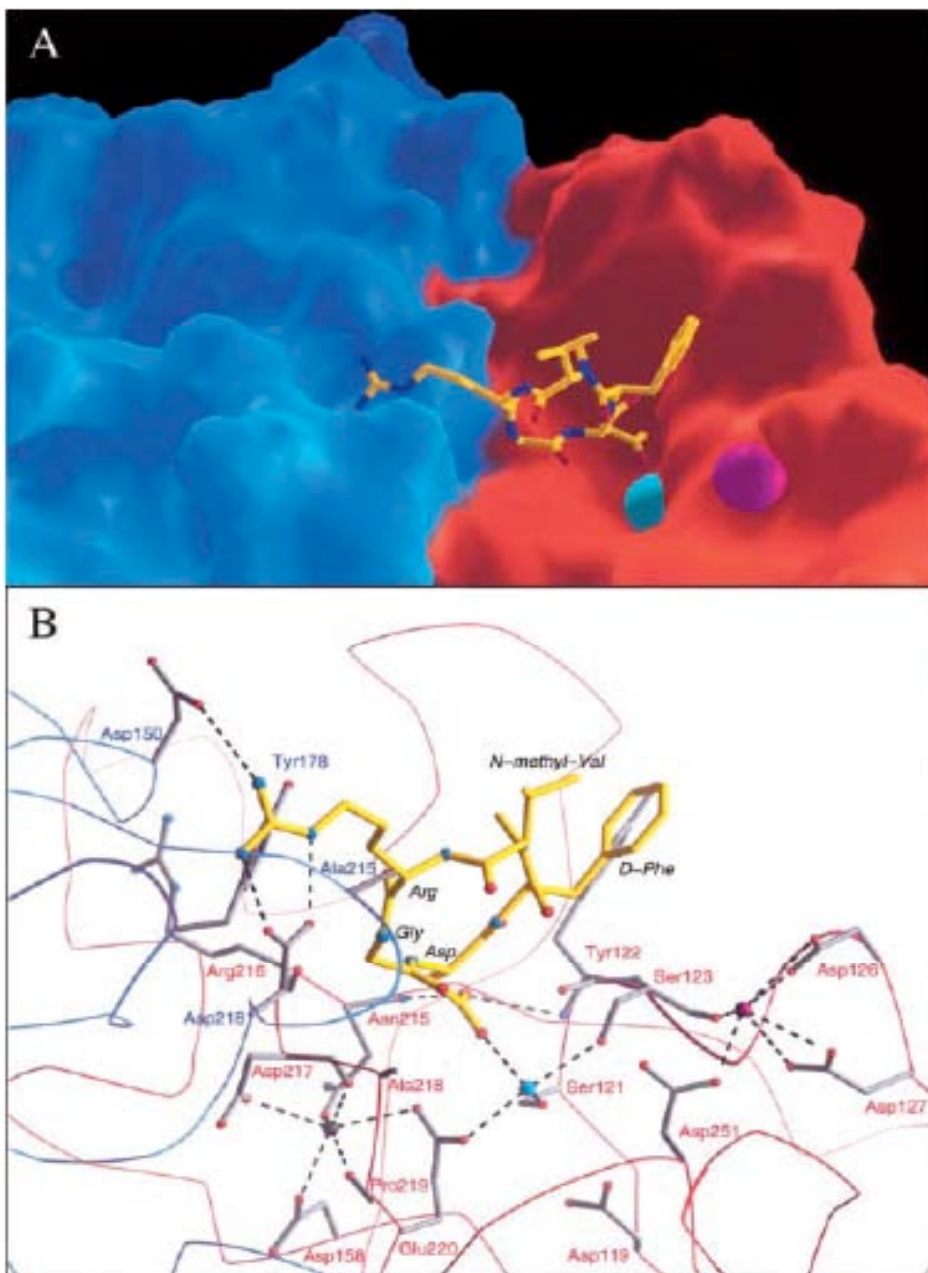


Fig. 4. Ligand binding site of $\alpha\text{V}\beta\text{3}$ integrin. (A) The ball-and-stick model. Violet and cyan marks show metal ions in MIDAS and ADMIDAS sites respectively. (B) In this model the peptide is shown in yellow; αV and β3 residues are labelled blue and red respectively. Oxygen and nitrogen atoms are colored red and blue respectively. The dotted lines represent hydrogen bonds and salt bridges (Xiong et al., 2002).

The structure of extracellular domains of $\alpha\text{V}\beta\text{3}$ in complex with ligand mimetic peptide $\text{cyclo(RGDf-N}\{\text{Me}\}\text{V)}$, revealed by Xiong (Xiong et al., 2002), has established a basis for understanding integrin-RGD recognition. According to this model, glycine residue of the RGD-sequence lies at the interface between α and β subunits near to the surface integrin providing hydrophobic interaction. Arginine and aspartate residues both point away from the

binding pocket in opposite directions; arginine is close to Tyr178 of α_V subunits, and aspartic acid carboxylic group coordinates metal ions at the MIDAS region in the β_3 subunits (Fig. 4).

The structures of other ligand-binding integrins are not yet known, but the $\alpha_V\beta_3$ - cyclo(RGDf-N{Me}V) complex has provided a base for recent studies of ligand docking in other RGD-dependent integrins. The homology modelling led to proposals of $\alpha_V\beta_3/\alpha_{IIb}\beta_3$ ligand binding selectivity (You, 2002), but until now there is no $\alpha_V\beta_3/\alpha_V\beta_5$ selectivity found; the smallest molecules designed as $\alpha_V\beta_3$ ligands show biselectivity (Meyer et al., 2006). The high sequence homology of the β_3 and β_5 subunits allowed development of the ligand binding model for $\alpha_V\beta_5$ receptor. According to this model the bigger part of the binding pocket is highly conserved, especially regarding all residues surrounding MIDAS, ADMIDAS, and LIMBS; the hardly achieved selectivity for $\alpha_V\beta_5$ is based on the larger size of the binding pocket of $\alpha_V\beta_3$ (Marinelli et al., 2003).

X-ray scattering (Mould et al., 2003) and electron microscopy (Takagi et al., 2003) indicated that in the absence of ligand a headpiece of $\alpha_5\beta_1$ is remarkably similar to the crystal structure of the extracellular domain of an $\alpha_V\beta_3$ integrin. There is no atomic resolution structure available for $\alpha_5\beta_1$ in complex with its physiological ligand – fibronectin. However, based on electron microscopic studies model Takagi (Takagi, 2004, Takagi et al., 2003) supposes that the $\alpha_5\beta_1$ binds fibronectin in quite a similar to $\alpha_V\beta_3$ way (Fig. 5), leaving in doubt the earlier two-site binding model, which proposes that the RGD loop in the Fn10 domain and the synergy site in the Fn9 domain latch simultaneously on to widely separated binding pockets on the β_1 and α_5 subunits respectively. Regarding the studies that show minimal effects of dissociation rate but severe effects of the association rate for mutants of residues in the synergistic binding site (Humphries et al., 2003, Xiong et al., 2001) the model that FnIII domain 9 in fibronectin indirectly supports binding of the Fn10 domain to the integrin was proposed (Takagi, 2004).

Despite structural differences in β -propeller of α_{IIb} and α_V integrins, the binding mode of $\alpha_{IIb}\beta_3$ ligands is basically similar to all RGD-recognizing integrins (Meyer et al., 2006, Claasen et al., 2005, Feuston et al., 2003, Adair and Yeager, 2002). The putative structural difference is a deeper ligand binding “pocket”, which demands a longer ligand side chain to establish hydrogen binding. Such a structure explains the $\alpha_{IIb}\beta_3/\alpha_V\beta_3$ selectivity that can be achieved by varying the effective distance between the carboxylic and basic function in the ligand (Meyer et al., 2006).

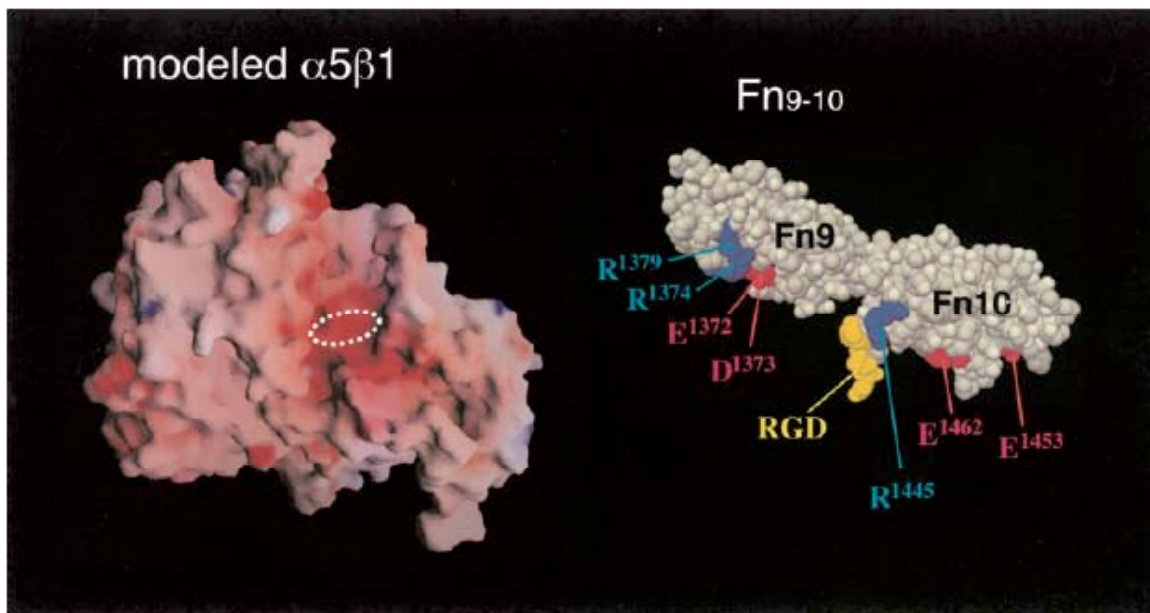


Fig. 5. Model of $\alpha 5\beta 1$ -Fn interface (Takagi, 2004). A molecular surface $\alpha 5\beta 1$ headpiece model (left) coloured from red (<-25 kT) to blue (>25 kT) according to electrostatic potential ranging. The dotted oval indicates an approximate location of the RGD-docking site. The structure of the Fn9-10 (right), fragment of RGD loop is shown in yellow; basic and acidic residues are coloured blue and red respectively.

1.3 Integrin clustering

The clustered integrins are detected on the cell surface (Schneider and Engelman, 2004, Li et al., 2003). Studies in the field of integrin clustering showed its dependence on integrin activation by their ligands; ligand-bounded receptors enhance their tendency to cluster (Yauch et al., 1997, LaFlamme et al., 1992). From another side, clustering may increase the avidity of the receptors and may also lead to additional intracellular signals stimulation. Integrin clustering as well as ligand binding is required to engage interactions with a full complement of cytoskeletal and signaling proteins (Miyamoto et al., 1995).

The cytoplasmic tails of the integrin β subunits are able to directly interact and self-assemble (Laplantine et al., 2002, LaFlamme et al., 1992) that could be important for receptor clustering and further nucleation of focal adhesions. Experimental evidence of $\alpha v\beta 3$ transmembrane domain interaction (Adair and Yeager, 2002, Vinogradova et al., 2002) and their ability to form homodi- and trimers (Li et al., 2003, Li et al., 2001) form the basis for models of $\alpha v\beta 3$ integrin clustering (Fig. 6) (Gottschalk and Kessler, 2004). In these models $\beta 3$ subunits form homotrimers, whereas αv subunits form homodimers.

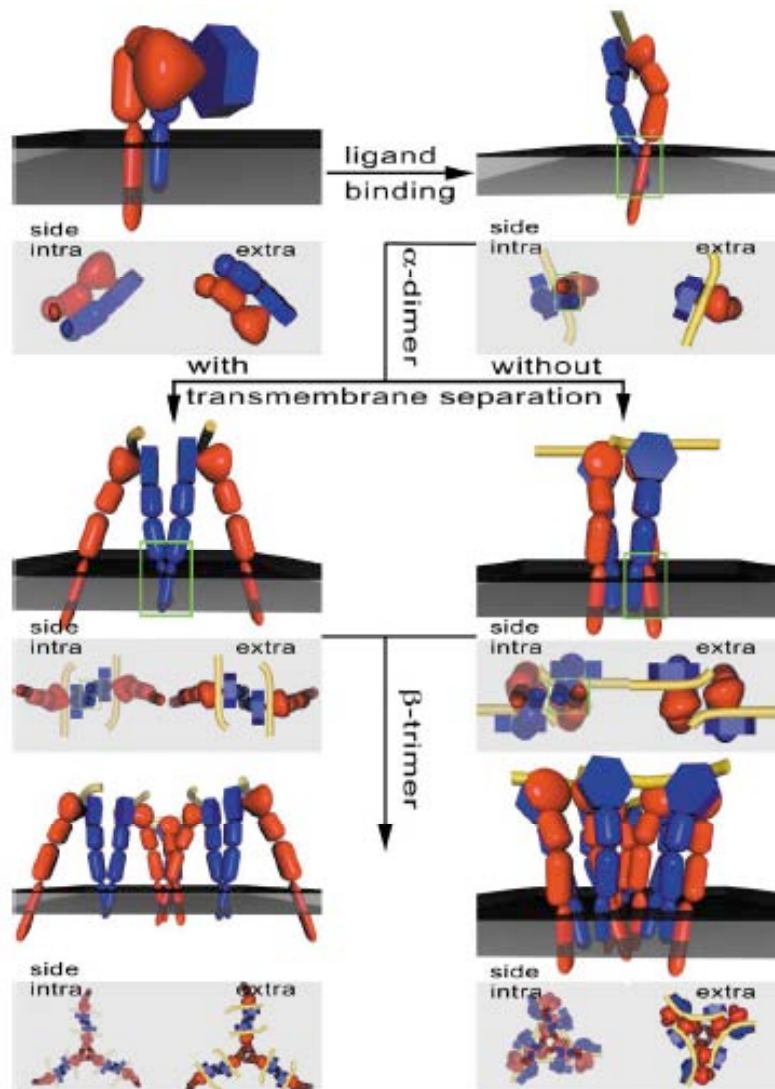


Fig. 6. Two possible models of $\alpha v\beta 3$ clustering. The α subunit is colored blue, the β subunit is colored red (Gottschalk and Kessler, 2004).

1.4 Focal adhesion formation

Focal adhesions (FAs) were first identified in electron-microscopy studies 36 years ago (Abercrombie et al., 1971). These high-density regions were found located on the plasma membrane of cultured cells, in the sites of tight contact of the membrane with substrate. Later was also shown the presence of FAs *in vivo* at cell matrix junctions (Fuchs et al., 1997). In the FAs, various proteins are associated with cytoplasmic tails of integrins linking them to actin-cytoskeleton (Fig. 7); integrins do not have actin-binding sites by themselves. In addition to integrins, FAs could contain some other receptors including syndecans (Woods et al., 2000, Woods et al., 1998, Zimmermann and David, 1999), layilins (Bono et al., 2001, Borowsky and Hynes, 1998), and signaling molecules (Wei et al., 1999, Tang et al., 1998, Myohanen et al., 1993), but their role in adhesion regulation is not yet clear.

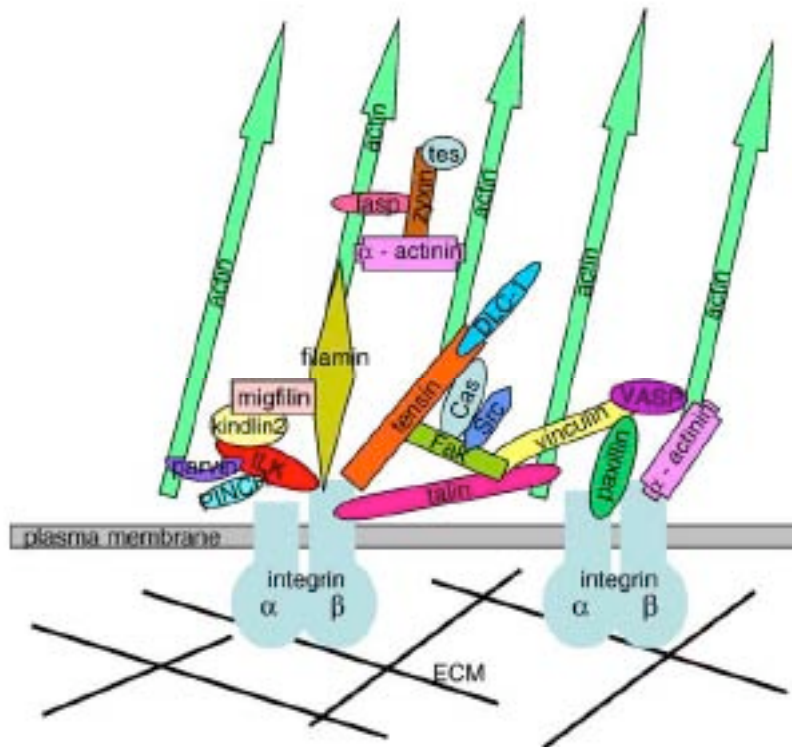


Fig. 7. Schematic illustration of interactions of several components of focal adhesions (Lo, 2006)

There are more than 200 proteins that could be associated to FA formation on the cytoplasmic part of membrane (Fig. 8) (Zaidel-Bar et al., 2007). These are not only cytoskeleton binding proteins such as talin, vinculin, and α -actinin, but also tyrosine and serine/threonine kinases, tyrosine phosphatases, modulators of small GTPases and other enzymes. The interactions between FA components can be mediated by some known binding motifs including the SH2 domain that is responsible for tyrosine-phosphorylated proteins recognition, binding proline-rich motifs SH3, LIM- and PDZ domains. Most proteins have so many binding sites that they cannot engage all of them simultaneously; the regulation of binding partner selection remains elusive.

The selectivity of substrate recognition is managed by integrins that bind ligands and nucleate FAs. Quantitative fluorescence microscopic studies demonstrate the diversity of FAs depending on what integrins are engaged (Zamir and Geiger, 2001a, Zamir and Geiger, 2001b). Variations in the structure and molecular composition of cell-matrix adhesions have been found, that mainly contained either $\alpha v \beta 3$ or $\alpha 5 \beta 1$ integrin depending on the ligand (Olski et al., 2001, Katz et al., 2000). Therefore Zamir and Geiger (Zamir and Geiger, 2001b) suggested a hypothetical model how focal adhesions of two different types are segregated (Fig. 9).

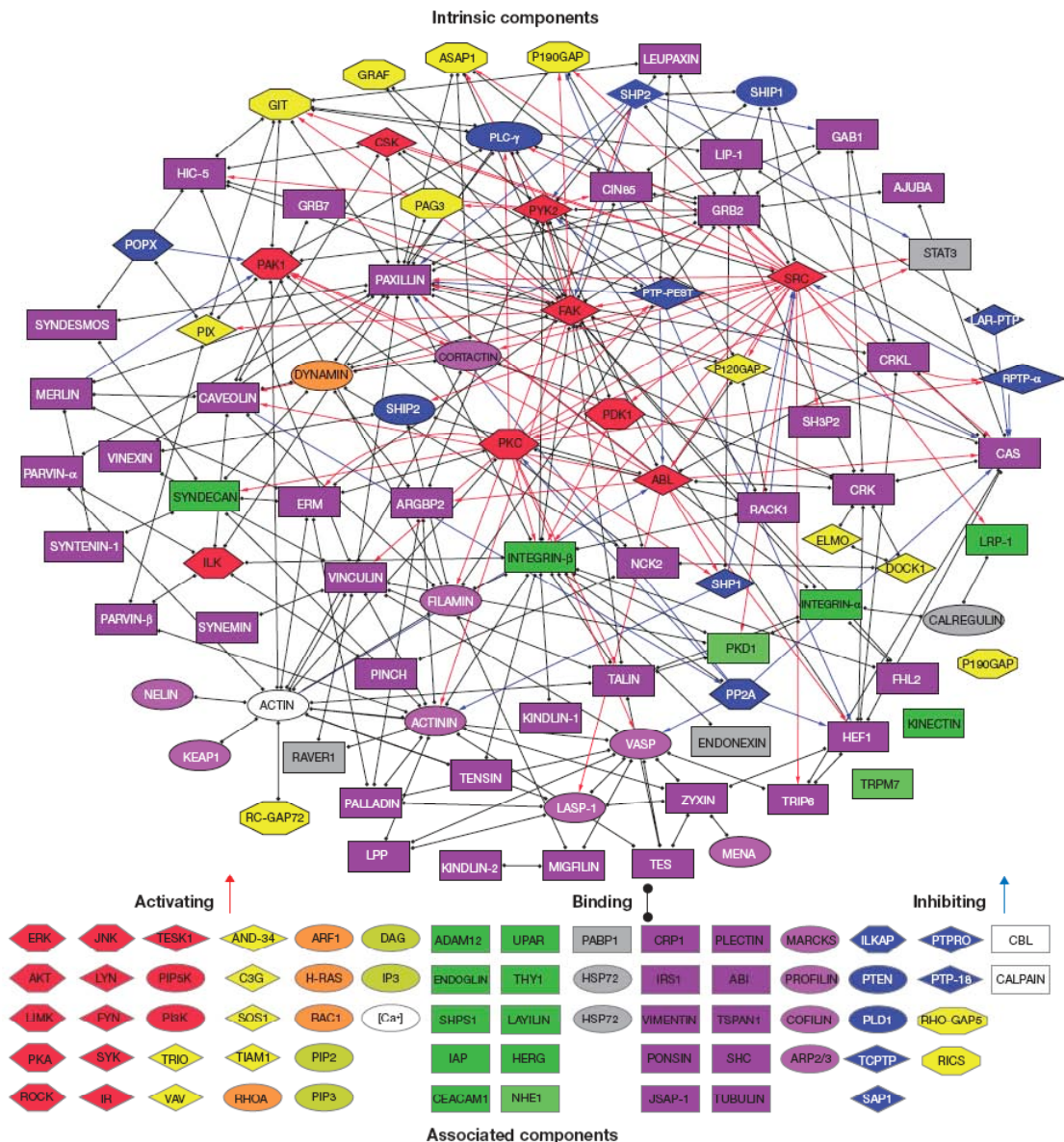


Fig. 8. A scheme of the interactions between the various constituents of cell-matrix adhesions. The components are coloured taking into consideration their structure; different stile lines illustrate the type of interactions between the components. Black lines with full circles at their ends denote non-directional binding interactions, blue arrows represent directional inhibition and red arrows represent directional activation interactions (Zaidel-Bar et al., 2007).

1.4.1 Vinculin, paxillin, and focal adhesion kinase (FAK)

Vinculin, paxillin, and FAK are of the “senior” members of FAs. The **vinculin** is a ~1000 aa molecule containing a globular head and long flexible tail (Winkler et al., 1996). The vinculin head has α -actinin and talin binding sites as well as a site for binding the vinculin tail (Kroemker et al., 1994). Therefore a “closed” conformation of vinculin exist, in which intramolecular interaction between the head and the tail masks binding sites for α -actinin,

talin, F-actin, and VASP located in the middle part of the molecule. The switch of vinculin to the “open” conformation is induced by phosphoinositol 4,5-biphosphat (Gilmore and Burridge, 1996). Both “open” and “closed” conformations of vinculin are able to bind paxillin.

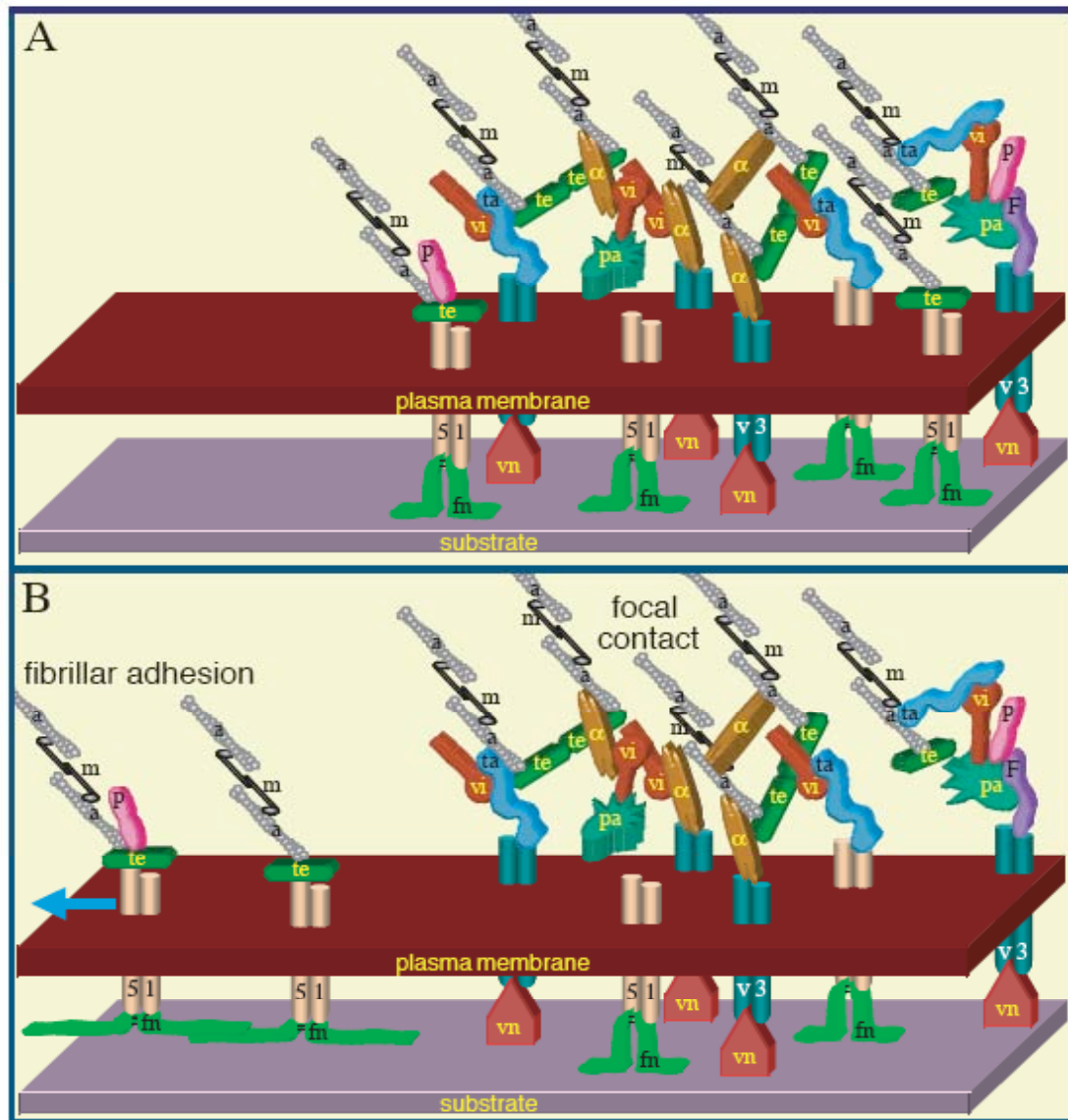


Fig. 9. A molecular model of segregation of two types of focal adhesions. (A) Initial adhesions contain both $\alpha_5\beta_1$ integrin, which binds primarily to fibronectin and $\alpha_V\beta_3$ integrin, which binds primarily to vitronectin. (B) Since substrate-attached vitronectin forms a rigid matrix, $\alpha_V\beta_3$ integrin remains immobile despite the applied contraction force. In contrast, $\alpha_5\beta_1$ integrin is bound to a relatively soft fibronectin matrix and thus translocates centripetally owing to the actomyosin driven pulling. Abbreviations: a, actin; α , α -actinin, F, FAK; fn, fibronectin; m, myosin II; P, parvin/actopaxin; pa, paxillin; ta, talin; te, tensin; vi, vinculin; vn, vitronectin; S1, $\alpha_5\beta_1$ integrin; V3, $\alpha_V\beta_3$ integrin (Zamir and Geiger, 2001b).

Paxillin is a multi-domain protein that was found localized in focal adhesions through its LIM domains (Turner, 2000). Paxillin binds directly to the cytoplasmic domain of integrin receptor (Liu et al., 1999, Schaller et al., 1995), as well as to the vinculin and many other proteins involved in effecting changes in the organization of the actin cytoskeleton. Located in the cell-matrix adhesions, paxillin is tyrosine-phosphorylated in contrast to the large non-phosphorylated cytosolic pools (Cattelino et al., 1997). The paxillin phosphorylation by FAK/Src kinases works as a switch in the regulation of cell-matrix adhesion formation (Zaidel-Bar et al., 2007). The role of paxillin in targeting of Rac activated effectors and the importance in DOCK180/ELMO pathway was revealed (see section 1.5) (Zaidel-Bar et al., 2005, Brown et al., 2002).

Playing a prominent role in integrin signalling **FAK** is one of non-receptor proteins tyrosine kinases. Lacking a transmembrane domain on the N-terminal FAK has a β -integrin binding site (Schaller et al., 1995), whereas its C-terminal region is rich in protein-protein interactions sites, including paxillin-binding one. About 100 residues on the FAK C-terminal part design a focal adhesion targeting (FAT) region, which provides targeting FAK to the FA complex (Hildebrand et al., 1993). Clustering of integrins leads to a phosphorylation of FAK at its central catalytic domain promoting so-called FAK pathway in integrin signalling (see section 1.5)

1.5 Integrin signalling

Anchoring of the cell to the ECM through integrin receptors is necessary for survival. The integrin binding and clustering could activate signals either for cell proliferation or for differentiation. Associated with cytoplasmic part of integrin proteins are not only a physical link to actin cytoskeleton that is necessary because of an absence of actin-binding site at the receptor. The adapter proteins assist in translation of integrin signalling in both directions: the extracellular binding activity of integrins is regulated from inside of the cell (inside-out signalling), while the binding of the ligands initiate signals into the cell (outside-in signalling) (Giancotti and Ruoslahti, 1999).

Activation of integrins by inside-out signalling precedes the binding of integrins to extracellular proteins. Inactive integrins are in a bent state with closed headpieces (Fig. 10). When they become activated by growth factor signalling which is transmitted by binding of adaptor molecules to their cytoplasmic tails the integrins extend, swing out and open their headpieces representing the activated form. This conformational change is a prerequisite for ligand recognition (Luo, 2007).

The ECM binding initiates clustering of recruited integrins, association of FA proteins and reorganisation of the actin cytoskeleton. In turn, changes in actin filament assembly assist FA formation and integrin clustering. Such positive feedback allows for protein aggregations detected by microscopy. Clustering of proteins results in growing FA. The size of a mature FA in a fibroblast could reach several micrometers in length. High concentration of involved proteins facilitates integrin signalling.

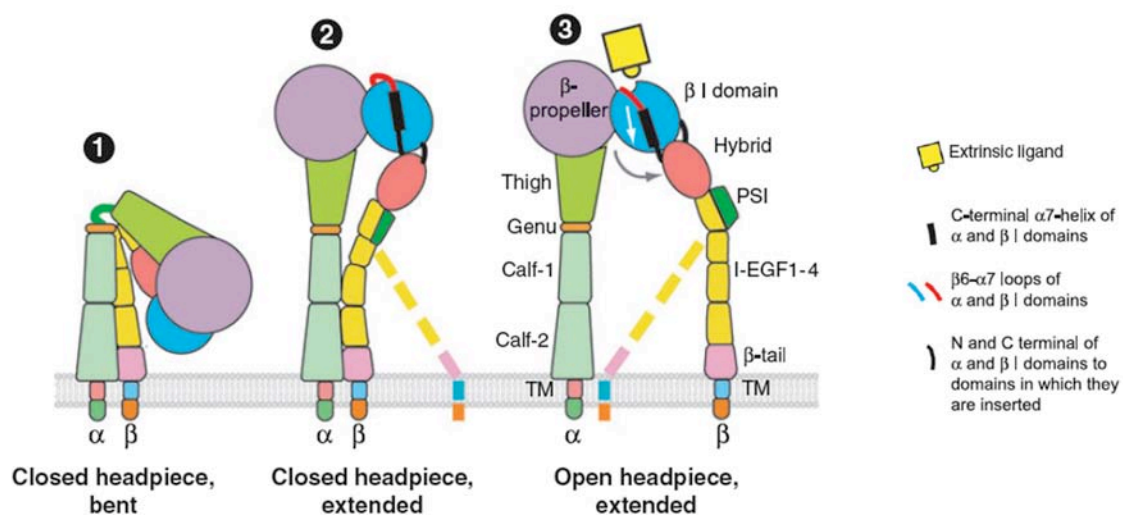


Fig. 10. Rearrangement of domains during activation of integrins lacking an I/A domain. The β subunit lower legs are flexible and are therefore shown in what may be the predominant (solid representation) and less predominant (dashed lines) orientations (Luo, 2007).

1.5.1 FAK pathway

FAK interacts with the cytoplasmic tail of β integrin either directly or through talin and paxillin. Clustering of integrins results in phosphorylation of FAK at Tyr397 (Calalb et al., 1995) that leads to formation of phosphotyrosine docking sites for SH2-domain-containing proteins. In addition to phosphoinositide 3-kinase (PI3-kinase), phospholipase C (PLC)- γ , adapter protein Grb7 (Akagi et al., 2002), the prominent binding partners are Src family kinases. The binding of the SH2 domain of Src induces further Src activation. The activated FAK with recruited Src is able to bind paxillin and Cas, a multifunctional adapter protein (Schaller et al., 1999).

With proline-rich sites for SH3-domain-containing proteins FAK binds two regulators of small GTPases: GRAF (GTPase-activated protein for Rho) and ASAP1 (GTPase-activated protein for Arf1 and Arf6) (Randazzo et al., 2000, Liu et al., 2002) that direct signal to cytoskeletal reorganisation. Thus the integrins signal could transfer through FAK to signaling pathways that regulate small GTPases of the Rho and Arf families.

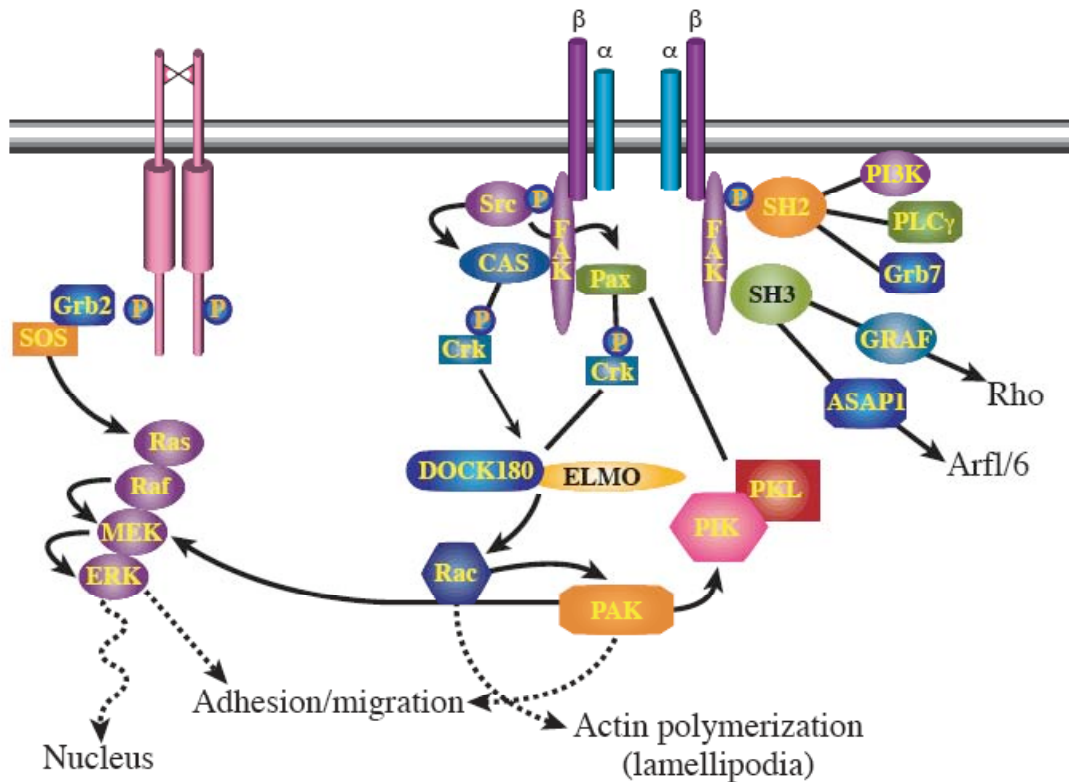


Fig. 11. Proposed interactions among the proteins involved in integrin signalling (Parsons, 2003).

Phosphorylated by FAK Cas is important for sending downstream signals through Sh2/SH3 adapter protein Crk (Vuori et al., 1996). Rac is a proposed effector of the Cas-Crk complex, which plays a prominent role in cell migration (Cary et al., 1998, Klemke et al., 1998). The Rac activation could involve recruitment of DOCK180 and ELMO (Brugnera et al., 2002). Thus FAK signal through Cas, Crk, DOCK180, and ELMO stimulates GTP loading of Rac. Proposed by Parsons (Parsons, 2003) schema of involved in integrin signalling proteins (Fig. 11) shows signals transduction through FAK to Rac and p21-activated kinase (PAK) playing a role in modulating cell adhesion and migration, actin polymerization and MAP kinase signalling.

1.5.2 Integrin regulation of cytoskeleton reorganisation

Cell shape, motility and polarity are regulated by Rho family G-proteins, molecular switches that control cytoskeleton reorganization. Two of these family members, Cdc42 and Rac, stimulate the formation of protrusions at the leading edge: Rac controls extension of lamellipodia and Cdc42 controls extension of filopodia (DeMali and Burridge, 2003). Integrin binding to ECM could be an activator of both these small GTPases (Price et al., 1998), promoting early phase of adhesion. The later phase, the maturation of adhesions is

associated with RhoA activity (DeMali and Burridge, 2003), under influence of RhoA and tension, FAs grow in size to become larger, more stable structures. Integrin engagement leads to a transient depression in RhoA activity (Ren et al., 1999). The decrease in RhoA activity also could be induced by paxillin phosphorylation (Tsubouchi et al., 2002). But during cells adhesion to fibronectin, this initial dip of RhoA activity could be followed by activation (Ren et al., 1999). Fig. 12 illustrates the scheme of Rho inhibition

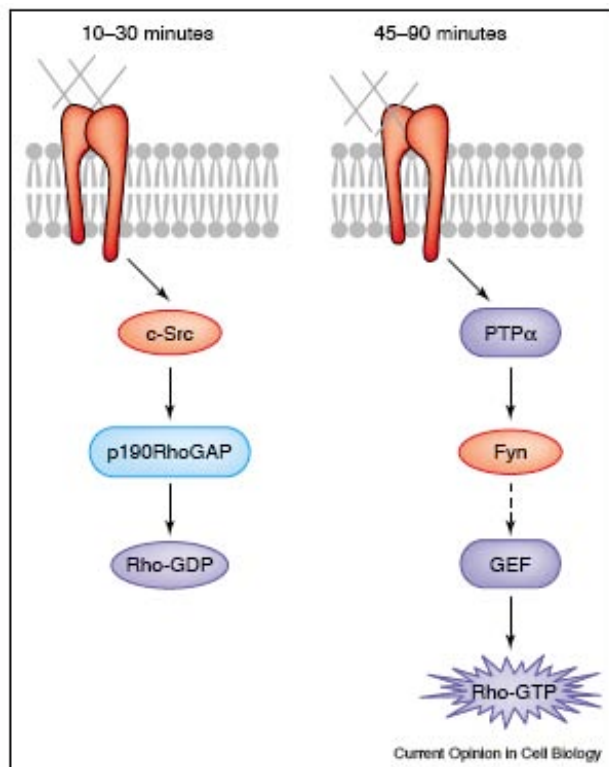


Fig. 12. Role of Src family kinases in the inhibition and reactivation of Rho activity (DeMali et al., 2003).

and further reactivation proposed by DeMali (2003). The time-dependent effect characterizes signal only from some integrins; other integrin receptors could induce a signal through protein tyrosine phosphatase- α (PTP α) earlier than in 45-90 minutes.

In addition to coordination of cytoskeleton remodelling through Rho family GTPases integrin signals are also able to control actin polymerisation through a prominent component of FAs vinculin. The major nucleation of actin polymerisation is actin-related protein 2/3 (Arp 2/3) complex (Fig. 13). The link between Arp 2/3 complex and ligand-bounded integrins was found only in the newest adhesions and not seen in more mature FAs (DeMali et al., 2002). Binding of the Arp 2/3 complex to vinculin does not stimulate the complex activity, but localizes polymerisation to new sites of integrin engagement.

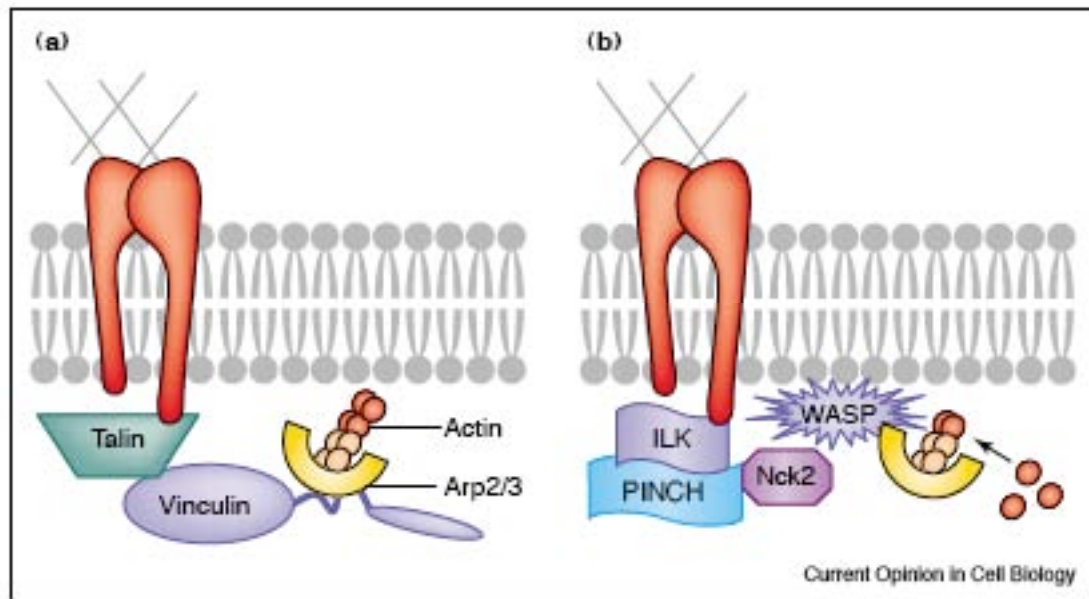


Fig. 13. Link between the actin polymerization machinery and integrins (DeMali et al., 2003).

Another mechanism of integrin-mediated control of actin polymerisation works via the proteins of Wiskott-Aldrich syndrome (WASP) family. Activated by Cdc42, Rac, or Nck WASP proteins stimulate Arp 2/3 complex (Higgs and Pollard, 2001, Rohatgi et al., 2001). The link between the NF-kappaB-inducing kinase (Nik) and integrin β subunit is proposed by a complex integrin-linked kinase (ILK) and particularly interesting Cys-His protein (PINCH) (Hannigan et al., 1996). This pathway promotes actin polymerization at sites of integrin clustering.

1.6 Biofunctionalised surfaces

Modification of surfaces is a widely employed technique for controlling cell attachment, proliferation, and differentiation (Barbucci et al., 2005, Carlsson et al., 1979). Many studies examined the ability of adsorbed ECM proteins to regulate cell behaviour on biomaterial's surfaces. Such proteins as laminin, collagen, and fibronectin are able to stimulate proliferation or differentiation of different type cells via integrin signals (Hashimoto et al., 2006, Stephansson et al., 2002, Nony and Schnellmann, 2001). The selection of the protein as promoter of a certain cell response have to be done taking in consideration that even the same cell lines could change their ability to bind certain ECM protein; e.g., activated by the tissue injury fibroblasts bind fibrin and fibronectin instead of type I collagen (Clark et al., 2004, Gailit et al., 1996), invading the fibrin clot in the wound space (McClain et al., 1996, McCarthy et al., 1988).

The covering of surfaces with ECM proteins by simple adsorption is the oldest and most popular method but nevertheless has some drawbacks. First of all, the amount and conformation of adsorbed proteins varies significantly among different substrates (Iuliano et al., 1993, Elwing et al., 1986). These bring uncontrolled factors in design of surfaces for cell attachment. This problem could be at least partly solved by non-adsorption methods of full-length protein immobilization, namely by covalent attachment.

The way of chemical immobilisation of the biologically active molecules should be chosen individually for every pair "protein-surface", and don't destroy the conformation of cell-binding amino acid sequences. There are some published methods of metal surfaces biofunctionalisation. Albumin has been covalently bound to titanium using aminopropylsilane (APS) and glutaraldehyde (Nanci et al., 1998). Cytokines like bone morphogenetic proteins (BMP-2 and BMP-4) have been bound to titanium with APS and carbonyl diimidazole (Becker et al., 2006) or plasma polymerized allylamine and EDC (Puleo et al., 2002). Fibrillar type I collagen was immobilised on tantalum oxide layer with silane coupling agent via linker (Muller et al., 2005). The methods of full-length proteins immobilisation often include cross-linking of the biomolecules for stabilization against enzymatic degeneration and for prolonged structural and mechanical integrity. For the cross-linking dialdehydes, diisocyanates, azides, and carbodiimides could be used (Khor, 1997).

Such covalent immobilization could be used for design of protein coatings that are much more stable than produced by physical adsorption methods. But the next weakness of the general idea to use the full-length proteins for surface modification is their tendency to deplete. Inserted in the tissue these proteins are objects of proteolytic degradation and need to be continuously refreshed. The long-term exploitation of these materials would be impossible.

Furthermore, using of the isolated from other organisms and purified proteins increases immune response and infection risks. This could be the most dangerous disadvantage of using the full-length proteins for medical applications. To avoid immunologic response, sensibility to degradation, as well as thermal and chemical instability, the surface materials could be modified not with full-length proteins but only with their parts, short amino acid sequences that mimic the adhesion domains of ECM proteins (Rowley et al., 1999, Cook et al., 1997, Lin et al., 1993, Lin et al., 1992).

1.7 RGD and other cell adhesion sequences

The RGD amino acid sequence is expressed in many ECM proteins, including fibronectin, fibrinogen, vitronectin, bone sialoprotein, osteopontin, thrombospondin, laminin, collagen,

von Willebrand factor and other large glycoproteins (Robey, 1996), (Blancher et al., 1996). The role of the RGD motif as primary cell attachment cue was revealed in 1984 by Pierschbacher and Ruoslahti (Ruoslahti and Pierschbacher, 1987, Pierschbacher and Ruoslahti, 1984). Later experiments with synthetic peptides showed that this 3-amino acid sequence in small molecules could promote cell attachment via integrin receptors as well as the full-length ECM proteins.

In addition to RGD some short sequences promoting the cell attachment are revealed. Mould (Mould et al., 1991) explored the Leu-Asp-Val (LDV) site contained in the connecting segment 1 region of fibronectin that is essential for $\alpha 4\beta 1/\alpha 9\beta 1$ integrin binding (Yokosaki et al., 1998, Tselepis et al., 1997). The motif KQAGDV is the proposed cell recognition site of fibrinogen despite two RGD sequences in the molecule (Tamura et al., 2004, Hautanen et al., 1989). KQAGDV binds only $\alpha IIb\beta 3$ but not $\alpha v\beta 3/\alpha v\beta 3$ receptors. Tripeptide KGD shows the same manner of integrin binding. The high selectivity of these peptides is explained by the structural difference of binding “pockets” of the integrins; the shorter side-chain of the lysine can bind αIIb but not αv (Tamura et al., 2004). Integrin $\alpha 5\beta 1$ is published to recognize RRETAWA sequence (Mould et al., 2000, Humphries et al., 2000).

However, the motif RGD is the most universal short sequence recognisable by many members of the integrin family, including $\alpha 5\beta 1$, $\alpha 8\beta 1$, $\alpha IIb\beta 3$, $\alpha V\beta 1$, $\alpha V\beta 3$, $\alpha V\beta 5$, $\alpha V\beta 6$, and $\alpha V\beta 8$. Tripeptide RGD mimics the recognition sites of native ECM proteins, and is able to inhibit in a competitive manner their binding to cell integrins, but affinity of the short RGD containing peptides is relatively low; e.g. hexapeptide GRGDSP is 1000 times less effective in cell attachment assays than fibronectin (Hautanen et al., 1989). The affinity of RGD-integrin was shown to be strongly dependent upon peptide content with addition of amino acids according to the fibronectin sequence: $RGD < RGD-NH_2 < RGDS < GRGDSP$ (Pierschbacher and Ruoslahti, 1987).

The conformation of the RGD-loop and its flanking amino acids both in full-length native proteins and in short synthetic peptides are mainly responsible not only for their different integrin activity (Hersel et al., 2003, Ruoslahti, 1996), but also provide selectivity of binding by different integrins (Meyer et al., 2006). Modern understanding of the structure of the extracellular domain of $\alpha V\beta 3$ integrin encourages attempts to construct the peptides for selective binding of the certain receptors. The structural difference between $\alpha IIb\beta 3$ and $\alpha V\beta 3$ allows the design of $\alpha V\beta 3/\alpha IIb\beta 3$ selective ligands, but the searching of $\alpha V\beta 5$ selective ligand has not been successful yet. $\beta 5$ and $\beta 3$ subunits probably have high homology; most known small molecules show $\alpha V\beta 3$ and $\alpha V\beta 5$ biselectivity (Meyer et al., 2006). The structure of binding pockets of others RGD-integrins, including fibronectin-specific $\alpha 5\beta 1$, have not yet been completely obtained.

1.7.1 Methods of RGD functionalisation

Broad application the new technique RGD-coating in the dental/orthopedic implant design, tissue engendering and numerous scientific approaches promotes development of a variety of methods of immobilizing the short peptides to many materials. RGD could be covalently attached to the polymer, glass or metal surfaces via functional groups (hydroxyl-, amino- or carboxyl groups) and/or linker molecules.

For immobilization of RGD peptides onto polymers in most cases linking via a stable covalent amide bond is used. This is usually done by reacting an activated carboxylic group on the surface with N-terminus of the peptide (Hersel et al., 2003). To avoid a potential problem of coupling to the surface of the peptide functional amino groups, their blocking with other groups could be used (Krijgsman et al., 2002, Quirk et al., 2001). The general drawback of this methodology is the necessity to remove the protecting groups afterwards; the harsh treatment in some cases could disrupt peptide bioactivity or affect long-term stability of the surfaces (Massia et al., 2000).

The functional groups on the polymer surfaces for peptide coupling could be generated by chemical or physical treatment, e.g. alkaline hydrolysis, reduction, oxidation, or plasma treatment (Hersel et al., 2003). Another alternatives are blending with a polymer containing functional groups, e.g. poly-L-lysine (Quirk et al., 2001, Yang et al., 2001), and co-polymerization (Bacakova et al., 2007, Deng et al., 2006, Park et al., 2004, Na et al., 2001).

The use of self-assembled monolayers (SAMs) is the next strategy of peptide immobilisation to the surface. The SAM-modification could be applied to metal as well as glass and polymers, providing two general methodologies: 1) coupling of the peptides to the functional groups of self-assembled molecules on the surface and 2) use of peptide-containing molecules, that are able to assemble in SAMs.

1.7.1.1 Self-assembled monolayers

Since Sagiv (Sagiv, 1980) reported in 1980 about formation of SAMs of octadecyltrichlorosilane (OTS) the SAM-technique becomes common in applications of surface science. Generally, a SAM is a single layer of molecules which are spontaneously formed upon solid substrates. The key advantage is that self-assembled monolayers are ordered, close-packed molecular assemblies. These thin ($10\pm 30\text{\AA}$) layers provide global changes in surface character.

SAM formation provides surface functionalisation by organic molecules terminated by functional groups like -SH, silanes, NH_2 , -CN, and -COOH (Chaki and Vijayamohan, 2002). The first two types of SAMs, alkanethiols and organosilanes, could be described as

$[-CH_2-]_n$ chains with a sulphur or silane ion anchor respectively. The end groups of molecules in such monolayers may be either hydrophobic (e.g., $-CH_3$) or hydrophilic (e.g., $-OH$, $-COOH$), providing additional possibilities to control surface reactivity by monolayer functionalisation (see sections 3.1.4).

Silanisation with silane compounds is a common method of modification of glass and other siliceous surfaces (SiO_2 , for example, as was performed in this work). Further immobilisation of biomolecules onto the silanised surface is commonly achieved with aminosilanes such as (3-Aminopropyl)-triethoxysilane (APTES) (Vansant, 1995). The reactivity of terminal aminogroups could be used for covalent binding to isothiocyanate (SCN) groups, for example.

Formation of SAMs of thiols is based on the interaction of sulphur atoms with gold (Ulman, 1989) silver (Shaporenko et al., 2005) or platinum (Perepichka et al., 2005). The advantage of a gold surface is its high resistance to oxidation. Since publication by Nuzzo and Allara in 1983 concerning dialkyldisulfides (Nuzzo, 1983) many other organosulphur compounds have been reported to form SAMs on the gold surfaces in recent years. The point of our interests, SAMs formed by octadecylthiol (ODT) molecules on gold surface are stable, compact and ordered structures (Vaughan, 1992), (Meucci, 1999); these monolayers are hydrophobic and weakly modifies their characteristics even in the presence of redox mediators (Mecheri, 2002). The advantages of the ODT SAMs makes them highly usable for surface functionalisation.

1.8 Patterning methodologies

The study of the effects of chemical and topographical surface patterning on cell attachment, growth and differentiation requires reliable microstructuring technology development. In the frames of the two-dimensional chemical patterning the soft lithographic as well as photolithographic technologies are commonly used.

The photolithography has originally been developed for the fabrication of semiconductor devices. The basic idea is a patterning of surfaces as a result of UV irradiation through a mask, and could be applied to UV-sensitive polymers. A method of multi-step metal-polymer coating with final deletion of polymer layer proposed by Scotchford (Scotchford et al., 2003) allows the composition of the two metal layers. The limitation of the photolithographic methods concerns the physical resolution of the mask structure, mask thickness, and requirement of photosensitive materials.

The “soft lithography” is a general name for a group of technologies that use electrometric materials to create chemical structures on the surface. The microcontact printing (μ CP) and microfluidic patterning (μ FLP) are two of them.

Methods of μ FLP use soft-polymer stamps for creation of microchannels pattern to deliver fluids to selective areas on the surface. The elastic polymer partly contacts with the substrate, protecting respective areas; unprotected substrate is open for biomolecules of solution that fills up channels of elastic muster (Nalayanda et al., 2007, Situma et al., 2005). The critical point of the method is time that is sufficient for biomolecules absorption or binding to the surface; in the case of surface-sensitive molecules this time could be relatively short and patterning procedure could perform without drying of the surface (Holden et al., 2004).

μ CP is the most widely used technique of soft lithography. Originally developed for microelectronics applications, μ CP has become popular for patterning of surfaces for cell adhesion because of its simplicity, cost-effectiveness and flexibility. The common procedure is illustrated in Fig. 14. The main element of the technique is an elastomeric stamp that is formed by moulding of liquid-phase polymer (usually polydimethylsiloxane) over a microstructured master. The first step of μ CP is covering the stamp with “ink”, a solution of molecules that later will be transferred to the surface. The molecules absorb on the stamp, covering it with homogeneous layer. Second step, actual stamping procedure transfers “ink” to substrate material. Final step is optional and allows backfilling of the non-stamped areas with second molecule.

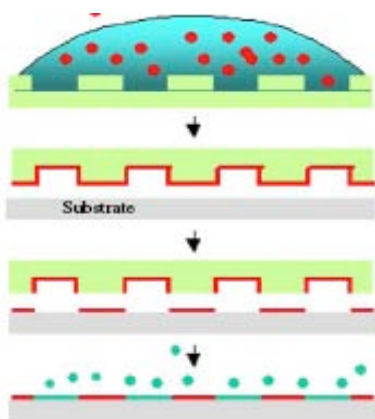


Fig. 14. Schematic representation of the microcontact printing (μ CP) technique (Falconnet et al., 2006).

The μ CP technology is successfully applied for stamping of polymers (Na et al., 2006) as well as biomolecules (Oliva et al., 2003) via their absorption to materials of stamp and later of substrate. Printing patterned SAMs extends their utility, providing a flexible method of structured surface design. Printed onto the metal alkanothiols is a suitable pattern for further treatment by etching that deletes non-protected metal (Wilbur, 1996).

1.9 Motivation/ Outlook

Combining the new technologies in creating topographically well defined 2D and 3D surfaces structures with optimal biocompatibility for different purposes, e.g. stem cell differentiation and tissue regeneration, is challenging. Multiple biomolecules have to be oriented arranged in defined patterns. This requires the development of different bioconjugation strategies that could be combined.

The aim of this work is to create novel strategies of RGD-peptide coupling that could be easily applied to homogeneous but predominantly to structured surfaces. For this purpose a novel method to bind RGD-peptides covalently to aminated surfaces was developed and their biocompatibility was examined. Furthermore, a method for 2D surface patterning was designed to which the novel RGD-coupling procedure could be successfully and reproducibly transferred.

2 MATERIALS

2.1 Chemicals

Acetone (Sigma Aldrich Chemie GmbH, Taufkirchen, Germany)

Agarose (Invitrogen GmbH, Karlsruhe)

Antibodies:

Rabbit polyclonal phospho-paxillin (tyr118) antibodies (Cell Signaling, USA)

Mouse monoclonal anti-human paxillin antibodies (BD Bioscience Pharmingen, USA)

Mouse monoclonal anti-human vinculin antibodies (Sigma Aldrich Chemie GmbH, Taufkirchen, Germany)

Rabbit polyclonal anti-human fibronectin antibodies (Sigma Aldrich Chemie GmbH, Taufkirchen, Germany)

Rabbit polyclonal anti-phosphohistone H3 antibodies (Upstate, USA)

CyTM2-conjugated goat anti-rabbit antibodies (Dianova, Hamburg, Germany)

CyTM2-conjugated goat anti-mouse antibodies (Dianova, Hamburg, Germany)

CyTM3-conjugated goat anti-rabbit antibodies (Dianova, Hamburg, Germany)

CyTM3-conjugated goat anti-mouse antibodies (Dianova, Hamburg, Germany)

Butanethiol (Sigma Aldrich Chemie GmbH, Taufkirchen, Germany)

Chloroform (Sigma Aldrich Chemie GmbH, Taufkirchen, Germany)

Deoxyribonucleoside triphosphates (dNTPs)(Promega GmbH, Mannheim)

Dithiotritol (Invitrogen GmbH, Karlsruhe)

Dimethylsulfoxide (AppliChem GmbH, Darmstadt, Germany)

Dulbecco's modified Eagle medium with 4.5 g/L Glucose, Sodium Pyruvate (PAA Laboratories GmbH, Cölbe, Germany)

Ethanol, absolute (Aldrich, Germany)

Fetal calf serum (Invitrogen GmbH, Karlsruhe)

Fibronectin 0,1 % solution from bovine plasma (Sigma Aldrich Chemie GmbH, Taufkirchen, Germany)

Geneticindisulfat (G418®) (Carl Roth GmbH + Co KG, Karlsruhe, Germany)

GoTaq® Polymerase (Promega, Mannheim, Germany)

HEPES (4-(2-hydroxyethyl)-1-piperazineethanesulfonic acid) (Carl Roth GmbH + Co KG, Karlsruhe, Germany)

Hexylthiol (Sigma Aldrich Chemie GmbH, Taufkirchen, Germany)

H-Gly-Arg-Gly-Asp-Ser-OH (Bachem, Weil am Rhein, Germany)

MMLV reverse transcriptase (Promega, Mannheim, Germany)

Non-essential amino acids (Invitrogen GmbH, Karlsruhe)

Octadecylthiol (Sigma Aldrich Chemie GmbH, Taufkirchen, Germany)

Oregon Green® 488 phalloidin (Invitrogen GmbH, Karlsruhe)

Phenylmethanesulfonyl fluoride (AppliChem GmbH, Darmstadt, Germany)

Pluronic® F-68 10% solution (Sigma Aldrich Chemie GmbH, Taufkirchen, Germany)

Penicillin-streptomycin mixture (Invitrogen GmbH, Karlsruhe)

Polyethelenglicol-3350 (Sigma Aldrich Chemie GmbH, Taufkirchen, Germany)

Pyromycin-dihydrochlorid (AppliChem GmbH, Darmstadt, Germany)

Potassium hexacyanoferrate(II) trihydrate, $K_4[Fe(CN)_6] \cdot 3H_2O$, (Sigma Aldrich Chemie GmbH, Taufkirchen, Germany)

Potassium hexacyanoferrate(III), $K_3[Fe(CN)_6]$, (Sigma Aldrich Chemie GmbH, Taufkirchen, Germany)

Potassium thiosulfate, $K_2S_2O_3$, (Sigma Aldrich Chemie GmbH, Taufkirchen, Germany)

Potassium hydroxide, (Sigma Aldrich Chemie GmbH, Taufkirchen, Germany)

Random hexamer primers (Promega, Mannheim, Germany)

RNAtidy G (AppliChem GmbH, Darmstadt, Germany)

Triton® X-100 (AppliChem GmbH, Darmstadt, Germany)

Trypsin / EDTA (Invitrogen GmbH, Karlsruhe)

Trypsin inhibitor from soybean (AppliChem GmbH, Darmstadt, Germany)

2.2 Buffers

TAE: 40 mM Tris / acetate, pH 8.3, 1 mM EDTA

1x PBS: 137 mM NaCl, 2.7 mM KCl, 6.5 mM Na_2PO_4 , 1.5 mM KH_2PO_4 , pH 7.5

PBS-Tween: 1x PBS, 0.05% (v/v) Tween 20

1x APBS: 103 mM NaCl, 2.0 mM KCl, 5 mM Na_2PO_4 , 1.1 mM KH_2PO_4 , pH 7.5

Hepes Buffer: 5 mM KCL, 140 mM NaCl, 1 mM MgCl_2 , 0.9 mM CaCl_2 , 25 mM HEPES, pH 7.4

2.3 Solutions

Antibodies:

Mouse monoclonal anti-paxillin (diluted 1 : 1000 in 2,5% BSA / PBS)

Mouse monoclonal anti-vinculin (diluted 1 : 1000 in in 2,5% BSA / 0,1 % Triton X100 / PBS)

Rabbit polyclonal anti-phosphopaxillin (diluted 1 : 250 in 2,5% BSA / PBS)

Goat-anti-mouse CyTM3 antibodies (diluted 1 : 400 in 2,5% BSA / PBS)

Goat-anti-rabbit CyTM3 antibodies (diluted 1 : 400 in 2,5% BSA / PBS)

Goat-anti-mouse CyTM2 antibodies (diluted 1 : 300 in 2,5% BSA / PBS)

Goat-anti-rabbit CyTM3 antibodies (diluted 1 : 300 in 2,5% BSA / PBS)

Butanethiol (2 mmol and 10mmol in ethanol)

DAPI (1 mM in PBS)

Octadecylthiol (2 mmol in ethanol)

Oregon Green® 488 phalloidin (diluted 1 : 100 in PBS)

Phenylmethanesulfonyl fluoride (PDMF), stock (0,25 M in Ethanol)

Pyromycin-dihydrochlorid (10 mg/ml stock solution in HEPES buffer)

Trypsin inhibitor from soybean (STI), stock (1 mM in water)

2.4 Cultured cell lines

MC3T3-E1 pre-osteoblastic cells, mouse embryo/fetus calvaria fibroblasts (DCMZ ACC 210)

Mouse B16 beta3–GFPintegrin–expressing melanoma cells (Ballestrem et al., 2001)

Rat embryonic fibroblasts (REF52) stably expressing YFP-paxillin (Zimmerman et al., 2004)

Swiss mouse 3T3 fibroblasts L1, embryonic cell line (ATCC CL-173)

Xenopus tadpole fibroblasts (Pudney et al., 1973)

2.5 Equipment

Centrifuges:

Biofuge fresco (Kendo, Langenselbold, Germany)

Multifuge^R 3S-R (Kendo, Langenselbold, Germany)

Confocal Microscope System Zeiss LSM-510 Meta (Jena, Germany) equipped with

Argon laser (458, 488, 514 nm excitation)

Diode Pumped Solid State (DPSS) laser (561 nm)

Diode 405-30 laser (405 nm)

Helium-Neon Laser (633 nm excitation)

Software: LSM Image Browser

IKA Ultra Turrax® Homogenizers (IKA Labortechnik, Staufen, Germany)

Fluorescence microscope DMIRE2 (Leica Microsystems, Bensheim) equipped with

Digital camera C4742-95-12 ERG (Hamamatsu, Heidelberg, Germany)

Software: Openlab 3.1.2 (Openlab, Heidelberg, Germany)

High vacuum coating unit (Institute for Applied Physics, FZK, Karlsruhe, Germany)

PCR cycler, Personal cycler and UNO II (Biometra, Göttingen, Germany)

pH meter pH 521 (WTW, Weilheim, Germany)

Scanning electron microscope LEO 1530 Gemini (Oberkochen, Germany)
equipped with FEG

Spectrophotometer, Bio-photometer (Eppendorf, Hamburg, Germany)

Spectrophotometer, Ultraspec 2100 pro (Amersham, Freiburg, Germany)

Water bath: Victor Recker (Krankenhaus-laborbedarf, Berlin, Germany)

Weighing balances, LC2201P and ISO9001 (Satorius, Göttingen, Germany)

2.6 Materials

Cell culture flasks 50 cm² and 250 cm² (Greiner Bio-One GmbH, Frickenhausen, Germany)

Glasses 15X15 mm and D12mm (Fisher Scientific GmbH, Schwerte, Germany)

Microscope Immersion Oil "Immersol" (Carl Zeiss Jena GmbH, Jena, Germany)

μ-Slid 8 well (Ibidi GmbH, München, Germany)

Petri dishes, polystyrene, 5 ml (Sarstedt, Nümbrecht, Germany).

Silicone elastomer Sylgrad 184 stamp (Dow Corning, US)

Grids for transmission electron microscopy (TEM grids) with 400 bars/inch (Agar Scientific, England)

3 METHODS

3.1 Functionalisation of surfaces

3.1.1 Aminosilanisation

To form functional aminogroups on the surface for further covalent binding to isothiocyanate end groups of synthetic peptides I used a procedure of silanisation of glass or SiO₂ slides with (3-Aminopropyl)-triethoxysilane (APTES). Both liquid and gas phase aminosilanisation provides formation of SAM on the surface.

For cleaning, glass and SiO₂ slides were rinsed with absolute acetone, ethanol, and finally distilled water. After drying under nitrogen the slides were aminosilanised for 30 seconds in 4% APTES in chloroform (liquid phase) or for 10 minutes in the presence of APTES vapour (gas phase) in a glass container under nitrogen. The aminosilanisation of slides was followed by chloroform rinsing and 1 h heating at 40°C to evaporate trace quantities of chloroform.

3.1.2 Fabrication of metal covered slides

A gold coating was applied to both glass and SiO₂ slides. At first, 15x15 mm² glass and 10x10 mm² SiO₂ slides were cleaned by rinsing consecutively with acetone, absolute ethanol, distilled water and then dried under nitrogen. The coating of the slides with gold layer required at first the creation of a chromium layer (thickness 1-2 nm), which acts as an adhesion promoter between the glass and the gold. Both metal coatings were formed by e⁻ beam evaporation in a home built high vacuum coating unit. The evaporation was performed at a chamber vacuum of 10⁻⁸ mbar before evaporation and 10⁻⁷ mbar during evaporation and with typical evaporation rates of 0.02 - 0.03 nm/s. The control of metal layer thickness was performed by a quartz micro crystal balance. Deposition of a 50 nm gold layer required about 30 minutes after which the samples were kept in the chamber for 15 minutes for cooling down.

The deposition of a 50 nm silver layer on glass slides (with 1 nm chromium layer as adhesion promoter) was performed in the same way. The silver-covered samples were not used for the preparation of RGD-functionalised structured samples because the silver layer was completely floated and resolved during the etching procedure as described in the following section.

3.1.3. Microcontact printing and thiol SAMs formation

To design a patterned gold surface a method of microcontact printing (μ CP) was chosen. μ CP technology allows the creation of a pattern by printing of thiol SAM (in this work, ODT) onto the gold surface. As a stamp a polydimethylsiloxane (PDMS) form was used, taken from a microfabricated silicon master. 3.5×10^{-2} M solution of ODT in ethanol was used as ink. The printed ODT-monolayer protected appropriated areas of gold underneath during the next step of pattern design, etching of gold, which was done as follows. 20 μ l of ink (ODT in ethanol) was dropped on stamp surface and after 20 sec the liquid was blown away and the stamp surface was dried under nitrogen. After 40 sec the stamp was pressed onto the gold substrate for 60 sec and removed again.

By the immersion of the substrates in aqueous solution of 3.2 mg potassium hexacyanoferrate(II) trihydrate ($K_4[Fe(CN)_6] \cdot 3H_2O$), 33 mg potassium hexacyano-ferrate(III) ($K_3[Fe(CN)_6]$), 190 mg potassium thiosulphate ($K_2S_2O_3$) and 400 mg potassium hydroxide in 10 ml deionised water the metal is reduced and removed solely at those surface areas which were not covered with thiol layer by μ CP.

After the etching process the samples were rinsed with water and dried under nitrogen. In the last step the samples were aminosilanised (as described in section 3.1.1) for functionalisation of glass areas with amino groups.

For μ CP and etching slides were immediately used after gold evaporation.

3.1.4 Biofunctionalisation with RGD-peptides

3.1.4.1 RGD peptides

The peptides functionalised with isothiocyanate anchor were synthesised in Prof. Dr. Kessler laboratory (TU Munich). The linear peptides PDIT-Ahx-Ahx-GlyArgGly-AspSer-OH (GRGDS) and PDIT-Ahx-Ahx-GlyArgGlyAspSerPro-OH (GRGDSP) including their corresponding controls PDIT-Ahx-Ahx-GlyArg β AlaAspSer-OH (G β ADS) and PDIT-Ahx-Ahx-GlyArg β Ala-AspSerPro-OH (G β ADS) were synthesized by Solid Phase Peptide Synthesis (SPPS) on tritylchloride polystyrene (TCP) resin (Barlos et al., 1989a) according to Fmoc strategy (Barlos et al., 1989b; Pearson et al., 1989) The cyclic peptides c(-RGDfK-) and c(-RGDfKG-) as well as the corresponding control peptides c(-R β ADfK-) and c(-R β ADfKG-) were synthesized in a similar way as described by Kantlehner et al. 1999 (Kantlehner et al., 1999) and afterwards coupled in solution with the spacer-anchor fragment OH-Ahx-Ahx-PDIT, to give the corresponding desired functionalised compounds PDIT-Ahx-Ahx-c(-RGDfK-), PIDT-Ahx-Ahx-c(-RGDfKG-), PDIT-Ahx-Ahx-c(-R β ADfK-) and PDIT-Ahx-Ahx-c(-R β ADfKG-).

3.1.4.2 RGD peptide coupling

The lyophilized peptides were dissolved in DMSO at 4 mg/mL and diluted with 100 mM Na₂HPO₄ pH 9.5 to the desired concentration; for cell adhesion assays, the final concentration was 0.4 mg/ml. During coupling isothiocyanate groups of peptides bind the NH₂-groups on the aminosilanised glass (or SiO₂) surfaces. The coupling to unstructured and micro structured surfaces was carried out in a wet chamber at room temperature.

After four times 10 min washing with PBS the slides were washed two times with DMEM before being used for cell-adhesion.

3.1.4.3 PEG or Pluronic® passivation

The cell adhesion experiments showed that biofunctionalisation of structured surfaces requires an additional blocking/passivation step before or during the peptide coupling to prevent unspecific absorption of peptides to gold-ODT layers (see section 4.9.6). Three different modification of the passivation treatment were performed:

- (1) 10 min incubation of the structured surfaces with 5% PEG solution followed by 2 hours peptide coupling;
- (2) 10 min incubation of the structured surfaces with 5% Pluronic® solution followed by 2 hours peptide coupling;
- (3) 2 hours peptide coupling in the presence of 2 mM Pluronic® in coupling solution.

I proved that all these methods could be applied to “gold-ODT – NH₂-glass” structured surfaces, but for further tests of structured RGD-functionalised surfaces I have made a choice in favour of peptide coupling in the presence of Pluronic®.

3.1.5 Coating of the surfaces by absorption

3.1.5.1 Fibronectin coating

0,1% fibronectin (Sigma) solution diluted 1 : 5 in water was incubated overnight in plastic μ -slide wells at 4°C. 100 μ l of solution per well was used. After washing with PBS 100 μ l of 1% pure BSA (Promega) in PBS was added in the well for 30 minutes. After washing 3 times for 10 min with PBS the slides were used for cell-adhesion.

3.1.5.2 Absorbed RGD-peptides on the surfaces

1 mg/ml peptide solution in PBS was incubated overnight in plastic μ -slide wells at 4°C. 100 μ l of solution per well was used. After washing with PBS 100 μ l of 1% pure BSA (Promega) in PBS was added in the well for 30 minutes. After washing 3 times for 10 min with PBS the slides were used for cell-adhesion.

3.1.6 Fabrication of homogeneous thiol layers on gold

3.1.6.1 Fabrication of homogeneous ODT-SAMs

Gold coated glass (50nm thickness of gold layer) were incubated for 2 minutes in 3.5×10^{-2} M solution of ODT in ethanol, before being rinsed with water and then dried under nitrogen.

3.1.6.2 Fabrication of homogeneous layers of short thiols

Gold coated glass (50 nm thickness of gold layer) was incubated for 2 minutes in 2 mM or 10 mM solution of hexylthiol or butanethiol in ethanol. Next they were rinsed with water then dried under nitrogen.

3.1.7 Alternative patterning: Gold evaporation through the mask

Glass slide was APTES-silanised in liquid phase (see section 3.1.1). Immediately after silanisation the TEM grids with through slits (400 bars/inch) was fixed on the slide. The slide with mask was placed in a high vacuum coating unit and coated with 1nm chromium and 25 nm gold (see section 3.1.2). After 15 minutes cooling in the chamber the samples were ready for further preparation.

3.2 Cell biology methods

3.2.1 Cell culturing

Working with cell cultures was always performed under sterile conditions. Mouse 3T3 Swiss fibroblasts were cultured in Dulbecco's modified Eagle medium (DMEM with 4.5 g/l glucose, sodium pyruvate) supplemented with 10% FCS, 1% penicillin-streptomycin mixture, and 1% non-essential amino acids at 37°C at 7% CO₂ supply, 95% humidity. Rat embryonic fibroblasts (REF52) stably expressing YFP-paxillin and mouse beta3-GFP integrin-expressing melanoma cells were cultured at the same conditions additionally supplied with

pyromycin-dihydrochloride (final concentration: 1 mg/ml), and geneticindisulphate (G418®) (final concentration: 1.5 mg/ml) respectively. *Xenopus* tadpole cells were cultured in DMEM with 4.5 g/l glucose and sodium pyruvate, supplied with 10% FCS, 1% penicillin-streptomycin mixture, 1% non-essential amino acids and 25% H₂O at 24°C at 7% CO₂ supply, 95% humidity.

After reaching approximately 70% confluence, the cultivated in 50 cm² flasks cells were split 1:4 (every 2-4 days). For this, the medium was removed and 1 ml of 0.05% trypsin/ 0.02% EDTA solution pre-warmed to 37°C was added to the culture and left in the incubator at 37°C for approximately 5 minutes until detached from the flask. Trypsin activity was stopped by addition of the cell culture medium to the flask.

3.2.2 Cell adhesion assay

The confluent cell cultures were detached by trypsin/ EDTA treatment. To remove trypsin from cell suspension in DMEM, 5 µl of 1 mM soybean trypsin inhibitor (STI) per every 5 ml medium was added (final concentration of STI was 10 µM), followed by 3 min centrifugation at 900 rpm. After removal of the supernatant, the concentration of the cell suspension was reduced to 1.4×10^5 cells in 10 µM STI in DMEM. To avoid serum-fibronectin contamination cell adhesion assays were performed in serum free medium.

In the 5 ml polystyrene Petri dishes peptide or protein functionalised glass surfaces were covered with 5 ml of cell suspension and incubated at 37°C and 7% CO₂ for a time sufficient for cell spreading depending on the specific cell line that was used.

3.2.2.1 Phenylmethanesulfonyl fluoride (PMSF) as trypsin inhibitor

PDMS was used as an alternative trypsin inhibitor in the cell adhesion assay procedure. After re-suspension of cells adherent to the cell culture dishes, 50 µl of 0,25 M PMSF in 100% ethanol was added to every 5 ml of cell suspension; final concentration of PMSF was 2.5 mM. Adding of the trypsin inhibitor into the solution was followed by 3 min centrifugation at 900 rpm. After removal of the supernatant, the concentration of the cell suspension was reduced to 1.4×10^5 cells DMEM. Further procedures were exactly the same as described in section 3.2.2.

3.2.2.2 Cell adhesion assay in the presence of Pluronic®

The cell assay procedure was as described in 3.2.2, excluding the addition of 5 µl of 10% Pluronic® solution in the serum-free cell-cultivation medium in every 5 ml Petri dish.

3.2.3 Cell proliferation assay

The cells were seeded in 5 ml Petri dishes with test samples as described in section 3.2.2 in concentration 0.7×10^5 cells in 10 µM STI in serum free DMEM. After 4 hours of incubation at 37°C and 7% CO₂ serum free medium was replaced by supplemented with 10% FCS DMEM. Formaldehyde fixation of attached to samples cells was performed in 4, 24 and 48 hours after cell seeding. To enumerate cells in the mitotic phase the immunostaining with antibodies against phosphorylated histone H3 was performed. Total number of cells was counted with DAPI staining.

3.2.4 Competition assays

The competitive assays were performed for (1) RGD-peptides absorbed on the plastic bottom of µ-slide wells and (2) RGD-peptides that were coupled to amino-functionalised glasses.

(1) 200 µl of 1 mM RGD-peptide solution in PBS was added in a µ-slide well and incubated overnight at 4°C. After washing with PBS, 200 µl of pure BSA in PBS was incubated in a µ-well 30 minutes at RT and then it was washed 3 times with PBS, before addition of cell suspension with simultaneously supplied with the soluble RGD peptide (see below).

(2) The RGD-functionalised slide was placed onto the bottom of a µ-slide well. 200 µl of pure BSA in PBS was incubated in a µ-well for 30 minutes at RT. The µ-well was washed three times with PBS followed by addition of cell suspension together with the soluble RGD peptide.

The cells were trypsinised, and the cell suspension was supplied with STI as described in the section 3.2.2. The final concentration was 0.7×10^5 cells in 10 µM STI in DMEM (without FCS). 200 µl of the cell suspension was placed in the well of a µ-slide. Simultaneously 6 µl of stock solution of H-Gly-Arg-Gly-Asp-Ser-OH (0,1 M in PBS) was added into the suspension; the final concentration of the soluble peptide in the well was 3 mM. After 1 hour incubation at cell cultivation conditions, the cell suspension was removed; the surface attached cells were washed, fixed and stained as described in the following section.

3.2.5 Immunocytochemistry

Slides with attached cells were rinsed three times with PBS and fixed in 4% formaldehyde / PBS for 10 min at RT. Cells were permeabilised in 0.5 % Triton X-100 for 10 min and washed three times with 0,1 % Triton X100 / PBS prior to blocking with 2.5% bovine serum albumin / PBS for 1 hour. Components of focal adhesion complex such as paxillin, phosphopaxillin, and vinculin were detected with respective monoclonal or polyclonal first antibodies (see section 2.3), and incubated in the antibody solution overnight at 4°C. For every 15x15 mm² sample slide 150 µl of antibody solution was used. After washing with PBS (3 times) a solution of secondary goat-anti-mouse or goat-anti-rabbit fluorophor-coupled antibodies was added for 30 min at 37°C. A washing step (PBS, 3 times) was followed by counterstaining with Oregon Green® 488 phalloidin, 30 min, at RT. A nuclear staining with DAPI was carried out for 3 min at RT. After three washes with PBS the samples were mounted in elvanol.

When *Xenopus* fibroblasts were analysed PBS was replaced by APBS due to the different osmolarity of amphibian cells.

3.3 Microscopic methods and surface quality control

3.3.1 Microscopy and image analysis

Fluorescence of fixed and stained cells were recorded on a Leica DM IRE2 inverted research microscope with 5x, 10x, 20x, 40x, and 63x objectives, equipped with a 16 bit greyscale digital camera. Narrow band filters A4, L5, and Y3 were used for registration of blue (DAPI), green (GFP and Oregon Green® 488), and red (Cy3) fluorescence correspondingly. Images exposure times were dependent on signal strength. Greyscale images from every filter were handled, coloured and overlaid with Openlab 3.1.2 software package.

3.3.1.1 Statistics

For statistical data images made on Leica fluorescent microscope were used. The size of an image of the surface made with the 40x objectives is 0.03 mm². The number attached to the surfaces cells was counted on a minimum of 30 images for every sample slide. To ensure data accuracy the results of calculations for a minimum of 3 different slides were used. The numbers of adhered cells were calculated to 1 mm² and presented as mean ± standard deviations. Statistical significance was proved with Student's t-test.

3.3.2 Confocal laser scanning microscopy

Confocal microscopy is a technique for obtaining high resolution scans of optical slices through specimen without having to cut the specimen mechanically.

Due to the precise lenses and the confocal way of gathering backscattered light, confocal microscopes have a higher in-depth resolution than ordinary light microscopes and filter out most of the photons coming from out of focus planes. Zeiss LSM-510 Meta Confocal Microscope System equipped with an Argon laser (458, 488, 514 nm excitation), Diode Pumped Solid State (DPSS) laser (561 nm), Diode 405-30 laser (405 nm), and Helium-Neon Laser (633 nm excitation) was used.

DAPI fluorescence was excited at 405 nm with Diode 405-30 laser, and detected through a 420–480-nm band-pass filter; pinhole 90 μm . Cy2, Oregon Green, GFP and YFP fluorescence was excited at 488 nm with Argon laser, and detected through a 518–550-nm band-pass filter; pinhole 96 μm . Cy3 fluorescence was excited at 561 nm with DPSS laser, detected through long pass filters at 575 nm; pinhole 78 μm . To improve the signal to noise ratio the mode of averaging of 4 lines per frame was chosen. LSM Image Browser software was used for image export to TIF-files.

3.3.3 Scanning electron microscopy

To investigate surface topography scanning electron microscopy (SEM) was used. In a SEM, a focused electron beam is scanned along the sample, and detection of secondary or backscattered electrons allowed to image probe surface.

Here, the SEM observations were performed with high-resolution (1.5 nm) microscope LEO 1530 Gemini equipped with FEG. Imaging with secondary electrons provided investigation of gold samples without any additional coating of the surface.

3.3.4 Contact angle measurement

For the contact angle measurements drops of 50 μl of the peptide solution were placed on 4 different amino functionalised cover glasses and were removed after 0.25, 1, 2 and 4 hours by rinsing the samples with bidistilled water. This experiment was performed with peptide concentrations of 0.625 mg/ml, 2.5 mg/ml and 10 mg/ml. Contact angles investigations were carried out with bidistilled water using an OCA 20 from data physics (Germany) operated in the sessile drop method. The drop volume was 0.5 μl .

3.3.5 X-ray photoelectron spectroscopy (XPS) measurement

XPS experiments were performed in an ESCALAB-5 electron spectrometer (VG Scientific, East Grinstead, UK). The photoelectrons were excited by means of non-monochromatized MgK α radiation (200 W) in a sample area of about 50 mm². The kinetic energy of the electrons was measured by a 150° hemispherical energy analyzer operated in the constant analyzer energy mode (CAE) using 20 eV pass energy for elemental spectra. The photoelectron take-off angle was set to 45° with respect to the sample normal. The binding energy scale was calibrated using a value of 285.0 eV for the adventitious C 1s photoelectron peak and controlled by means of the well-known peaks of metallic Cu, Ag, and Au, respectively.

3.4 Molecular biology methods

3.4.1 Isolation of RNA

Total RNA was isolated from cultured mouse 3T3 Swiss fibroblasts. A confluent cell monolayer of a 50 ml cultured flask was scratched from the bottom and suspended in 1 ml of PBS. After 5 minutes centrifugation at 900 rpm the cell pellet was immediately homogenized in RNAtidy G. RNAtidy G is a solution of phenol and guanidine isothiocyanate, and dissolves cell components while maintaining the RNA integrity. The cell suspension was homogenized in 500 μ l RNAtidy with ultrasonic homogenizer IKA Ultra Turrax®. For removal of proteins, 100 μ l chloroform was added and vigorously agitated by hand for 15 sec. After 10 000 rpm centrifugation for 15 minutes at 4°C, the upper aqueous phase containing the RNA was transferred into a sterile tube. A second chloroform extraction was performed and RNA was precipitated at -80°C for at least 1h with two volumes of absolute ethanol and 1/10th volume 3M sodium acetate solution. Following 30 minutes centrifugation at 10,000 rpm the RNA pellet was washed with 70% ethanol, dried at RT re-dissolved in an appropriate volume of DEPC water.

3.4.2 Quantitative and qualitative determination of total RNA

Following the RNA elution, RNA was diluted 1:1 with bromophenol blue loading buffer for gelelectrophoresis and 1:10 with DEPEC water for spectrophotometry (see sections 3.4.5 and 3.4.6).

3.4.3 Complementary DNA synthesis

The transcription is the process of overwriting genomic DNA in mRNA. With reverse transcriptase it is possible to transcribe mRNA in complementary DNA (cDNA) *in vitro*. In this study, for cDNA synthesis into a microcentrifuge tube 1 µg of total RNA and 1 µl random hexamer primers (0.5 µg/µl) were added. After mixing by pipetting, the mixture was heated at 70°C for 10 minutes and quickly chilled on ice to allow random hexamer primers to bind to mRNA. The sample was briefly centrifuged and 4 µl of 5x first strand buffer, 2 µl 10 mM DTT, 1 µl 10 mM dNTP mix and 1U RNase inhibitor dithiothreitol were added to the sample. After gently mixing, 0.5 µl (100 U) of reverse transcriptase was added. The reaction was incubated at 42°C for 50 minutes then inactivated by heating at 70°C for 15 minutes and stored at -70°C or used directly for PCR (see section 3.4.4). To control specificity of reverse transcription, -RT was also performed using all the other components together with DEPC water instead of the reverse transcriptase.

3.4.4 Polymerase chain reaction (PCR)

PCR is a process of exponential amplification of DNA material using artificial oligonucleotides (Meuer et al., 2001). There are three general steps in PCR: melting of DNA template, annealing of primers, and extension. The DNA amplification proceeds by temperature cycling of the sample. To control temperature for each step a Thermocycler could be used.

At the melting step, by heating at 95°C DNA template splits into two single-stranded molecules. Decreasing of the temperature on the melting step allows small oligonucleotides that serve as primers to associate with the single stranded DNA molecules. The annealing temperature depends on oligonucleotides contents and could be chosen as 3-4°C lower than $T_m = 2^\circ\text{C} \times (\Sigma(\text{A+T})) + 4^\circ\text{C} \times (\Sigma(\text{G+C}))$. On the extension (amplification) step, beginning with primers heat stable Taq DNA polymerase copies the complete DNA. The optimum temperature for amplification normally is 72°C.

In this work PCR was used to check the expression of integrin genes by mouse 3T3 Swiss fibroblasts. To a final volume of 50 µl, reaction buffer (5 x Green GoTag FlexiBuffer), nucleotide mix (2.5 mM each), primers (25 µM each), 10 ng DNA template, 1.5 U GoTaq as polymerase, and water was added. PCR run in the cycler; the cycler program was designed according request for every primers pair.

Table1. Primers used for RT-PCR assays.

Integrin subunit	Forward primer	Seq. location	Reverse primer	Seq. location	Fragm. size (bp)	Annealing T(°C)	Num. of cycles
α IIb	5'-TGGTGGTGGC AGCAGAAGAA-3'	2397 - 2417	5'-GTAGGGAGG AGACG TTGAAC-3'	2898 - 2918	521	55 °C	36
α V	5'-GTGGGAGACT TCAATGGTGA C-3'	990 - 1010	5'-CTGTCTACATCT GTA GCTCCC -3'	1536 - 1557	567	55 °C	36
α 5	5'-AAAAGAAACT TCAGTGGGCC-3'	3121 - 3141	5'-GAGTCTGAGAT CAG GAGGACT -3'	3341 - 3362	241	55 °C	34
β 1	5'-GCTAT CGTGCATGTT GTGGAG -3'	2316 - 2337	5'-GTTATAATCC ATGC CAGGGAC-3'	2737 - 2758	442	55 °C	36
β 3	5'-GAAGGAGAAC CTGCTGAAGG-3'	3228 - 3248	5'-GGTTGC TAGT AAGC TTGCGC-3'	3552 - 3572	344	55 °C	36
β 5	5'-GAGGATC TAC GGACCTT TCTG-3'	1824 - 1845	5'-CACCACCA GTG CAAAGATGAG-3'	2174 - 2195	371	55°C	32
β 6	5'-GGCTAAAGT GGAG CTGTCAG -3'	738 - 758	5'-CTGCTGTCTGC AA GGAGAAG-3'	1108 - 1128	390	55°C	32
β 8	5'-CAAAGGACAG TGTGCGGAAG-3'	1425 - 1445	5'-GTTGACACAG TGCTGTGCTG-3'	1759 - 1779	354	50°C	36
GAPDH	5'-ACCACAGTCC- ATGCCATCACT-3'		5'-GTCCACCACCC TGTTGCTGTA-3'		400	55°C	25

3.4.5 Agarose gel electrophoresis

The agarose gel electrophoresis was used for size-separation of the DNA or RNA fragments. Generally the electrophoretic mobility of DNA/RNA fragments depends on the fragment size and to a lesser extent on the conformation of the DNA/RNA. Type and concentration of agarose as well as applied voltage and electrophoresis buffer used also affects the electrophoretic mobility. Agarose gels could be used to resolve DNAs in the great range: of 50bp to 20 kbp in length. Work with smaller sized DNAs requires a relatively high (2 – 3%)

concentration of agarose gel. For the visualisation of the DNA bands ethidium bromide is used.

For separation of PCR products 300 - 600 bp length 1% agarose gel was used. The agarose was solved in 1x TAE, and heated in a microwave oven for approximately 1 minute until agarose powder was completely solved. After cooling the solution to $\sim 60^{\circ}\text{C}$, ethidium bromide was added, at final concentration 1 $\mu\text{g/ml}$. The solution was poured into a gel chamber and left to solidify at RT. Gels were electrophoresed at 80V for 40 min. The ethidium bromide bound DNAs were visualized under UV light.

Buffers and solutions:

50x TAE: 2 M Tris, 50 mM EDTA $\cdot\text{Na}_2\text{x} 2\text{H}_2\text{O}$, 1 M acetic acid, pH 8.3.

1% ethidium bromide stock solution: working concentration 0.5 $\mu\text{g/ml}$

10 x loading buffer: 57% glycerol, 100 mM Tris pH 8.0, 10 mM EDTA $\cdot\text{Na}_2\text{x} 2\text{H}_2\text{O}$, $\sim 0.001\%$ bromophenol blue.

3.4.6 Photometry

For quantification of RNA and DNA photometry was used. Due to their characteristics absorption maximum at 260 nm, nucleic acids can be photometrically quantified. Contamination with proteins which also have an absorption maximum at ultraviolet wavelengths, $\lambda = 280 \text{ nm}$, can falsify the result. Therefore, the ratio of absorption at both 260 nm to absorption at 280 nm greater than 1.9 for DNA, or greater than 1.8 for RNA is indicative of samples that are free of these contaminants. For uncontaminated nucleic acid solutions the Lambert-Beer law is applicable: 50 $\mu\text{g/ml}$ double-stranded DNA have an OD_{260} of 1.0; 40 $\mu\text{g/ml}$ single-stranded DNA or RNA have an OD_{260} of 1.0.

4 RESULTS

4.1 Biofunctionalisation of surfaces

4.1.1 RGD-peptides absorption vs. coupling

To create a surface with an optimal orientation of the peptide synthetic RGD-peptides used for surface biofunctionalisation in this study have an isothiocyanate anchor that is able to react with NH_2 groups of surfaces (Fig. 15). The necessary NH_2 -functionalisation of the surfaces was performed by liquid and gas phase amino-silanisation of glass or SiO_2 slides with APTES (see section 3.1.1).

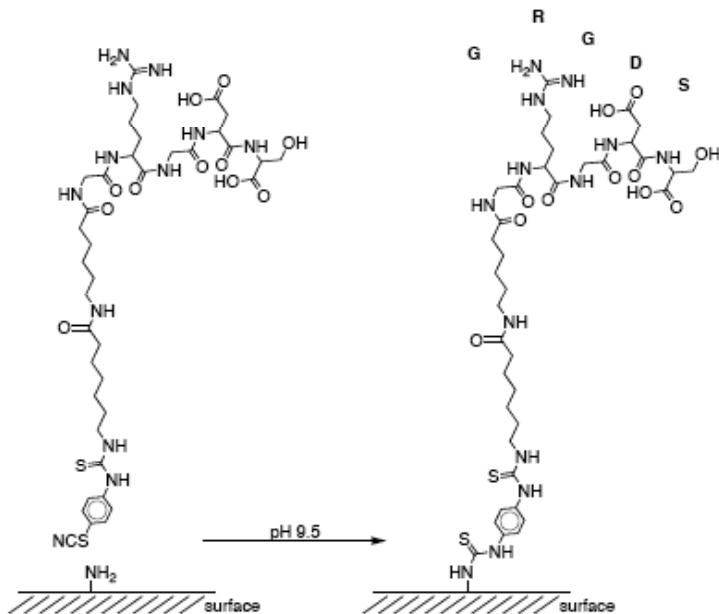


Fig. 15. Coupling of the linear GRGDS peptide to a surface amino group via an isothiocyanate anchor.

To investigate the behaviour of cells on the absorbed RGD-peptide we incubated linear GRGDS dissolved in PBS at pH 7.4 in a 1 mg/ml concentration on the plastic surfaces of μ -slide wells (Ibidi). The solution of commercial peptide GRGDS (Bachem) that has neither Ahx spacer nor isothiocyanate group was incubated in μ -slide wells at the same conditions. Fig. 16A and 16B show the differences in behaviour of mouse 3T3 Swiss fibroblasts on both peptides. The cells are fully spread on the absorbed GRGDS that was synthesised in the laboratory of Prof. Dr. Kessler while they spread to a less extent on the commercial peptide GRGDS (Bachem).

The competitive binding assay proved the specificity of RGD-recognition of surface absorbed GRGDS by the cells. When present in the cell assay medium at a concentration of 1.5 mg/ml

soluble GRGDS completely prevented spreading of fibroblasts on the surface; only round cells were found after 1 h of incubation of cell suspension in μ -slide well (Fig. 16C).

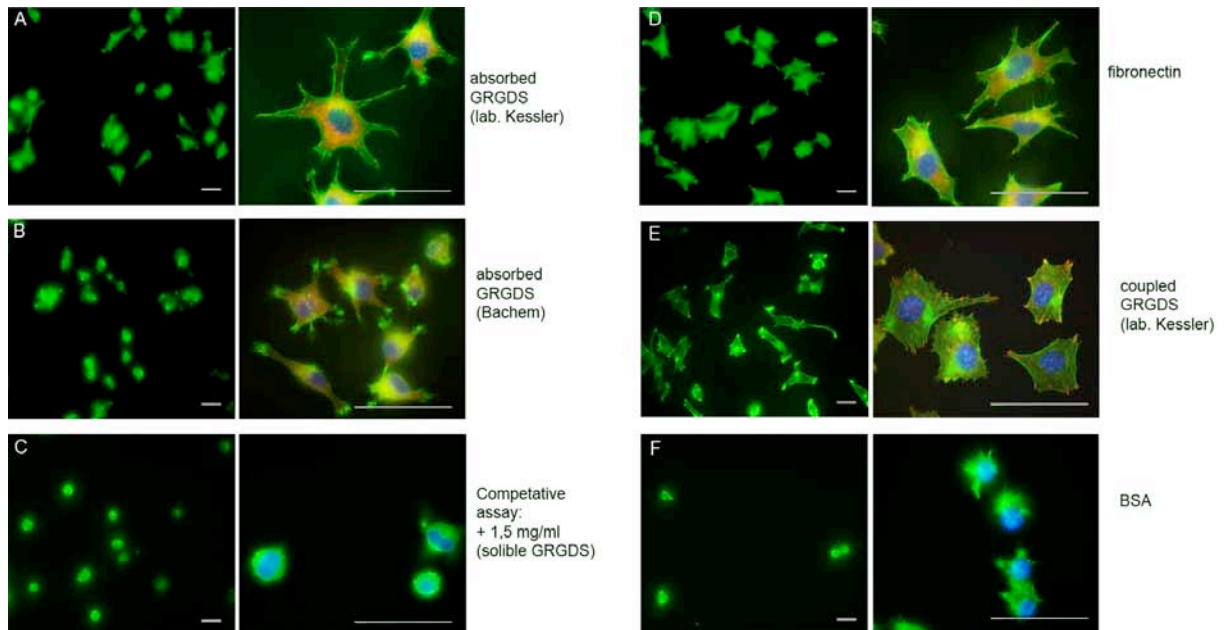


Fig. 16. Mouse 3T3 Swiss fibroblasts on the functionalised surfaces. The cells are fully spread on the absorbed GRGDS that was synthesised in laboratory of Prof. Dr. Kessler (A) and less extended spread on the commercial peptide GRGDS (Bachem) (B). Soluble GRGDS completely prevented cell spreading on the absorbed GRGDS from Kesslers Laboratory (C). The fibroblasts are fully spread on fibronectin (D) and coupled GRGDS (E), failing the spreading on pure BSA (F). The cells were stained for filamentous actin (green) and paxillin (red); nuclei were stained with DAPI (blue). Bars: 50 μ m.

Fig. 16D and 16E illustrate the spread morphology of 3T3 Swiss fibroblasts on the fibronectin layer and covalent couplings to the surface GRGDS peptide. On the both surfaces the fibroblasts demonstrate spread multi-polar cell shape and formed mature focal adhesions that were visualised with anti-paxillin staining.

To prevent unspecific adhesion by charge interactions samples were incubated with 1% pure BSA for 30 minutes before cells were seeded onto the surfaces. Fig. 16F shows the inert character of BSA to cells. The fibroblasts did not spread on BSA alone. Only few round cells were found attached on BSA extending very short protrusions.

4.1.2 Development of coupling conditions

To prepare a basic pH solution necessary for the reaction of peptide isothiocyanate groups with NH_2 groups of surfaces the lyophilized peptides after dissolution in DMSO at 4 mg/ml were diluted with 100 mM Na_2HPO_4 pH 9.5 to the desired concentration. The necessary

duration for coupling and most efficient peptide concentration was determined by contact angle measurement and cell adhesion assays. But first, the requirement of the NH_2 -group was tested by comparing untreated glass and amino-functionalised glass slides after incubation with GRGDSP-peptide solution. In the both cases the incubation conditions were the same. The cell adhesion assay showed significant difference in the 3T3 Swiss fibroblasts recognition of these surfaces; after 1 hour of incubation the cells spread on the GRGDSP-functionalised aminosilanised glass but remained round on the untreated glass that was incubated with GRGDSP at coupling conditions (Fig. 17).

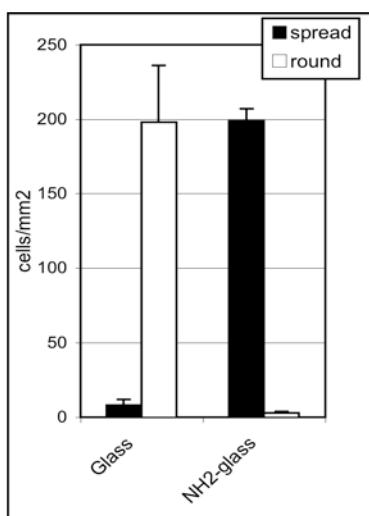


Fig. 17. Mouse 3T3 Swiss fibroblasts spread on the GRGDSP-functionalised aminosilanised glass. The cells stay round on the glass that was not treated with aminosilane but incubated with GRGDSP at coupling conditions.

4.1.2.1 Concentration of GRGDS

To define the optimal peptide concentration in the coupling solution the surfaces were functionalised with 0.004, 0.008, 0.04, 0.08, and 0.4 mg/ml GRGDS. The cell adhesion assay revealed different behaviour of mouse 3T3 Swiss fibroblasts on the tested surfaces. The calculated numbers of spread adhered cells and cells that are stay round after 1 hour of incubation were dependent on peptide concentration used during coupling procedure (Fig. 18). The typical saturation curve shows approximately equal numbers of the attached fibroblasts on the surfaces that were functionalised with 0.04, 0.08, and GRGDS. With increasing of the number of round cells the number of spread fibroblasts notably decrease at 0.008 mg/ml GRGDS; at 0.004 mg/ml GRGDS both parameters dramatically drop down demonstrating low suitability of this concentration for surface functionalisation.

The increase of the number of round cells at 0.008 mg/ml GRGDS could be explained by extension of the area that is accessible to initial cell attachment due to reduction of the areas covered by spread sells. A concentration of 0.4 mg/ml was chosen as the optimal

concentration for coupling; this concentration was 10 times higher than the minimum concentration sufficient to achieve saturation level of the tested parameters.

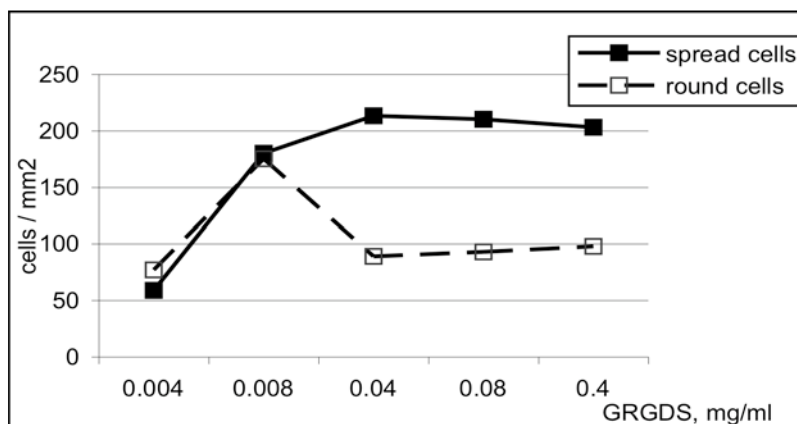


Fig. 18. 3T3 fibroblasts on the GRGDS-functionalised surface. The number of spread and round cells depends on the peptide concentration that was used during the coupling procedure.

4.1.3 RGD-peptide functionalisation of glass and SiO₂ slides

Both glass and SiO₂ slides could be functionalised with amino-groups by APTES silanisation producing NH₂-groups on the surfaces for further covalent binding of isothiocyanate-terminated peptides. For both slide types liquid and gas phase amino-silanisation was performed. Cell adhesion assay showed suitability of both substrates and allowed to compare two aminosilanisation procedures.

There were only slight differences in the numbers of spread 3T3 Swiss fibroblasts per 1 mm² of glass and SiO₂ slides that were first treated with APTES in gas or liquid phase and then functionalised with GRGDSP peptide (Fig. 19A). Fig. 19B and 19C demonstrate the similar shape of the cells on glasses that were treated in gas and in liquid phase. The images of the fibroblasts on the SiO₂ surfaces are not shown because of a high level of autofluorescence with these slides, disturbing microscopic investigations. For this reason glass as a material for development of the biofunctionalisation method has been chosen. The cell adhesion assay showed a higher number of round cells on the gas phase treated glass surfaces in comparison with the liquid phase silanised glass. This fact became a reason to prefer liquid phase silanisation for all further experiments.

4.1.4 Blocking reagents

Cell adhesion assays showed that 3T3 Swiss fibroblasts do not spread on amino-functionalised surfaces after 1 hour of incubation in cultural medium if the medium was not supplemented with FCS. Only a few cells attach to the surface, but they stay round showing the same cell shape as in the case of unspecific attachment to BSA covered plastic (Fig.

16F). Comparison of the cell attachment to untreated amino-functionalised glass and amino-functionalised glass that was covered with pure BSA (section 3.2.2), revealed only slight, not significant difference in the numbers of round attached fibroblasts (Fig. 20) that could be explained by the additional blocking effect of BSA.

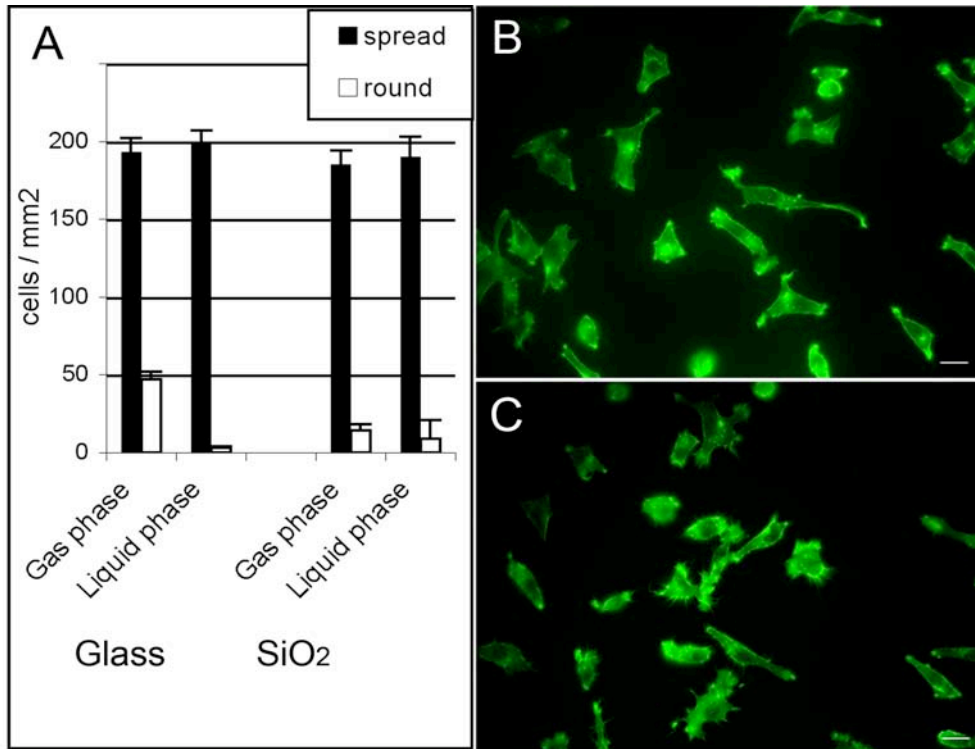


Fig. 19. Mouse 3T3 Swiss fibroblasts on the glass and SiO₂ GRGDSP-functionalised surfaces. (A) The calculated numbers of spread and round 3T3 Swiss fibroblasts per 1 mm² surface. (B) The similar cell shape on peptide-functionalised glass slides that were aminated using of gas (B) and liquid (C) aminosilanisation. Bars: 20 μm.

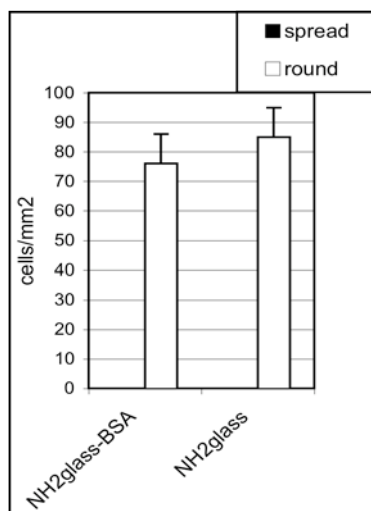


Fig. 20. Cell attachment to untreated amino-functionalised glass and amino-functionalised glass that was covered with pure BSA. The difference in the numbers of round attached fibroblasts is not significant.

4-methoxyphenylisothiocyanate (4MOPIT) was tested as a blocking reagent. NCS group of this chemical is similar to a coupling group of investigated peptides (Fig. 21). 4MOPIT should react with the surface -NH_2 groups that were not coupled with peptide more safely, preventing any possible chemical reactions on the surface other than BSA. After the 2h peptide coupling procedure followed by PBS washing, I performed incubation of the surfaces with 1 mg/ml 4MOPIT solution. To reach the final concentration 4MOPIT was dissolved firstly in DMSO at a concentration of 10 mg/ml and then diluted 10 times in 100 mM Na_2PO_4 , pH 9,5. The 4MOPIT treatment of peptide-functionalised slides was followed by 3 times washing with PBS and 2 times washing with cell cultured medium.

The cell assays showed nearly complete prevention of fibroblasts adhesion to the surface. Only a few round cells were found on the peptide-functionalised surfaces that were treated with 4MOPIT (data not shown). This complete blocking of the cell spreading demonstrated the futility of this chemical treatment as an intermediate step of the surface biofunctionalisation.

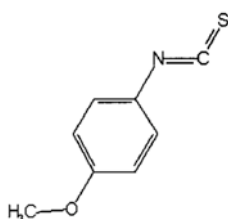


Fig. 21. Chemical formula of 4-methoxyphenyl-isothiocyanate.

4.2 Quality control of biofunctionalisation

4.2.1 X-ray photoelectron spectroscopy (XPS)

XPS measurements were performed to investigate the efficiency of peptide coupling. Fig. 22 shows results of the measurements for untreated, amino terminated, and finally peptide exposed glass surfaces. The N 1s peak at 400.2 ± 0.2 eV is attributed to -NH_2 (Gervais et al., 1988) and is a suitable indicator for the peptide uptake. Compared to simply aminated surfaces the N/C ratio increases by a factor of about 5 after peptide exposure, which justifies the desired immobilization of the peptide.

4.2.2 Contact angle measurement

The measurement of a water drop contact angle on the surface is used to estimate the surface hydrophilic properties. Amino functionalised glass substrates were investigated,

which treated with peptide solutions for different incubation times. In addition, three different concentrations of peptide solution were tested (Fig. 23) - 0.625, 2.5 and 10 mg/ml. For these peptide concentrations the contact angle of the water drops decreases with increasing exposure time of the substrate to the peptide solution.

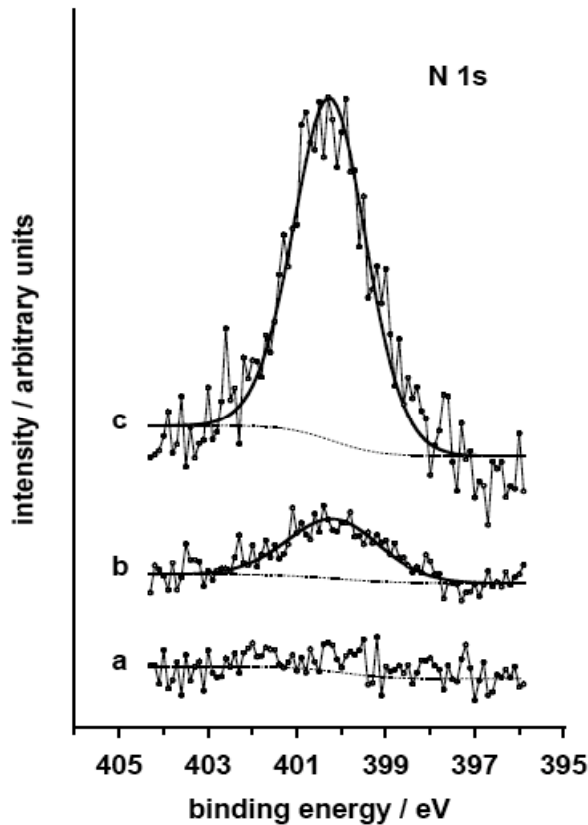


Fig. 22. XPS analysis.

Deconvolution of N 1s XPS spectra of a glass reference sample (a), an amino terminated glass surface (b), and an amino terminated glass surface after peptide exposure (c). The intensities are normalized to the overall carbon content.

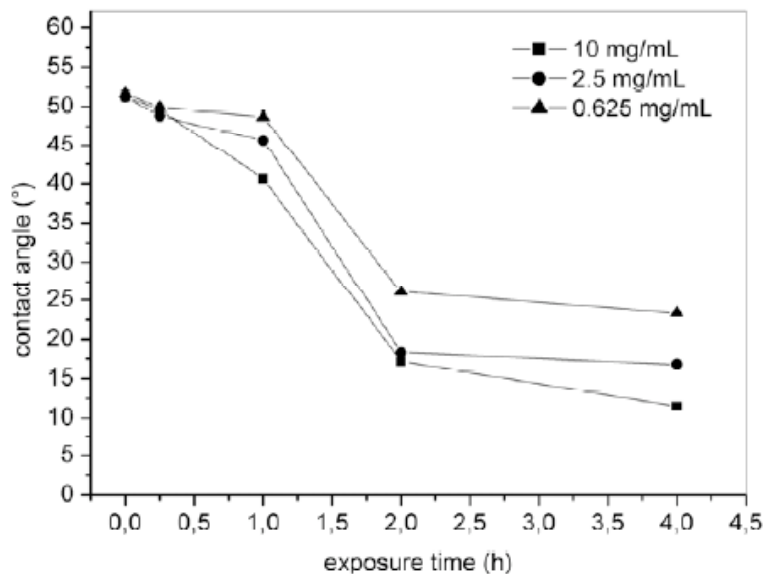


Fig. 23. Contact angle measurements. The graph shows the development of contact angles of water drops (0.5 μ l) on aminated glass substrates treated with peptide solutions of different concentrations for different times.

As the polarity of the peptide is higher compared to that of the amino functionalised glass substrate, this decrease in the contact angle can be explained by an increasing number of peptide molecules coupled to the amino groups. It was obvious that the contact angle decreased rapidly between one and two hours irrespective of the peptide concentration while the contact angle decrease after further two hours was negligible. This observation can be interpreted as a time dependent reaction between the peptide and the amino functions.

This tendency was reproduced for all used peptide concentrations, showing decreasing of contact angle with increasing concentration of the peptide, but this difference observed with different peptide concentrations was not significant. The final contact angle reached with peptide solutions of 0.625 mg/ml was 23°, while 2.5 mg/ml and 10 mg/ml showed saturation at contact angles of 17° and 12° respectively.

4.2.3 Rhodamine-GRGDS

Rhodamine coupled GRGDS peptide (rhodamine-GRGDS) was synthesised to detect peptide on the surface. Aminosilanized glass that was treated with rhodamine-GRGDS at coupling conditions was investigated on a fluorescent microscope. In comparison with untreated aminosilanised glass the rhodamine-GRGDS coupled samples showed high fluorescence in the red spectrum (Fig. 24).

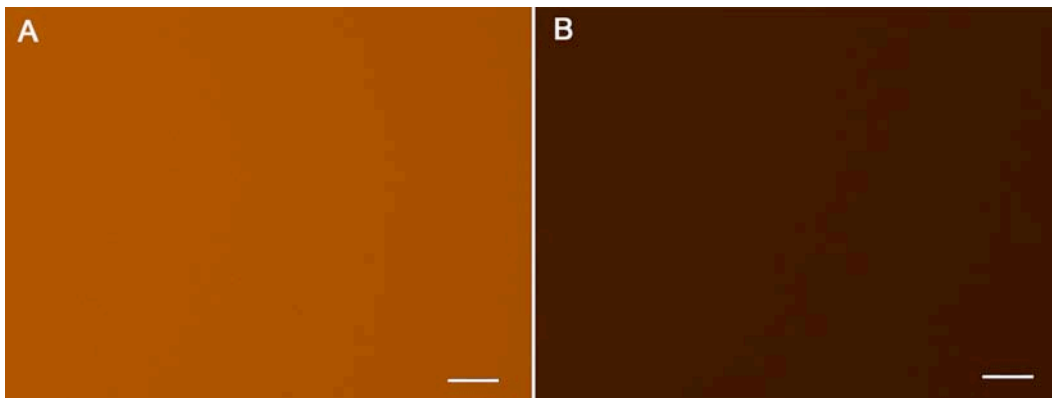


Fig. 24. Fluorescence on the red channel of light fluorescent microscope of aminosilanised glass. The glass was treated with rhodamine-GRGDS (A) and untreated (B). Bars: 20 μ m.

4.3 Cell adhesion assay as readout system for biocompatibility

4.3.1 Mouse 3T3 Swiss fibroblasts express RGD-binding integrins

RT-PCR analysis revealed the pattern of RGD-binding integrins expressed by mouse fibroblasts 3T3 Swiss fibroblasts. Except for the α 8-subunit all integrin receptors which have

been characterized to recognize the RGD peptide (Hynes, 2002) are detected. The most prominent β -subunit was $\beta 6$ followed by $\beta 3$ and $\beta 5$ while $\alpha 5$ showed strongest expression among the α subunits (Fig. 25). GAPDH served as internal standard.



Fig. 25. RT-PCR analysis revealed the RGD-binding integrins expressed by mouse 3T3 Swiss fibroblasts.

4.3.2 Fibroblasts adhesion on biofunctionalised surfaces in the presence and absence of FCS

The influence of fetal calf serum (FCS) in the culture medium on the adhesion of mouse 3T3 Swiss fibroblasts onto RGD-functionalised glass slides was also tested. In presence and absence of FCS cells adhered and spread onto investigating surfaces. However, similar tests of aminosilanised glass that were not treated with RGD peptides showed that the cells still spread onto the NH_2 -glass when assays were performed in the presence of FCS (Fig. 26), which they did not in the medium without FCS (Fig. 17). To explain these results it is proposed that proteins contained in FCS absorb to NH_2 -glass during incubation of the cell suspension and promote adhesion of fibroblasts on the formed layer. Thus, cell spreading onto surfaces in FCS-containing medium is not only the result of specific recognition of RGD-peptides, and cannot be used as characteristics of the surface biofunctionalisation.

4.3.3 Trypsin inhibitors

For cell adhesion assays I used trypsin to re-suspend cells adherent to the cell culture dishes. This standard procedure during the process of harvesting cells stipulate for further deactivation of trypsin by the use of FCS as medium supplement. The cell adhesion assays performed in the absence of FCS required a trypsin inhibiting agent. Two candidates – trypsin inhibitor from soybean (STI) and phenylmethanesulfonyl fluoride (PMSF) were tested.

Both inhibitors were added in suspension of detached from cultured dishes cells in cell-cultured medium without FCS. The adding of inhibitor was followed by 3 minutes

centrifugation at 900 rpm, discard of medium and repeated cells re-suspension with further achievement of standard used for cell adhesion assays concentration 1.4×10^5 cells/ml.

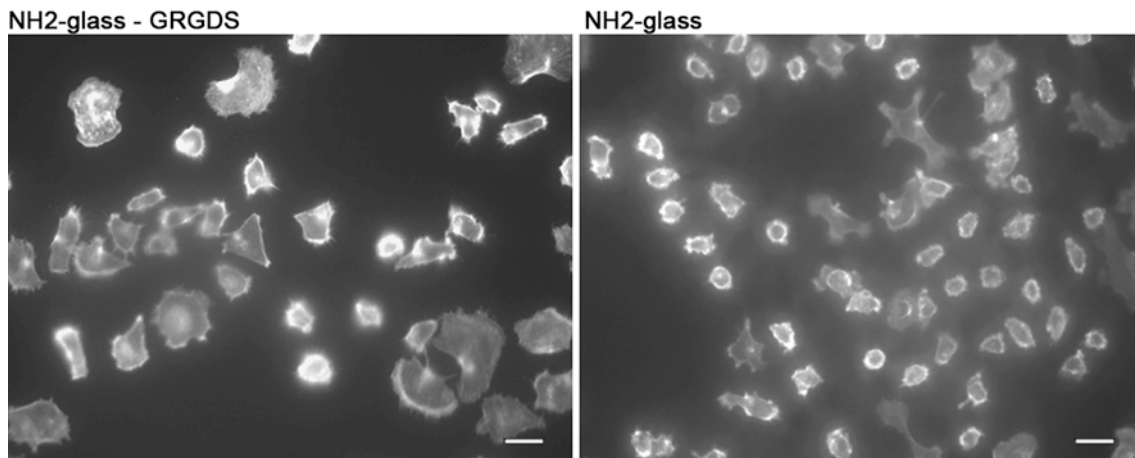


Fig. 26. Mouse 3T3 Swiss fibroblasts in the supplemented with FCS medium. The cells spread on both the RGD-functionalised and RGD-untreated aminosilanised glass. The cells were visualised by actin-cytoskeleton staining with Oregon Green® 488-phalloidin. Bars: 20 μ m.

Development of the method was performed with fibronectin coated polystyrene slides. Treated with trypsin inhibitor the mouse 3T3 Swiss fibroblasts suspension was incubated with the slides for 1 hour at 37°C. The cells adhered to the fibronectin coated surface and spread (Fig. 16D). The obvious differences in cell adhesion pattern for these two methods – with STI and with PMSF – were not found. However the addition in cell suspension of the stock solution PMSF in ethanol caused the destruction of some cells. Taking into consideration the possible influence of intracellular proteins release by cell damaging on the results of surface tests, we applied STI as a trypsin inhibitor for further experiments.

4.3.4 Cell adhesion: duration and classification

The time necessary for initial cell attachment to the surfaces was shown to be around 10-12 minutes (Cohen et al., 2006). The initial substrate recognition is followed by cell spreading. The time sufficient for full spreading is dependent upon cell type and suitability of the substrate. I have found that mouse 3T3 Swiss fibroblasts reach the full spreading onto fibronectin layers as well as onto RGD-functionalised surfaces within 1 hour. After 1-hour incubation at cell culturing conditions the fibroblasts formed mature focal adhesions in the sites of attachment to the substrate; the cytoskeleton staining reveals formed lamellipodia and actin stress fibres in contact with the focal adhesions.

For all cell assays a 1 hour adhesion period was used, unless stated differently. The number of fully spread cells was counted and noted as number of “spread cells”. The cells that retained a round shape, not spreading at all, were noted as “round cells”. The cells that were not round, formed very short lamellipodia and filopodia but no focal adhesions, were termed “flattened” (Fig. 27).

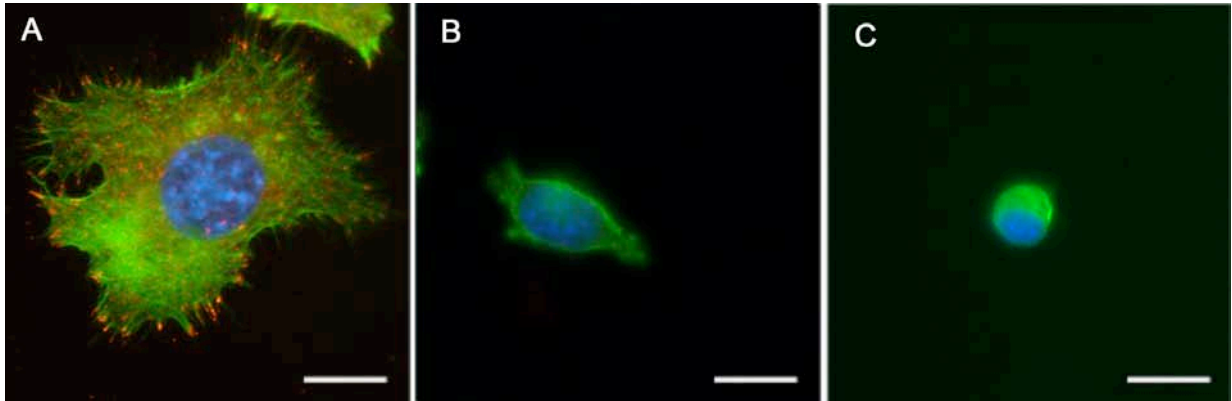


Fig. 27. Fibroblasts on the surface: spread, flattened, and round. (A) Fully spread mouse 3T3 Swiss fibroblasts on uniform GRGDS-functionalised surface. (B) Flattened cell attached to c(-R β ADfK-)-surface. (C) Round attached to aminosilanised glass. Phospho-paxillin staining for focal adhesions in red; actin filament labelling with phalloidin in green; staining of nuclei with DAPI in blue. Bars: 10 μ m.

4.4 Comparison of cell adhesion behaviour to different peptides

4.4.1 Mouse fibroblasts spread on the RGD-functionalised surfaces

After establishment of optimal peptide conjugation conditions and adhesion assays different linear and cyclic peptides were compared. Mouse 3T3 Swiss fibroblasts spread on RGD-functionalised surfaces recognising linear peptides - GRGDS and GRGDSP - as well as cyclic ones - c(-RGDfKG-) and c(-RGDfK-) (Fig. 28).

For statistical evaluation spread cells and attached round cells were counted. Linear and cyclic RGD containing peptides showed similar abilities to induce cell spreading (Fig. 29). In contrast, on the untreated with RGD-peptides surfaces only round cells were found.

4.4.2 Fibroblast FA formation depends on used RGD-peptide

The spreading behaviours on the different linear and cyclic peptides were compared with regards to focal adhesions (FAs). To visualise the FAs the staining of paxillin, phospho-

paxillin, and vinculin was used. The proteins involved in FA formation aggregate into clusters that can be detected by immunohistochemistry.

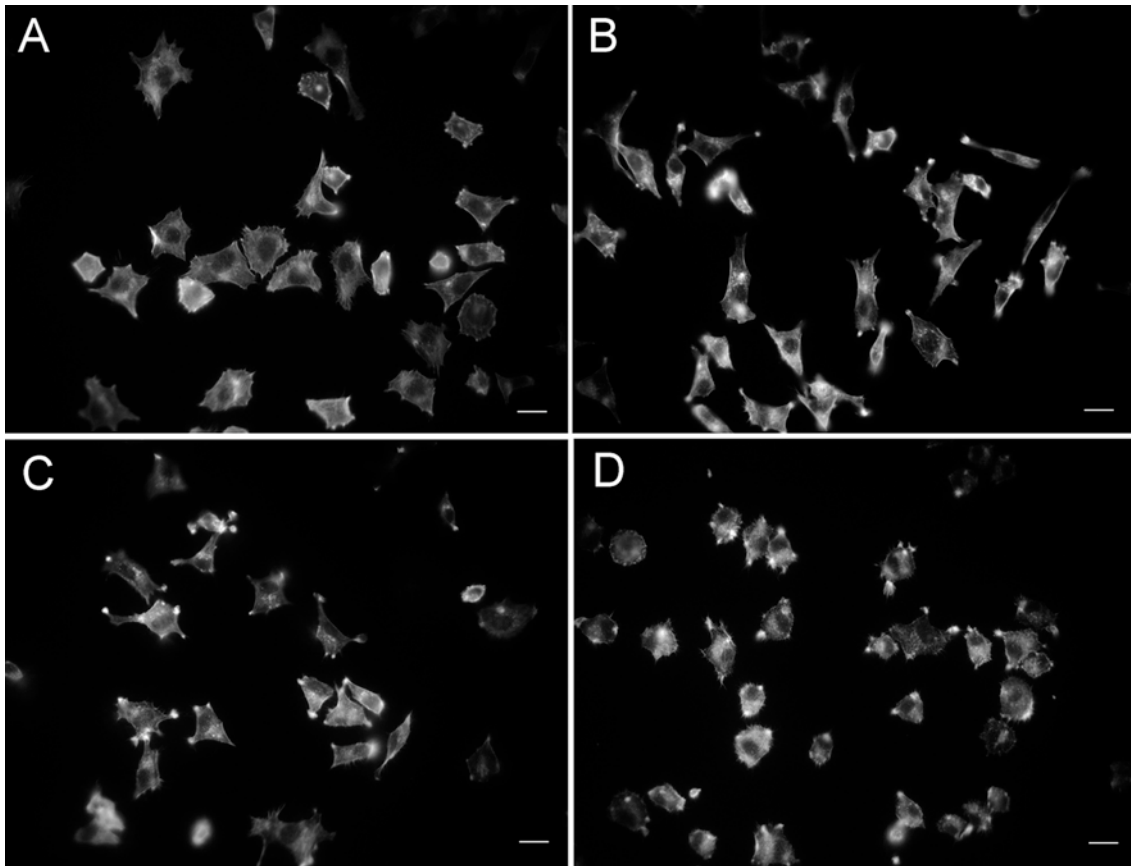


Fig. 28. Cell spreading behaviour on different RDG-containing peptides. Linear peptides GRGDS (A) and GRGDSP (B); cyclic peptides c(-RGDfKG-) (C) and c(-RGDfK-)(D). Mouse 3T3 Swiss fibroblasts are visualised with Oregon Green® 488 phalloidin staining. Scale bars 10 μ m.

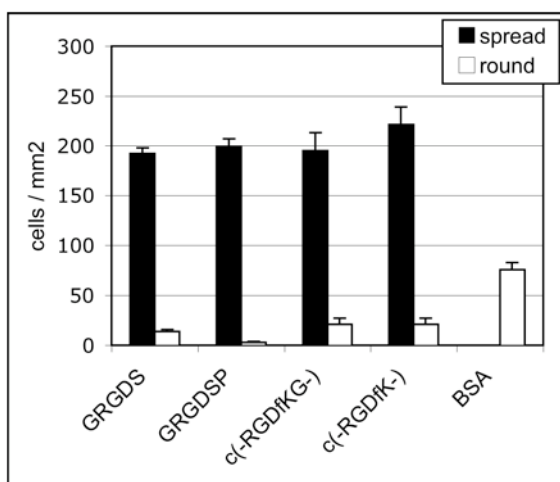


Fig. 29. Linear and cyclic peptides showed similar abilities to induce fibroblasts spreading. Linear peptides: GRGDS and GRGDSP, cyclic peptides: c(-RGDfKG-) and c(-RGDfK-). The cells did not spread on RGD-unfunctionalised aminosilanised glass covered only with BSA.

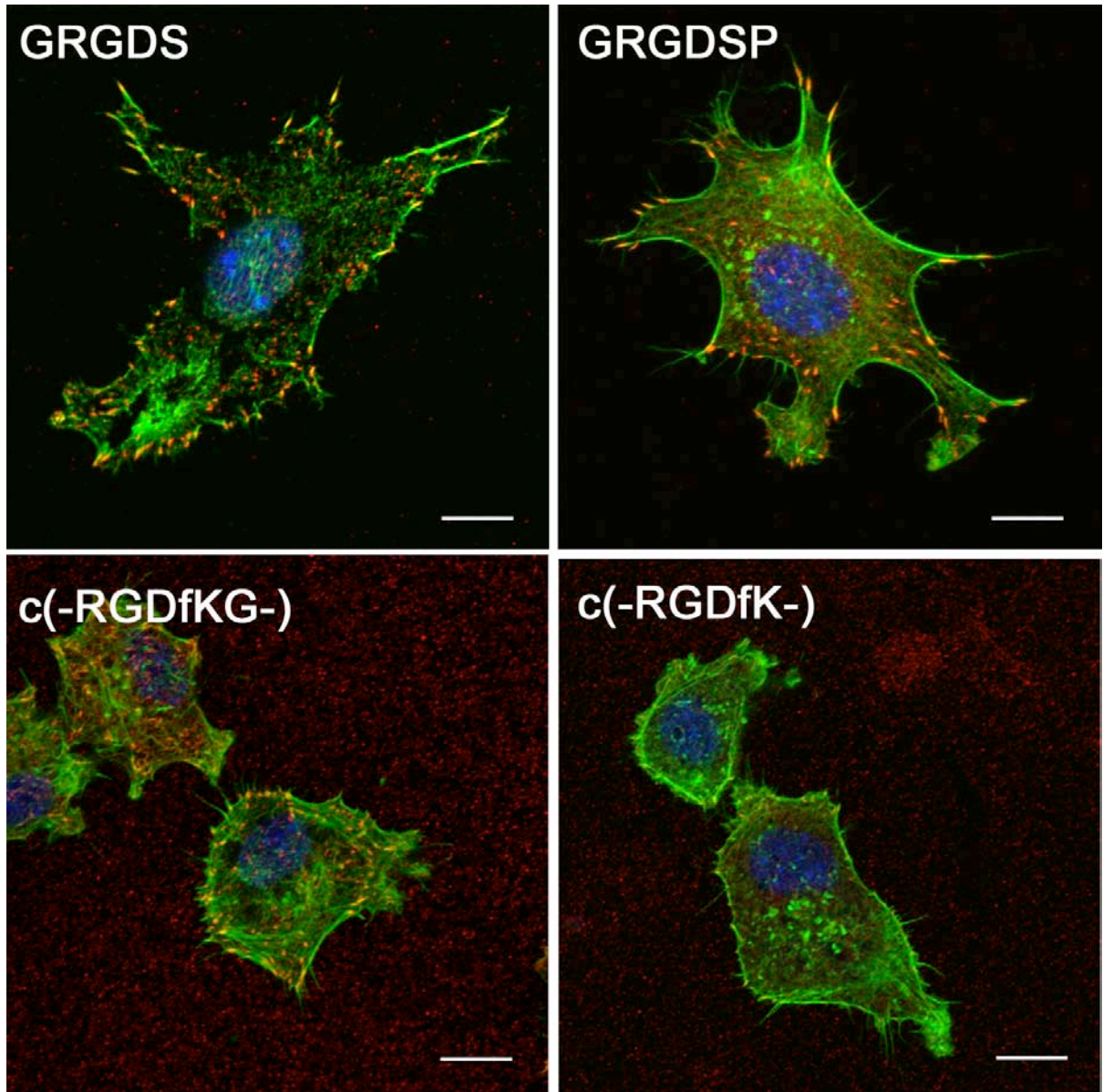


Fig. 30. Focal adhesion formation in mouse fibroblasts on different RGD-containing peptides visualized by vinculin staining. Confocal laser microscope. Vinculin staining for focal adhesions in red, actin filament labelling with phalloidin in green, staining of nuclei with DAPI in blue. Bars: 10 μ m.

Fig. 30 illustrates differences in the visualised with the vinculin FAs patterns of fibroblasts that spread on different peptides. Cells on both linear peptides and the cyclic peptide c(-RGDfKG-) formed focal adhesions at cell protrusions. Focal adhesions were predominantly found at the periphery of the cells, and at the end of F-actin bundles indicating properly spread cells. In contrast, focal adhesions were rarely detected in cells spread on the cyclo(-RGDfK-).

Paxillin and phosphopaxillin staining has demonstrated similar difference in FAs formations for 3T3 Swiss fibroblasts on the liner and cyclic peptides (Fig. 31).

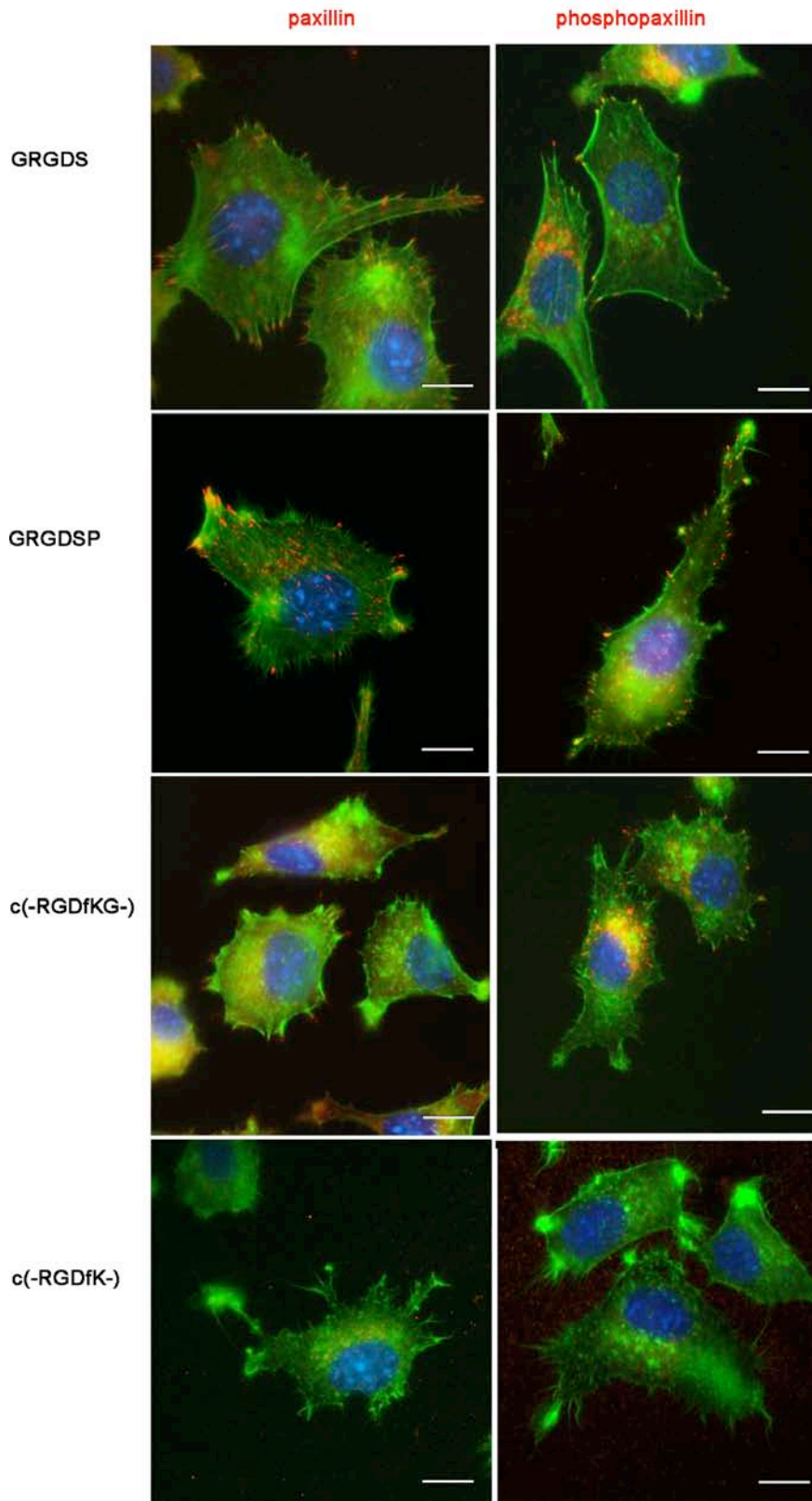


Fig. 31. Cell spreading behaviour on different RDG-containing peptides. Linear peptides GRGDS and GRGDSP; cyclic peptides c(-RGDfKG-) and c(-RGDfK-). Paxillin and phosphopaxillin staining for focal adhesions in red, actin filament labeling with phalloidin in green, staining of nuclei with DAPI in blue. Scale bars 10 μ m.

4.4.3 Counting of FAs allows to estimate cell spreading and the surface biocompatibility

To estimate cell spreading on different substrates the focal adhesions per cell were counted. Quite similar FAs numbers were found in cells on both linear peptides by vinculin or paxillin staining (Fig. 32), whereas less than half of them were detected in cells on the cyclic peptides. The difference between both cyclic peptides was most prominent in paxillin immunostaining because only few focal adhesions were formed per cell on c(-RGDfK-).

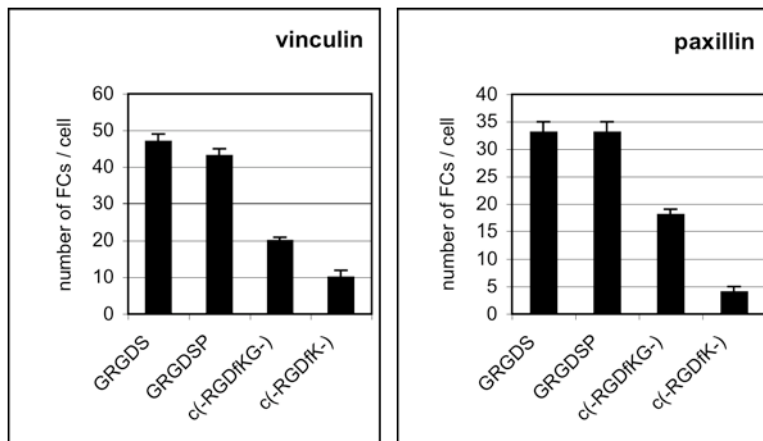


Fig. 32. Statistical evaluation of focal adhesion formation per cell on different substrates. Focal adhesions visualized by vinculin and paxillin staining. Statistical significant difference between linear and cyclic peptides, $p < 0.01$ (student t test).

The difference in adhesion efficiency was dramatic when the result was related to the total number of focal adhesion forming cells. About 95% of the cells plated on the linear peptides formed focal adhesions while 70% of the cells on c(-RGDfKG-) and only 20% of those on c(-RGDfK-) were positive for vinculin or paxillin.

4.4.4 The fibroblast FA formation on Nc(-RGDfK-)

The high background and the reduced numbers of FAs observed in adhered to the cyclic peptides cells as well as the spreading behaviour of the cells on the control peptide c(-R β ADfK-) led to a critical reconsidering of the peptide synthesis. The synthesis of the functionalised cyclic peptides was modified in order to be able to do the cyclization step and the coupling of the spacer and the isothiocyanate anchor on solid phase and on that way avoid possible undesirable reactions.

The peptide synthesised according the changed synthesis procedure - Nc(-RGDfK-) - was tested. Much better results were obtained as documented in Fig. 33 and 34. Vinculin, paxillin and phosphopaxillin staining revealed FAs in mouse 3T3 fibroblasts spread on Nc(-RGDfK-)-

functionalised surface; level of background staining was obviously lower than in the case of c(-RGDfK-) (Fig. 30, 31 and 33). Statistical evaluation showed 5 times higher number of paxillin-stained FAs in cells on Nc(-RGDfK-) than c(-RGDfK-) (Fig. 32 and 34). Number of spread on Nc(-RGDfK-) was similar to other RGD-peptides.

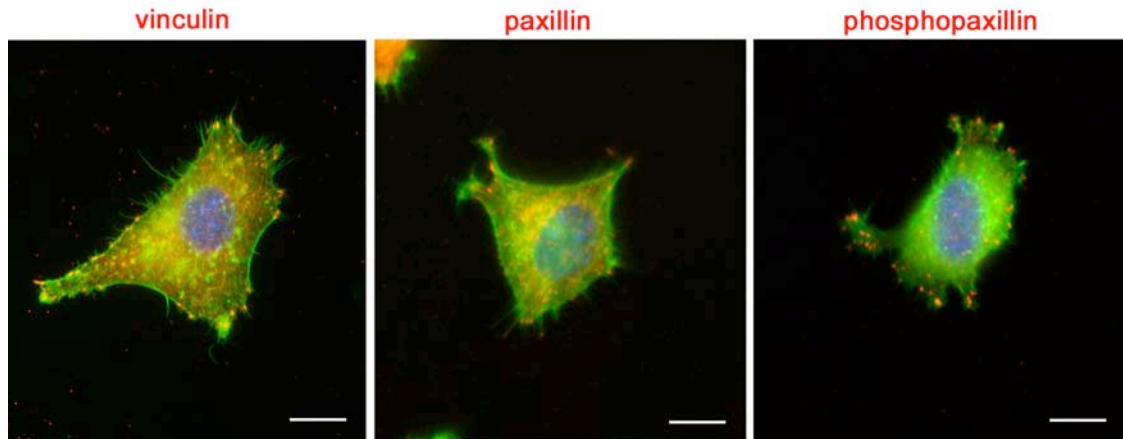


Fig. 33. Cell spreading behavior on Nc(-RGDfK-). Vinculin, paxillin and phosphopaxillin staining for focal adhesions in red, actin filament labeling with Oregon Green®-phalloidin in green, staining of nuclei with DAPI in blue. Scale bars 10 µm.

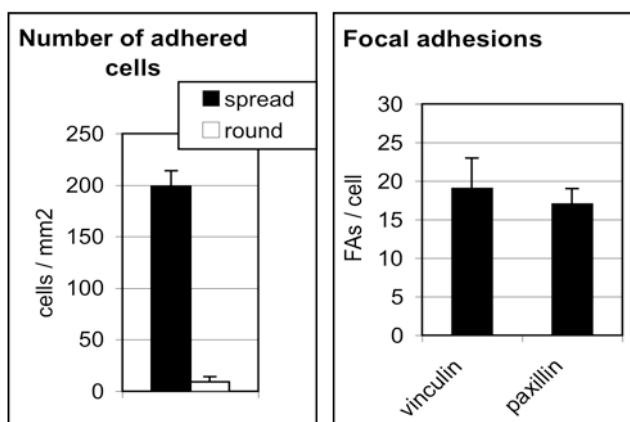


Fig. 34. Cell spreading behaviour on c(-RGDfK-); statistical evaluation. Number of spread and round 3T3 fibroblasts was counted. Focal adhesions were visualised by vinculin and paxillin staining.

4.5 Mouse 3T3 Swiss fibroblasts spread on fibronectin coating

To evaluate the biocompatibility of the new developed RGDS surface conjugation method the spreading behaviour of mouse 3T3 Swiss fibroblasts on fibronectin was investigated. The fibronectin coating was created by absorbed to plastic surface. Oregon Green® 488 phalloidin treatment revealed actin filaments of the fully spread cells; immunostaining of paxillin, vinculin and phosphopaxillin visualised mature FAs on the ends of actin stress fibres (Fig. 35). Diagram on the Fig. 35 shows average number of FAs per cell marked with vinculin and paxillin, which are in the range observed on linear peptides (Fig. 32).

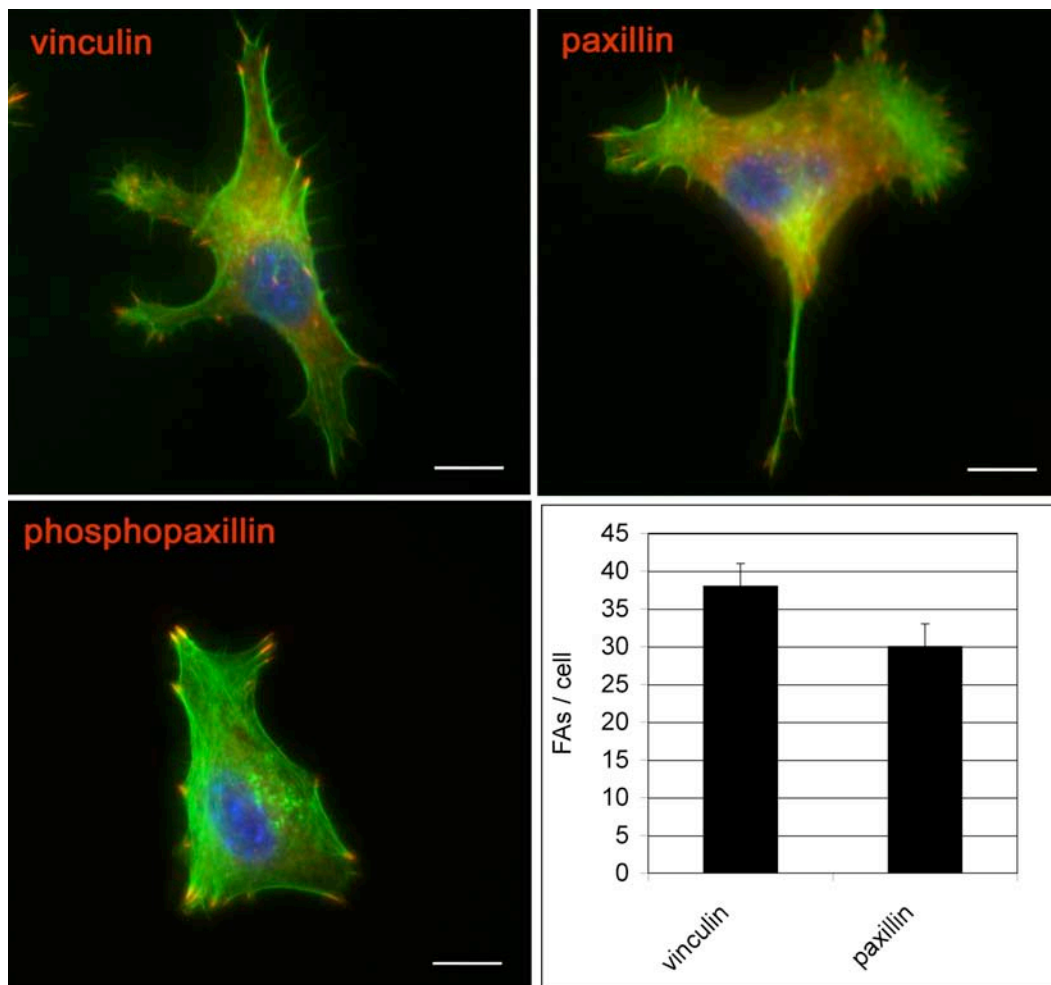


Fig. 35. Mouse 3T3 Swiss fibroblasts spread on fibronectin coating. Vinculin, paxillin and phosphopaxillin staining for focal adhesions in red, actin filament labeling with phalloidin in green, staining of nuclei with DAPI in blue. Scale bars 10 μ m.

4.6 Cell spreading behaviour of different cell lines spread on RGD-functionalised surface

4.6.1 *Xenopus* tadpole cells

To test applicability of the method of aminosilanised glass functionalisation with isothiocyanate terminated RGD peptides different cell lines were compared. *Xenopus* tadpole fibroblasts (XTC) showed extensive spreading behaviour on a GRGDS-surface (Fig. 36A). In contrast, only a few round cells were found on aminosilanised glass treated with BSA (Fig. 36B, C). Statistical evaluation showed that more than 90% of the XTC cells on the RGDS-functionalised surfaces were spread; this correlates well with spreading behaviour of mouse fibroblasts on the RGD-surface (Fig. 36C, 29).

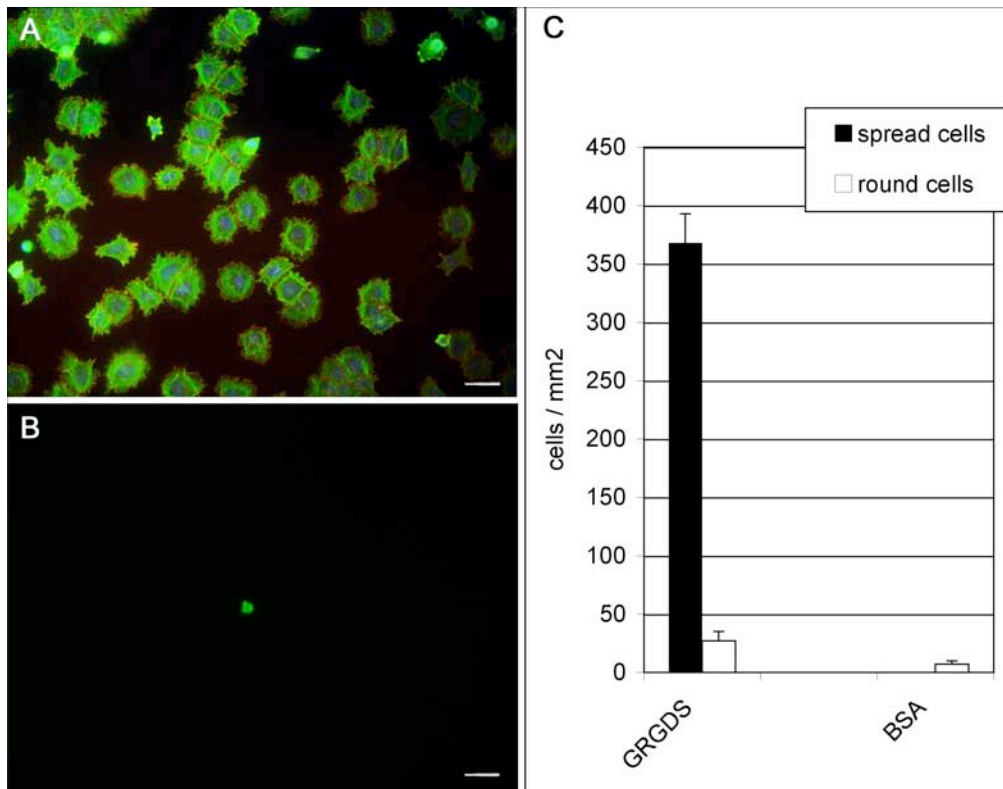


Fig. 36. XTC on RDGS-functionalised surface. (A) XTC spread on GRGDS; (B) only few round cells were found on BSA covered amino-silanised glass; (C) statistical evaluation of XTC spreading behaviour. Phosphopaxillin staining for focal contacts in red, actin filament labelling with phalloidin in green, staining of nuclei with DAPI in blue. Scale bars 50 μ m.

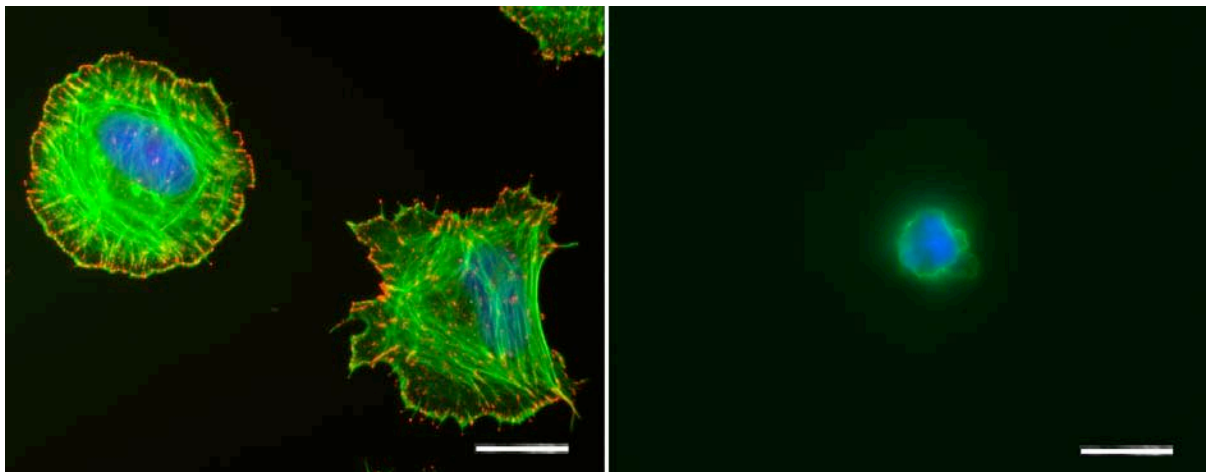


Fig. 37. XTC on RDGS-functionalised surface. (A) XTC spread on GRGDS forming FAs; (B) cells stay round on BSA. Phosphopaxillin staining for focal contacts in red, actin filament labelling with Phalloidin in green, staining of nuclei with DAPI in blue. Bars 20 μ m.

Phosphopaxillin staining revealed well formed focal adhesions on the end of actin fibres in the lamellipodia of the *Xenopus* fibroblasts on RGD-peptide. The fully spread morphology of

these cells sharply contrasts with the round shape of XTC on BSA covered aminosilanised glass (Fig. 37).

4.6.2 Rat embryonic fibroblasts (REF52) stably expressing YFP-paxillin

Rat embryonic fibroblasts (REF52) stably expressing YFP-paxillin demonstrated high level of fluorescence on the green channel even after formaldehyde fixation. REF52 cells incubated for 1 hour with GRGDS-functionalised surfaces spread and formed visible paxillin-clusters indicating focal adhesions (Fig. 38A). Phosphopaxillin staining, however, showed that FAs containing activated paxillin were distributed over the entire cell border (Fig. 38B).

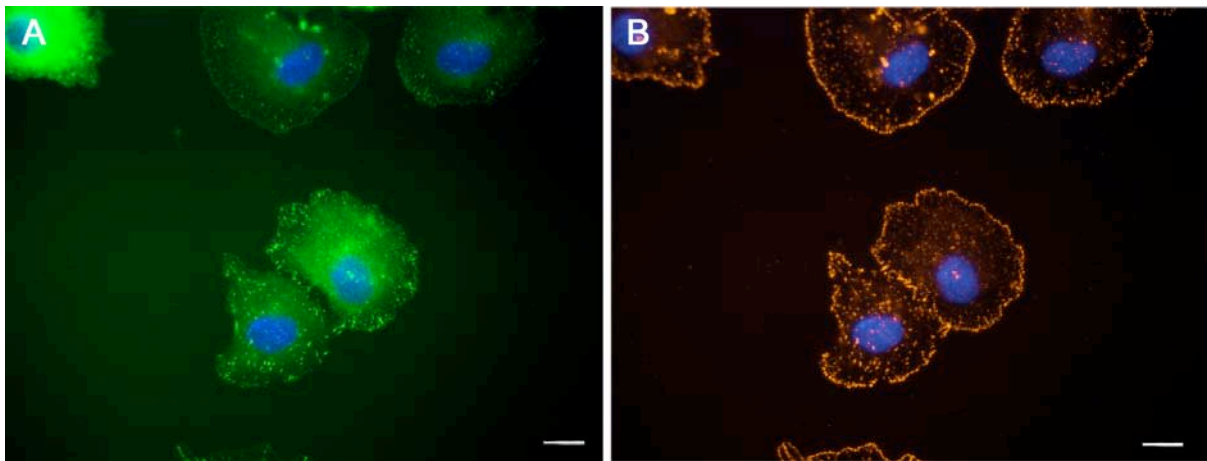


Fig. 38. REF52 fibroblasts spreading behaviour on RDGS-functionalised surface. (A) YFP-paxillin clusters on the green channel of fluorescence microscope; (B) phosphopaxillin staining in red. Scale bars 20 μm .

4.6.3 B16 beta3–GFP-integrin–expressing melanoma cells (beta3-GFP)

Behaviour of B16 beta3–GFP-integrin–expressing melanoma cells on the RGD-functionalised surface was tested. The cells spread on both linear and cyclic RGD-containing peptides (Fig. 39). GFP-integrin clusters were registered in living cells on GRGDS, GRGDSP, c(-RGDfKG-), and c(-RGDfK-) using the Leica fluorescence microscope. However, on GRGDS, GRGDSP, and c(-RGDfKG-), the integrin clusters were located in a similar manner in separated sites nearly the leading edge of lamellipodia; their location correlated well with FAs visualised by phosphopaxillin staining after fixation of cells. In contrast, in the case of c(-RGDfK-) the GFP-fluorescent signal was detected on hole basal cell membrane. The immunostaining did not reveal clusters of phosphorylated paxillin under the cell body and showed a high level of background fluorescence.

Adhesion assay showed that beta3-GFP-integrin cells spread on negative control R β AD-peptides as well as on RGD-peptides. Fig. 40 illustrates spreading behaviour of the cells on GR β ADS, GR β ADSP, c(-R β ADfKG-), c(-R β ADfK-) -functionalised surfaces and on amino-

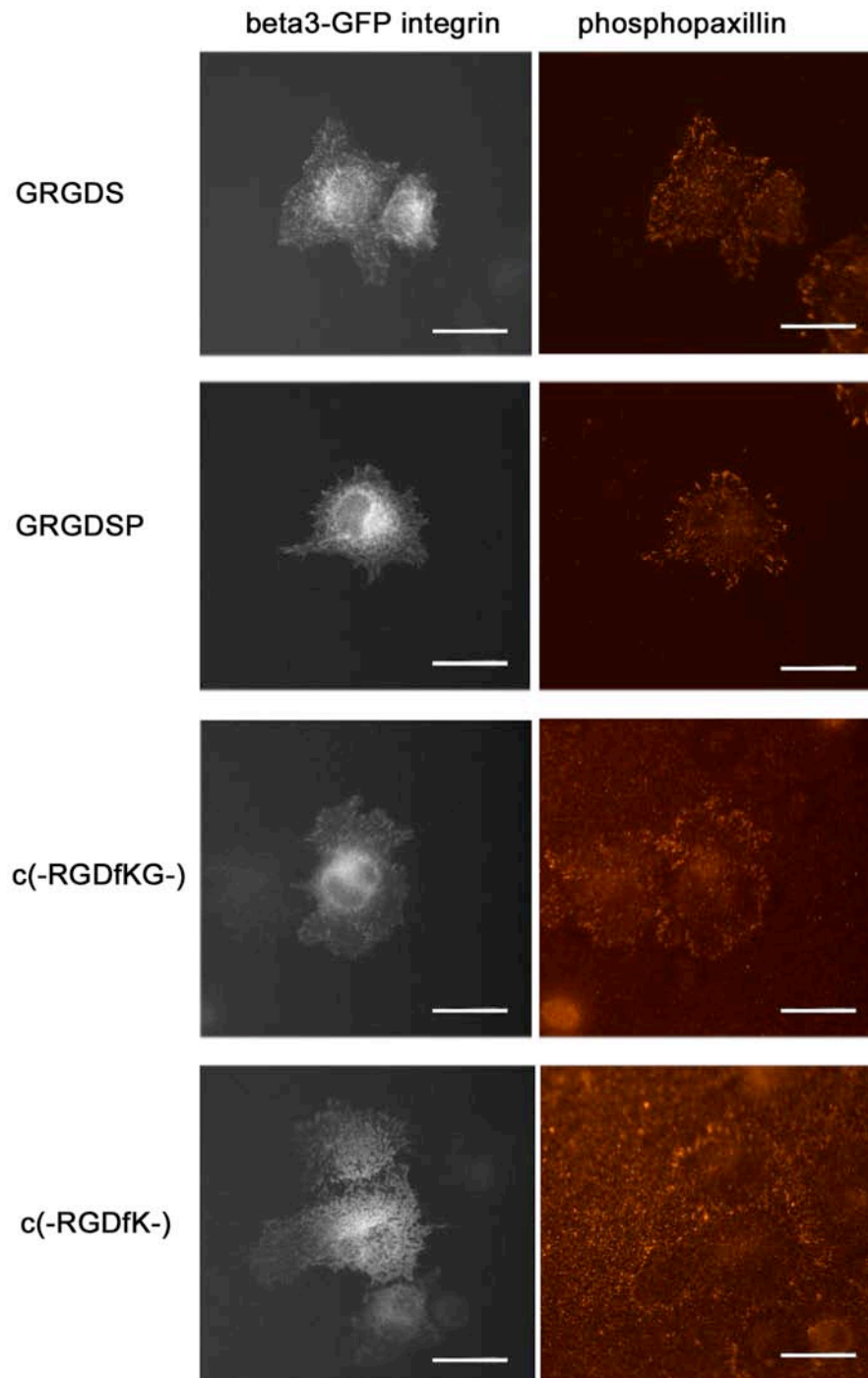


Fig. 39. B16 beta3-GFP integrin cells on RGD-peptides functionalised surface: linear GRGDS and GRGDSP, cyclic c(-RGDfKG-) and c(-RGDfK-). GFP-integrin clusters are visualised by fluorescence microscopy; phosphopaxillin staining in red. Bars: 20 μ m.

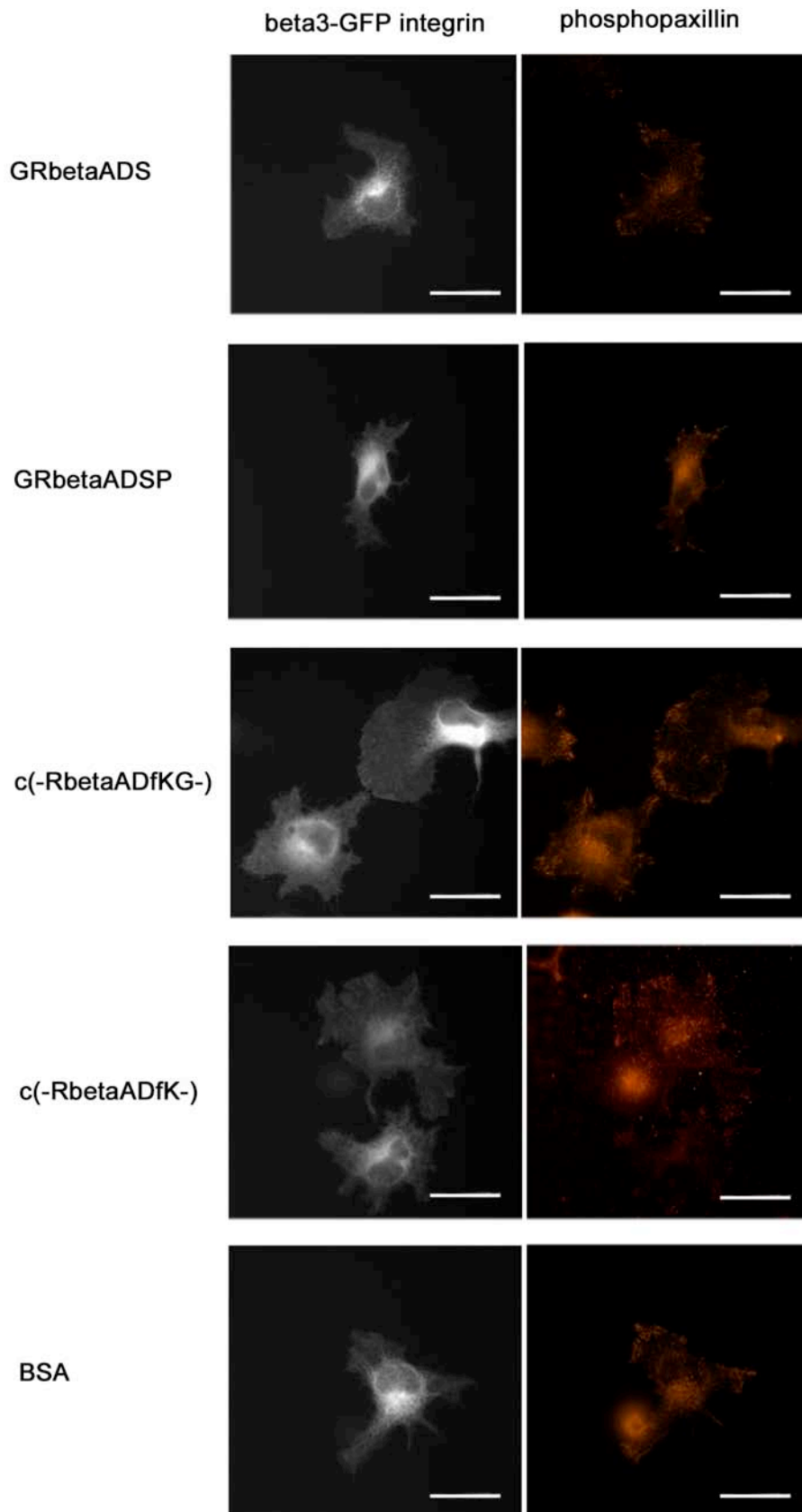


Fig. 40. B16 beta3-GFP integrin cells on control peptides: linear GR β ADS and GR β ADSP, cyclic c(-R β ADfKG-) and c(-R β ADfK-). GFP-integrin clusters are visualised by fluorescence microscopy; phosphopaxillin staining in red. Bars: 20 μ m.

silanised glass covered with BSA. Even on the control peptides and un-functionalised BSA surfaces the cells formed GFP-integrin clusters; phosphopaxillin staining showed FAs located in the corresponding sites of lamellipodia.

4.6.4 MC3T3-E1 pre-osteoblasts

The cell adhesion assay with mouse MC3T3-E1 pre-osteoblastic cells showed spreading of the cells on GRGDSP-functionalised surfaces. Paxillin and phosphopaxillin staining revealed mature FAs in the lamellipodia (Fig. 41). However, similar spreading morphology was observed for MC3T3-E1 cells on the surfaces functionalised with control GR β ADSP-peptide (data is not shown) as well as on unfunctionalised aminosilanised glass covered with BSA (Fig. 41).

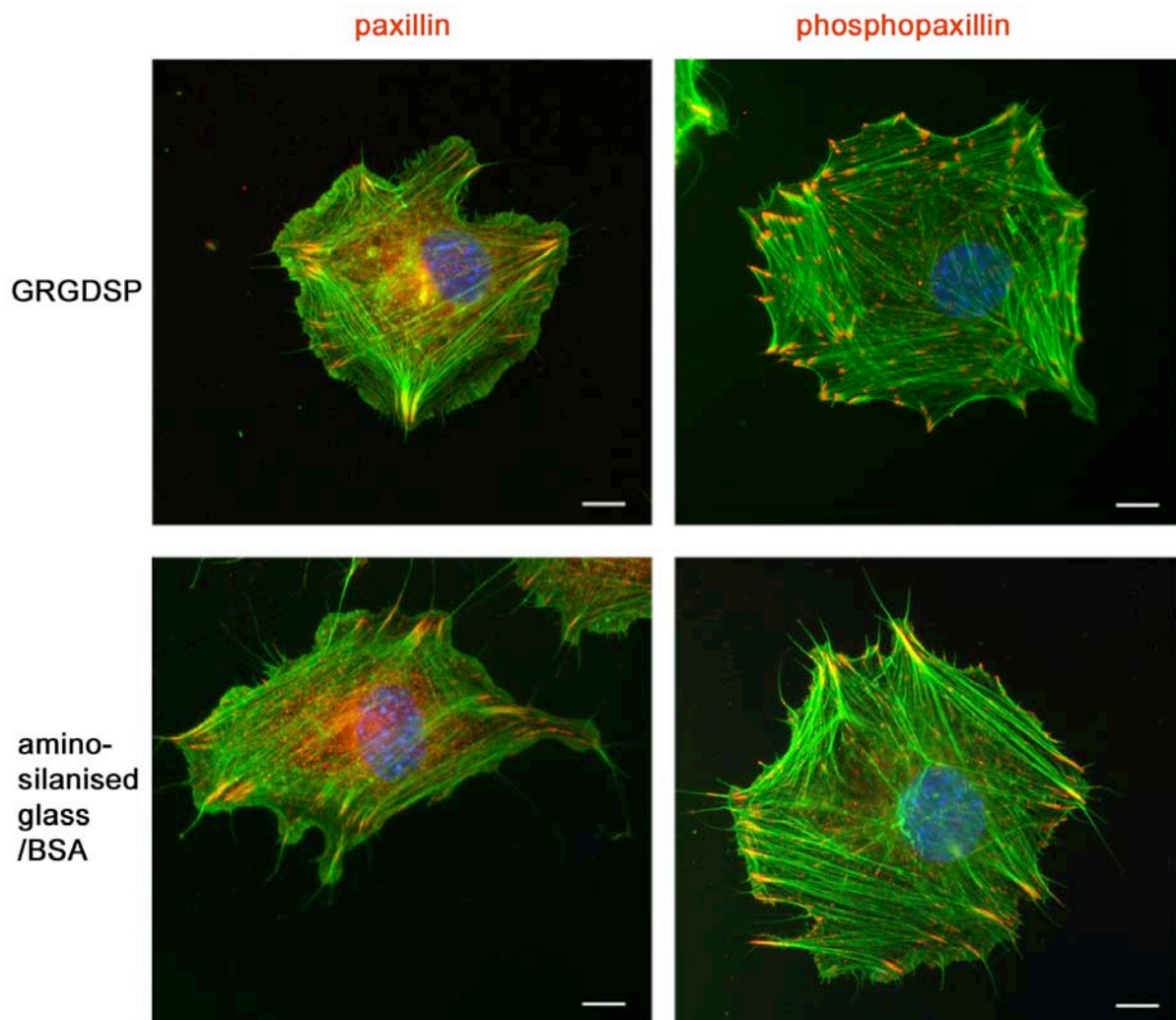


Fig. 41. MC3T3-E1 pre-osteoblasts on RDGSP-functionalised surface and on aminosilanised glass covered with BSA. Phosphopaxillin staining for focal contacts in red, actin filament labelling with Phalloidin in green, staining of nuclei with DAPI in blue. Scale bars 10 μ m.

4.7 Control of the surface biocompatibility

4.7.1 Control peptides

The control peptides were synthesized to prove specificity of RGD motif recognition by cells in adhesion assays. The chemical formulas of these peptides exactly repeat the formulas of the tested RGD-containing peptides with the only exception being that the Glycine in RGD motif is replaced with β Alanine. I have tested two linear – GR β ADS and GR β ADSP – and two cyclic – c(-R β ADfK-) and c(-R β ADfKG-) – control peptides. The cell adhesion assays showed no spread cells on the surfaces that were functionalised with the control peptides. However, the flattened cells on the c(-R β ADfK-) were found. They did not form focal adhesions, but demonstrated morphology that was dissimilar to the completely round shape of the cells on other negative peptides GR β ADS, GR β ADSP, and c(-R β ADfKG-) (Fig. 42).

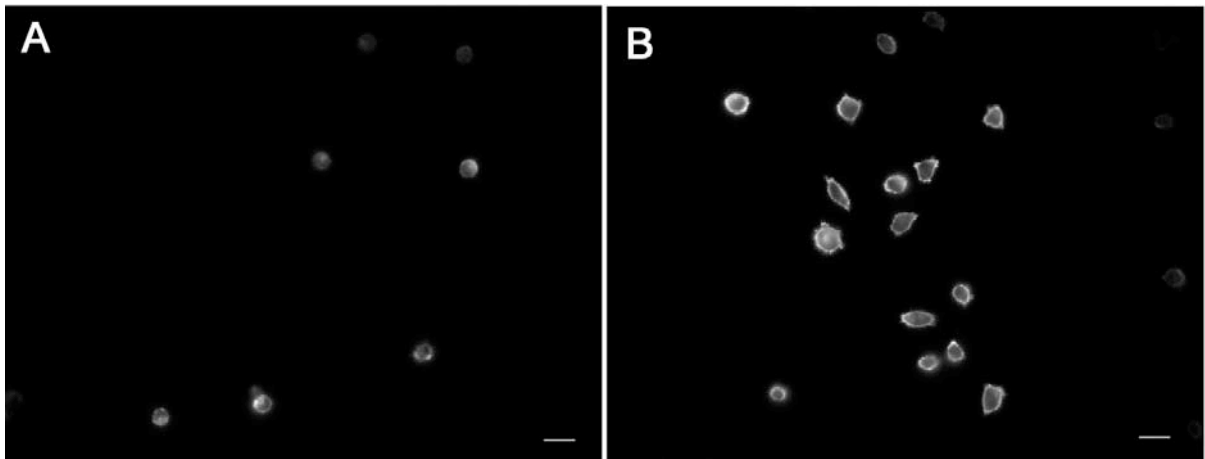


Fig. 42. Cell attachment to negative control peptides. The surfaces were functionalised with GR β ADS (A) and c(-R β ADfK-) (B). The cells were visualised with Oregon Green®-phalloidin staining. Bars: 10 μ m.

The number of attached cells was quite similar to the round fibroblasts on both linear negative peptides, and nearly twice higher than the number of cells on cyclo(-RGDfKG-) and cyclo(-RGDfK-). The flattened cells were found only on the cyclo(-RGDfK-) (Fig. 43). Thus, the control with scrambled RGD motif were not able to stimulate cell spreading accompanied with FAs formation, but the corresponding cyclic peptide c(R β ADfK-) promoted cell flattening on the surface.

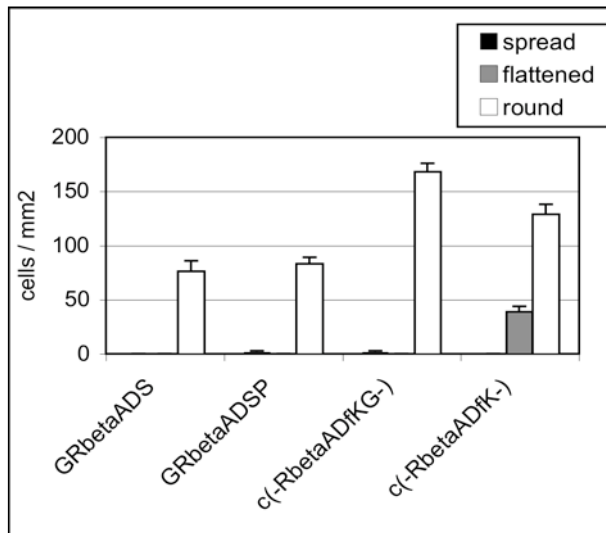


Fig. 43. Statistical evaluation of cell attachment to negative control peptides.

4.5.2 Competition assays

Soluble RGD peptides added to cell suspension during cell adhesion bind with RGD-receptors in a competitive manner, preventing adhesion. To prove that 3T3 Swiss fibroblasts indeed recognise the RGD motif on the functionalised surfaces I performed the cell adhesion assays on the surfaces in the presence of 1,5 mg/ml GRGDS. Indeed, soluble GRGDS in cell medium completely prevent cell spreading on linear GRGDS, GRGDSP, and on cyclic c(-RGDfKG-). Only a few round cells were found on these surfaces (Fig. 44A). Flattened and spread cells were found on c(-RGDfK-), although these cells had no FAs (Fig. 44B).

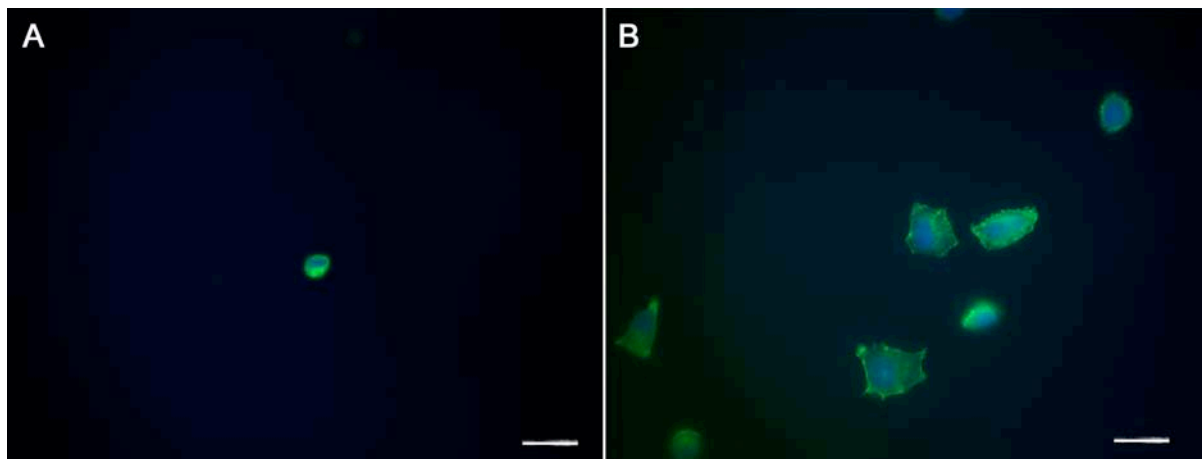


Fig. 44. Cell adhesion assay in the presence of soluble GRGDS. Cells attached to GRGDS (A) and c(-RGDfK-)(B) functionalised surfaces. Scale bars 20 μ m.

The counting of round and flattened cells that attached to RGD-functionalised surfaces in the presence of soluble GRGDS showed that 75% of the fibroblasts showed spreading behaviour on c(-RGDfK-) in presence of 1,5 mg/ml GRGDS (Fig. 45).

The test of fibroblasts adhesion on Nc(-RGDfK-) in the presence of soluble GRGDS showed no spread cells on the surface; less than 10 attached round cells per mm² were found.

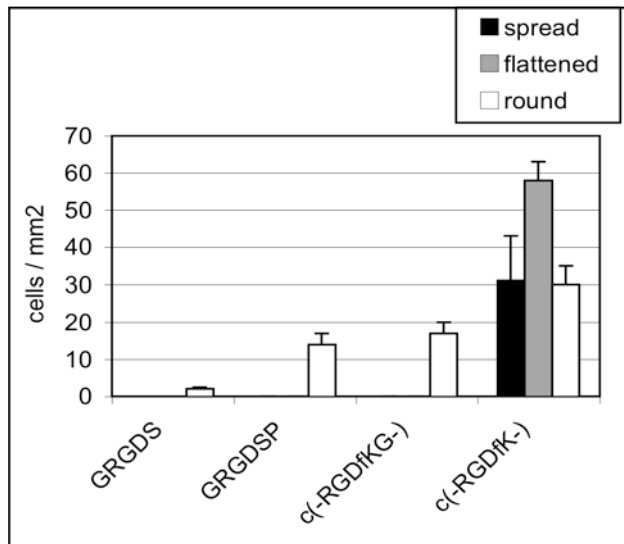


Fig. 45. Cell adhesion assay in the presence of soluble GRGDS. Statistical evaluation. Soluble RGD-peptide completely prevented cell spreading on GRGDS, GRGDSP, and c(-RGDfKG-), but on c(-RGDfK-) flattened cells were found.

4.7.3 Proliferation assays

To estimate the cell ability to proliferate on RGD-functionalised surfaces an enumeration of cells in mitotic stage was performed. Immunostaining of phosphorylated histone H3 revealed mitotic cells; comparison of their number with total number of surface adhered cells allowed calculation of the proliferation index. The diagram in Fig. 46 shows an increase with time in the number of mitotic cells cultivated on the GRGDS-functionalised surface for 4, 24 and 48 hours, that corresponds to an increase in the total number of surface adhered cells.

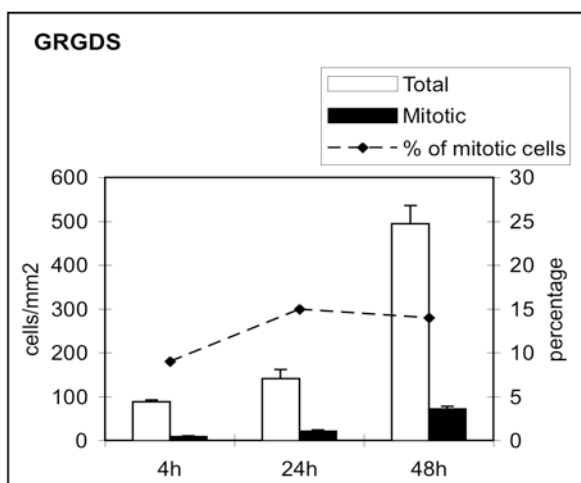


Fig. 46. 3T3 Swiss fibroblasts proliferate on GRGDS-functiona-lised surface.

The percentage of mitotic cells was relatively low during the first 4 hours that corresponded to cell cultivation in the serum free medium. Calculation of mitotic cells at 24 and 48 hours after cell seeding showed 15 and 14% of total cell number, respectively. Thus, on the GRGDS-functionalised surface mouse fibroblasts were able to grow and proliferate with stable velocity.

4.8 The RGD-functionalisation of the structured surfaces

Table 2. Notations used for designed surfaces.

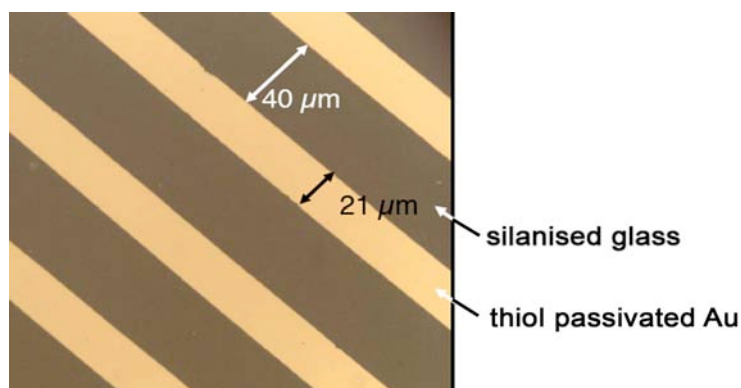
Notation	Surface
Homogeneous Au-ODT	Gold layer covered with octadecylthiol.
Homogeneous Au-BT	Gold layer covered with butanethiol.
Homogeneous Au-HT	Gold layer covered with hexylthiol.
Homogeneous Au-ODT/RGD	Gold layer covered with octadecylthiol that was aminosilanised and incubated with isothiocyanate terminated RGD-peptide for 2h at coupling conditions. When the step of aminosilanisation was missed, it was mentioned in the text.
Homogeneous Au-BT/RGD	Gold layer covered with butanethiol that was aminosilanised and incubated with isothiocyanate terminated RGD-peptide for 2h at coupling conditions.
Homogeneous Au-HT/RGD	Gold layer covered with hexylthiol that was aminosilanised and incubated with isothiocyanate terminated RGD-peptide for 2h at coupling conditions.
Homogeneous Au/RGD	Gold layer after incubation with isothiocyanate terminated RGD-peptide for 2h at coupling conditions.
Structured Au-ODT	Patterned surfaces created by μ CP with octadecylthiol on gold layer and further etching.

Structured Au-ODT/RGD	Patterned Au-ODT surfaces that was aminosilanised and incubated with isothiocyanate terminated RGD for 2h at coupling conditions.
Structured Au-BT/RGD	Patterned surfaces created by μ CP with BT on gold layer and etching that was aminosilanised and incubated with isothiocyanate terminated RGD-peptide for 2h at coupling conditions.
Structured Au-HT/RGD	Patterned surfaces created by μ CP with HT on gold layer and etching that was aminosilanised and incubated with isothiocyanate terminated RGD-peptide for 2h at coupling conditions.
Structured Au-through-mask	Patterned surface designed by gold evaporation through the mask on the previously aminosilanised glass.
Structured Au-through-mask/RGD	Structured Au-through-mask incubated with isothiocyanate terminated RGD peptide for 2h at coupling conditions.

4.8.1 Surface preparation: structured Au-ODT slides

To design a structured surface the microcontact printing (μ CP) method was applied. The grid of used silicone elastomer stamp allowed to create a pattern of alternate 21 μ m wide lines of octadecylthiol (ODT) on the metal (see section 3.1.3). During the etching procedure the unprotected metal layer can be reduced and removed from the surface, whereas ODT-passivated metal lines designed the structured pattern (Fig. 47). Both gold and silver can be used as a base for thiol SAMs (Shaporenko et al., 2005). I have found that ODT- μ CP cannot be applied for passivation of a silver layer. The 50 μ m silver layer was completely removed from the surface during the etching procedure including the ODT-covered areas. The ODT-printed gold layer demonstrated resistance to etching that was high enough to protect lengthy 21 μ m wide areas of homogenous metal from etching.

Fig. 47. Light microscope image of the Au-ODT structured surfaces: alternate lines of ODT-passivated Au and glass.



4.8.2 Metal: thickness of gold

To choose the suitable metal thickness electron microscopy of the etched ODT-printed gold slides was performed. I have tested 25, 50 and 100 nm gold layers. The precise thickness of the metal layer was controlled directly during the coating process with a quartz crystal microbalance.

Taking into consideration that etching duration depends on metal thickness, I have tested different treatment times using visual estimation for control of the metal release from the surface. Optimal etching duration for 25, 50 and 100 nm gold layers is was observed at 25, 40 and 60 minutes respectively.

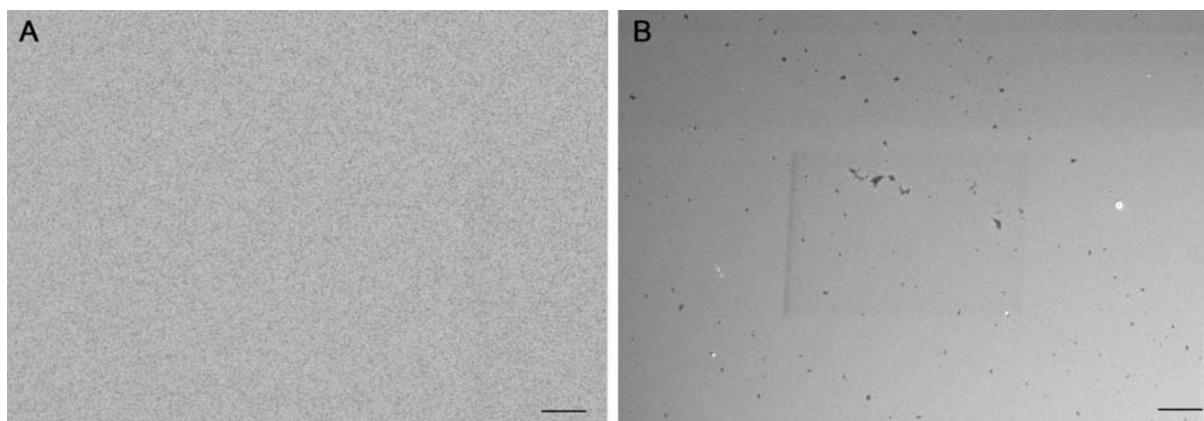


Fig. 48. Electron microscope image of gold areas on the structured Au-ODT slides. 25 nm gold slides before (A) and after (B) 20 minutes etching. Surface defects in (B) are seen as black spots. Bars: 1 μm.

Etched 50 nm gold layers demonstrated suitable surface quality while 25 nm etched layers demonstrated surface defects that were detected by electron microscopy (Fig. 48). The etching of 100 nm gold layers required 1 h treatment and refreshment of the solution during etching procedure.

4.8.3 Adapter metal

Titanium and chromium were tested as adapter metals to promote the gold attachment on the glass or SiO₂. For both metals a 1 nm thick layer was shown to be sufficient to promote a uniform gold layer.

Removal of the chromium as well as titanium layer from patterned surface during the etching process was controlled by visual estimation that was easy in the case of transparent glass but difficult for SiO₂ slides. The removal of the adapter metals required 3-4 minutes additional exposure in the etching solution. It was shown complete in the case of chromium; however, confocal laser microscope showed that removal of a titanium layer was incomplete (Fig. 49).

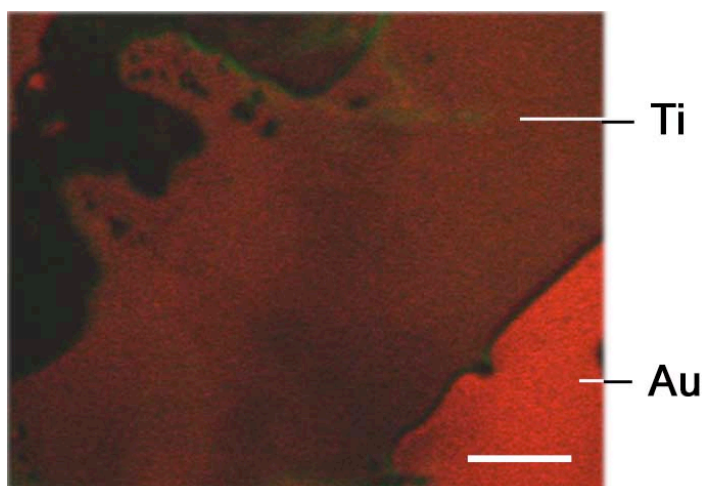


Fig. 49. Structured Au-ODT slides created with Ti as an adapter metal. The residue Ti layer was found after etching. Confocal laser microscope image. Bar: 5 μm .

4.8.4 Thiol stamping

I used thiol solution in ethanol in the μCP procedure to create SAMs on the some areas of the metal surface. ODT - $\text{CH}_3(\text{CH}_2)_{17}\text{SH}$ - was shown to be able to passivate a gold surface, creating a patterned structure during μCP .

As an alternative thiol-coating we have tested butanethiol (BT) - $\text{CH}_3(\text{CH}_2)_3\text{SH}$. μCP with 2mmol as well as 10 mmol BT in ethanol was not able to protect the gold layer during etching. Large fissures and holes were detected within the Au stripes as seen in the electron microscopic image (Fig. 50).

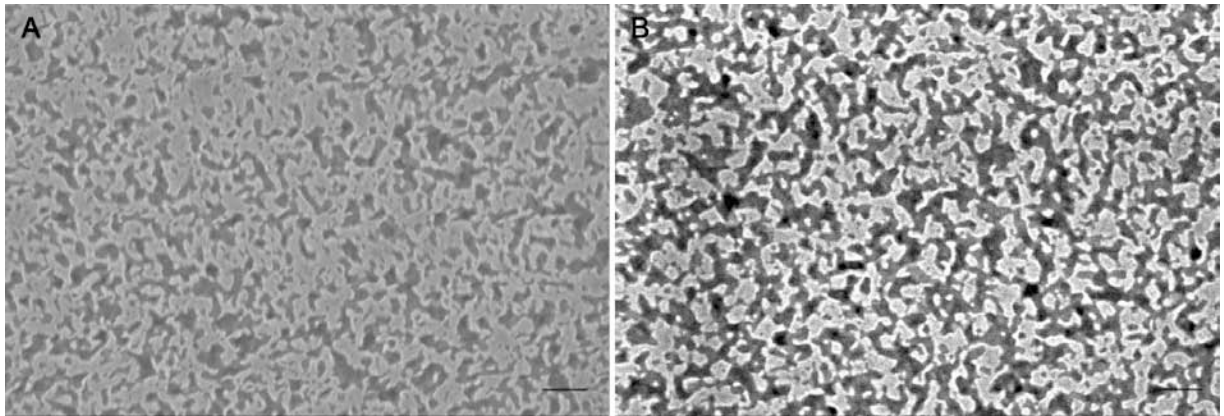


Fig. 50. Electron microscope images of gold areas on the structured Au-BT slides. 50 nm gold slides after 20 minutes treatment with 2 mmol (A) and 10 mmol (B) solution of butanethiol. Scale bars: 200 nm.

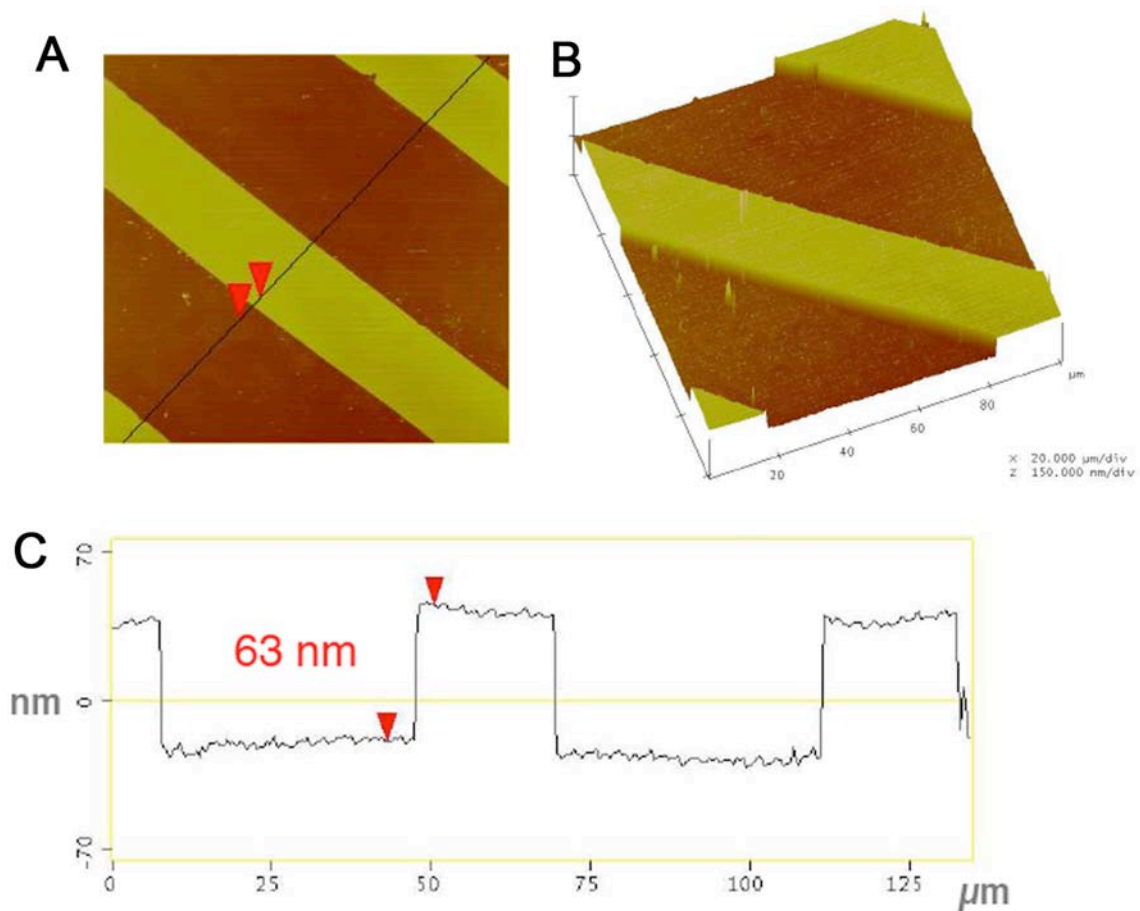


Fig. 51. AFM topography of the structured Au-ODT surface. (A) 2D image of 100 μm x 100 μm area of the glass-Cr-Au-ODT patterned surface after etching; 1 μm Cr, 50 μm Au. (B) 3D image of the same area, (C) cross-section.

4.8.5 Quality control by atomic force microscopy (AFM)

Selective etching of a 50 nm gold layer and its removal from glass created a 3D patterned structured surfaces. AFM measurement revealed topography of the glass slide covered with 1 nm chromium and 50 nm gold, then printed with ODT by μ CP and etched for 40 minutes. The tested $100\ \mu\text{m} \times 100\ \mu\text{m}$ area included Cr-Au-ODT as well as opened glass stripes (Fig. 51A). The cross-section of the investigated area (Fig. 51B) showed about 63 nm difference in the height of these two regions. The 3D structure of the surface visualised by AFM is shown on Fig. 51C.

4.8.6 Alternative patterning: Gold evaporation through the mask

As described in the section 3.1.7 an alternative patterning procedure was performed to produce gold stripes onto amino-silanised glass. Use of the mask with slips allowed creation of a patterned surface without an etching step. In Fig. 52 designed pattern is shown: alternate gold and amino-glass stripes (400 bars/inch). High magnification (Fig. 52B) revealed additional stripes on the pattern, located on both sides of main broad gold stripes looking like a “shadow”. It is proposed that such a “double” pattern was created because of features of evaporation of two different metals – chromium and gold – on the surface through the mask.

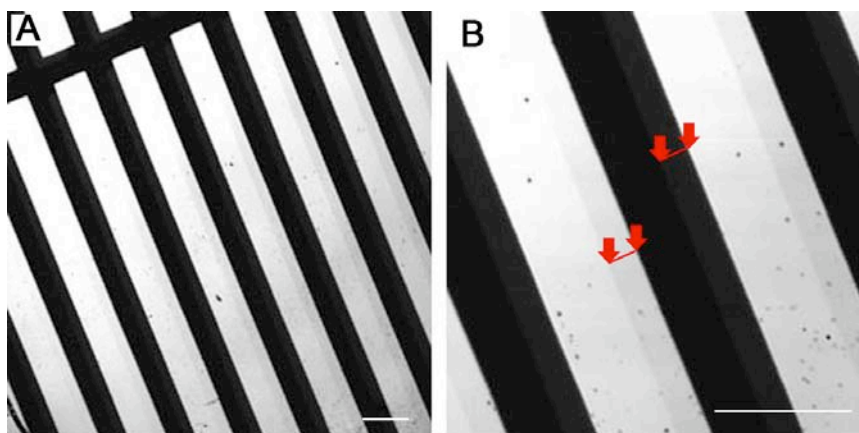


Fig. 52. The patterned surfaces created by gold evaporation through the mask. Confocal laser microscope image. The shadows are indicated by arrows. Bars: $50\ \mu\text{m}$.

The sources of these metals were located in the evaporation unit at a distance of about 20 cm; the evaporation through the relatively thick (exact thickness is not specified) mask could be a reason for incomplete overlaying of the metal coating areas. Fig. 53 demonstrates that a surface evaporated by this method is not homogeneous; there are areas with a different quality.

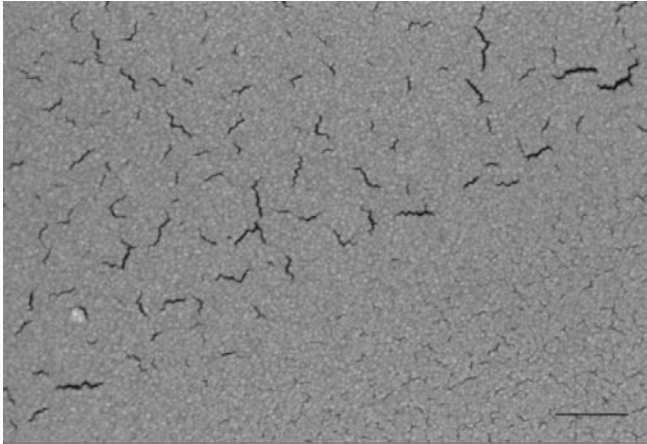


Fig. 53. Created by gold evaporation through the mask the patterned surface showing areas with a different quality. Electron microscope image. Bar: 200 μm .

4.9 Cell behaviour on the structured surfaces

4.9.1 Mouse fibroblasts spread on structured Au-ODT/RGD surfaces without any preferences

The structured surfaces, which combined gold-ODT and amino-silanised glass stripes, were treated with isothiocyanate terminated GRGDSP solution at coupling conditions. Adhesion assay showed that mouse fibroblasts spread on such surfaces but without any preference. The cells demonstrate filopodia, lamellipodia and focal adhesions on both regions – gold-ODT and NH_2 -glass (Fig. 54).

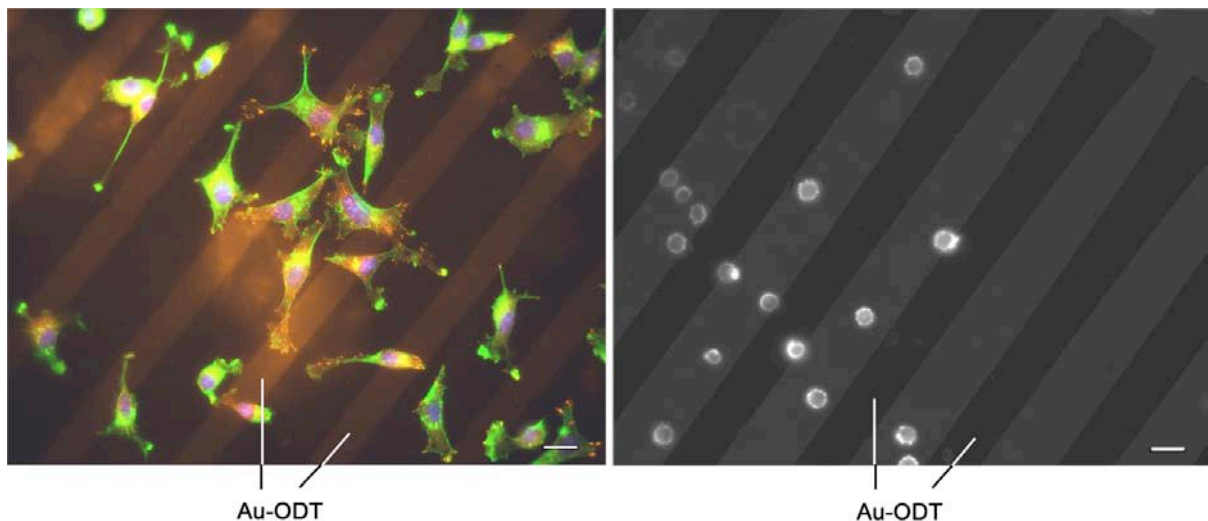


Fig. 54. Mouse 3T3 Swiss fibroblasts on structured surfaces. (A) RGDS-functionalised surface: Au-ODT and NH_2 -glass; the fibroblasts spread without any preferences. The cells were visualised by filamentous actin staining with phalloidin (green) and DAPI (blue); paxillin immunostaining (red) marks focal adhesions. (B) The fibroblasts don't spread on an unfunctionalised structured surface. The cells were visualised by filamentous actin staining with Oregon Green®-phalloidin. Bars: 10 μm .

An unfunctionalised structured surface not treated with RGD-peptide showed no spread cells on it; only a few round cells were attached (Fig. 54B).

4.9.2 Cells on the RGD-functionalised structured Au-through-mask surface

The pattern on the amino-silanised glass was created by gold evaporation through the mask on the previously amino-functionalised glass (see section 3.1.7). For RGD-functionalisation the slides were incubated for 2 hours with peptide solution at coupling conditions. Adhesion assay showed that mouse fibroblasts attach to the surfaces without any preference, spreading on NH₂-glass as well as on gold covered areas (Fig. 55).

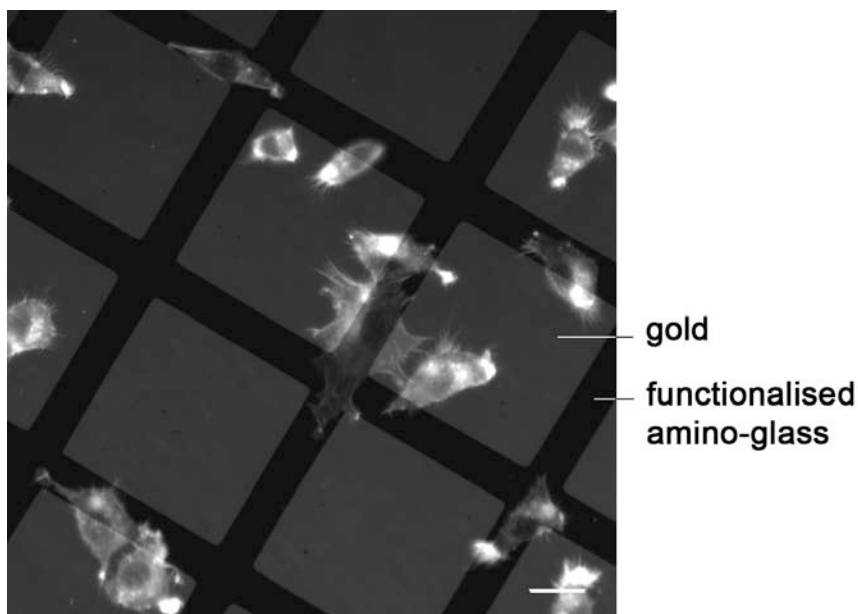


Fig. 55. RGD-functionalised structured surface: gold through the mask. Mouse 3T3 Swiss fibroblasts spread on the structured surfaces without preferences. Confocal laser microscopy. The cells were visualised by filamentous actin staining with Oregon Green®-phalloidin. Bar 20 μ m.

4.9.3 Cell behaviour on the homogeneous surfaces: Au and on Au/GRGDSP

To reveal the reasons of uniform fibroblast distributions on patterned surfaces the cell behaviour on homogeneous samples was investigated. At first, I have checked whether the adhesive properties of the pure gold can be changed by incubation with peptide solution. For this, cell assays for two types of surfaces were performed: (1) pure gold layer (50 nm thickness) on the glass and (2) gold covered glass modified by 2 hours incubation with coupling solution GRGDSP.

Indeed 3T3 Swiss fibroblasts spread on Au/GRGDSP but mainly remained round on the pure unfunctionalised gold surface, even after 1-hour in serum-free cell-cultivation medium (Fig. 56). Confocal laser microscopy revealed numerous filopodia and ruffling lamellipodia of the spread cells on Au/GRGDSP. More than 80% of the cells on unfunctionalised gold retained a complete round shape, others demonstrated slightly elongated – “spindle” – phenotype.

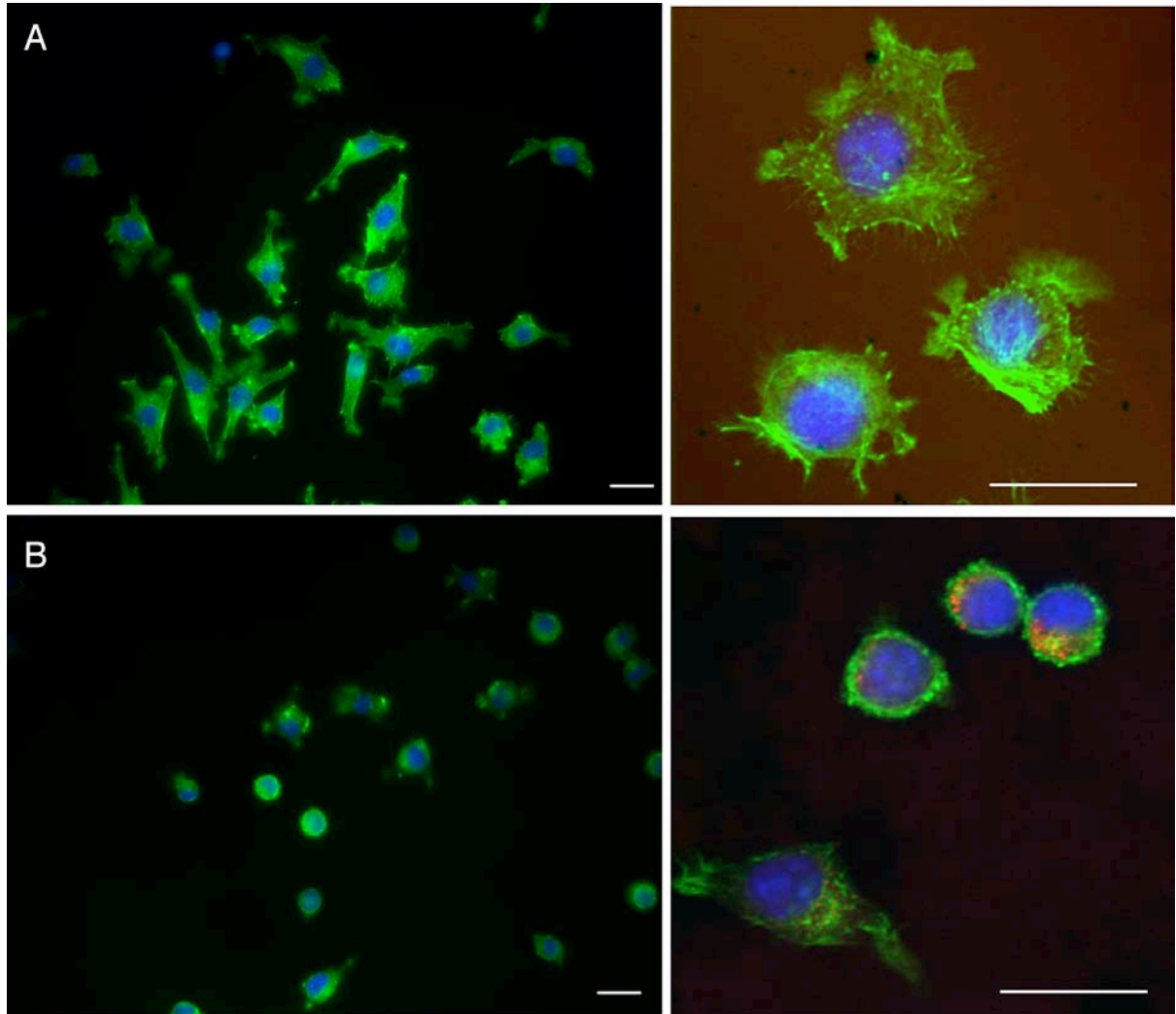


Fig. 56. Mouse 3T3 Swiss fibroblasts spread on Au/GRGDSP surface (A) but mainly stayed round on the unfunctionalised gold (B). The cells were visualised by filamentous actin staining (green) and DAPI (blue). Bars: 20 μm .

4.9.4 Homogeneous surfaces: Au-ODT/GRGDSP

Cell adhesion assays showed that in the serum-free cultivated medium mouse fibroblasts did not spread on Au-ODT if the surface was not treated with RGD-peptide. However, when the Au-ODT surface was treated with GRGDSP via adsorption or chemical coupling 3T3 Swiss fibroblasts recognized the peptide and adhered to the surface (Fig. 57).

The spreading cell morphology was not dependent upon whether or not the Au-ODT/GRGDSP slides were amino-silanised before GRGDSP treatment, showing the ability of RGD-peptide to adsorb on Au-ODT. Thus, the procedure of patterned surface design requires a passivation step to prevent RGD-absorption on Au-ODT areas.

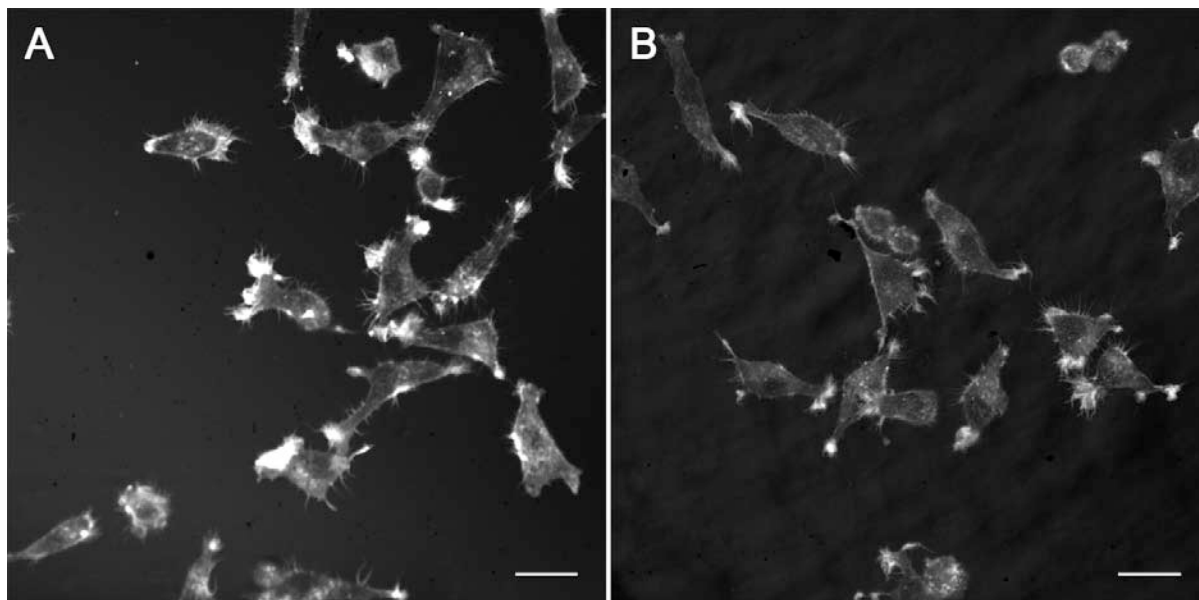


Fig. 57. Mouse 3T3 Swiss fibroblasts spread on Au-ODT/GRGDSP. The cell behaviour do not depend on whether the surface was not treated with amino-silane (A) or was amino-silanised (B) before incubation with GRGDSP; the fibroblasts spread on both samples. Confocal laser microscopy. The cells were visualised by filamentous actin staining. Bars: 20 μm .

4.9.5 Homogeneous surfaces designed with short thiols

The short thiols – butanethiol (BT) and hexylthiol (HT) – were tested as possible candidates for design of patterned surfaces instead or together with ODT. At first the cell behaviour on uniform Au-BT, Au-HT, Au-BT/GRGDSP, and Au-HT/GRGDSP surfaces was investigated. The RGD-functionalisation of the surfaces was included an aminosilanisation step, while Au-BT and Au-HT slides were fabricated without aminosilane treatment.

Adhesion assay showed that mouse fibroblasts spread neither on Au-BT nor on Au-BT/GRGDSP. After 1 hour incubation of suspended cells with both types of slides I observed only round cells on them. In contrast, the fibroblasts recognised GRGDSP on hexylthiol layer and spread onto the surface, but only attached and stayed round on hexylthiol alone (Fig. 58).

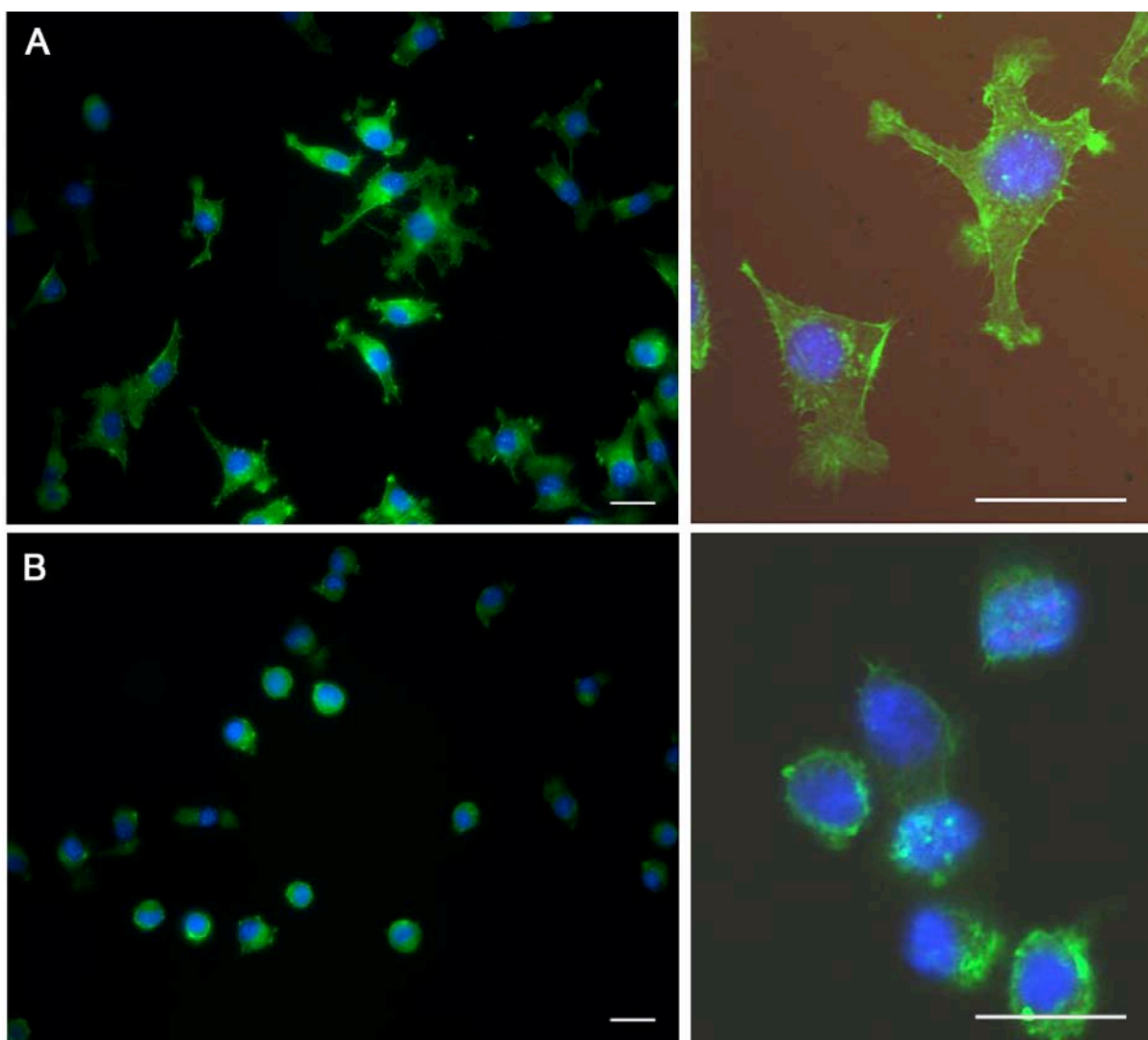


Fig. 58. Mouse 3T3 Swiss fibroblasts spread on Au-HT/GRDSP surface (A) and stayed round on Au-HT (B). The cells were visualised by filamentous actin staining (green) and DAPI (blue). Scale bars: 20 μm .

Thus hexylthiol was shown not to be able to protect the Au surface from RGD-functionalisation via absorption or coupling. In contrast, butanethiol was found to be a possible alternate candidate for the role of ink for μCP instead of ODT.

4.9.6 Passivation of ODT-gold: PEG and Pluronic®

To modify the pattern of RGD-peptides distribution on the structured surface Au-ODT/RGD via passivation of Au-ODT areas a polyethyleneglycol (PEG) and Pluronic® were used. A block copolymer Pluronic® F-68 (Sigma) based on ethylene oxide and propylene oxide has formula $(\text{PEO})_{75}\text{-(PPO)}_{30}\text{-(PEO)}_{75}$ (Fig. 59A) and molecular weight about 8400. PEG3500 (Sigma) has molecular formula $\text{H}(\text{OCH}_2\text{CH}_2)_n\text{OH}$ (Fig. 59B) and molecular weight about 3500.

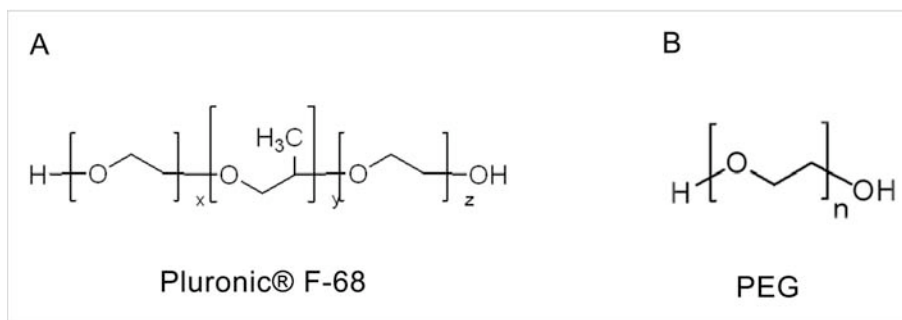


Fig. 59. Molecular formula of Pluronic® (A) and polyethyleneglycol (B).

For Pluronic® F-68: $x = 75$, $y = 30$, $z = 75$; for PEG3500 $n = 80$.

Overnight incubation of Au-ODT slides with 5% PEG as well as 2 mM Pluronic solution before GRGDSP coupling completely prevented cell spreading on the structured Au-ODT/GRGDSP surface (Fig. 60A). When duration of PEG treatment of Au-ODT samples was decreased till only 10 minutes before RGD-peptide coupling, mouse fibroblasts spread on the Au-ODT/GRGDSP surface (Fig. 60B). The cells were distributed mainly on the functionalised NH_2 -glass strips avoiding contact to gold-ODT. They spread and form focal adhesions on RGD-coupled NH_2 -strips. The same cells that were found attached on Au-ODT exhibited a round or flattened shape and did not form focal adhesions.

The similar pattern of the cell distribution was observed on the samples treated with Pluronic®. Fig. 60C shows mouse fibroblasts on the Au-ODT slide that was functionalised with GRGSP in the presence of 2 mM Pluronic® in coupling solution. Using of Pluronic® as well as PEG changed the cell behaviour on the structured Au-ODT/RGD surfaces. The fibroblasts demonstrated selective placement, mainly spreading on the areas between Au-ODT stripes. The treatment with Pluronic® by its own did not induce cell spreading on the surface (Fig. 60D).

Application of Pluronic® during cell adhesion assay was also tested. Added in the cell medium copolymer did not change cell adhesion behaviour. There were no differences found in cell distribution and spreading on Au-ODT/RGD surfaces in comparison with standard cell adhesion assay (data is not shown).

4.9.7 “Bridging” of the cells through unfunctionalised regions

The pattern of structured surfaces is thin enough to allowed cell bridging through unfunctionalised areas. The fibroblasts are able to anchor on the RGD-covered areas forming focal adhesions and filopodia (Fig. 61).

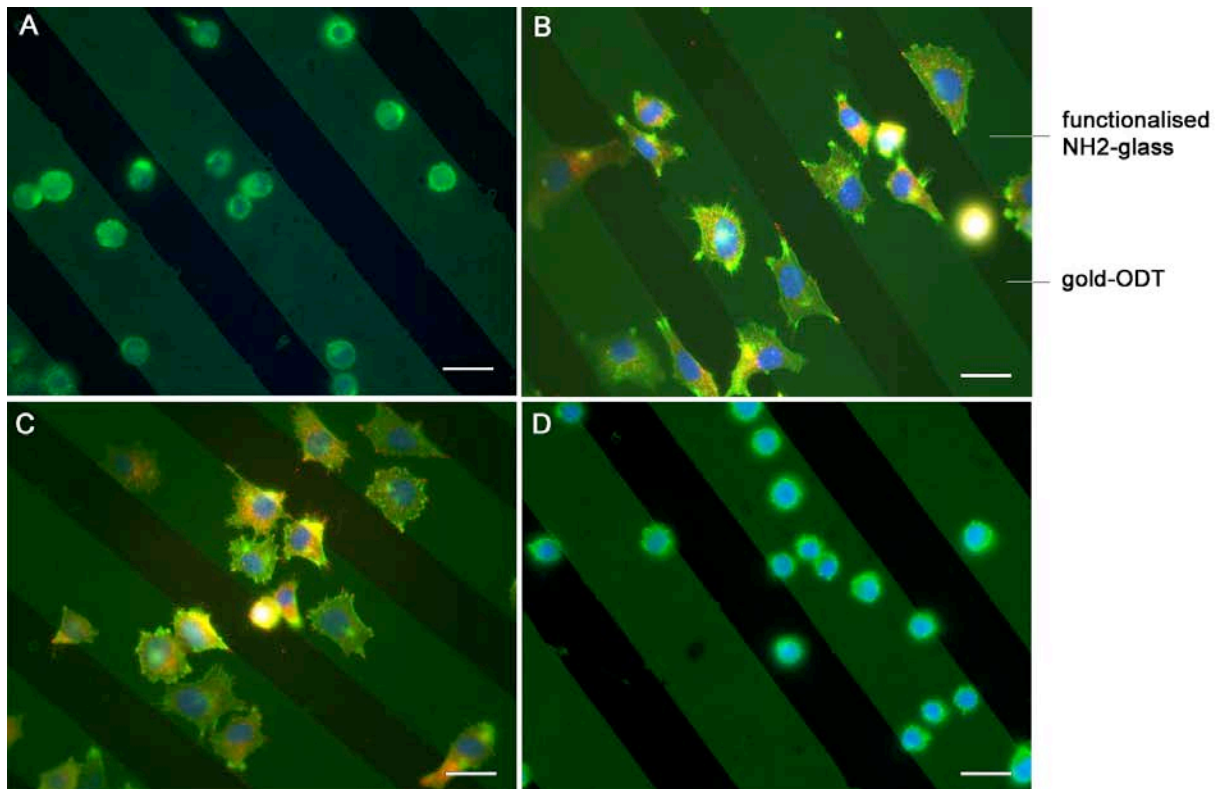


Fig. 60. Comparison of different passivation techniques by cell assays with mouse fibroblasts on the structured Au-ODT/GRGDSP surfaces. (A) Overnight treatment of the slide with 2 mM Pluronic® was followed by peptide coupling. (B) 10 min treatment with 5% PEG was followed by peptide coupling. (C) Peptide coupling was performed in the presence of Pluronic®. (D) The surface was only treated with Pluronic®.

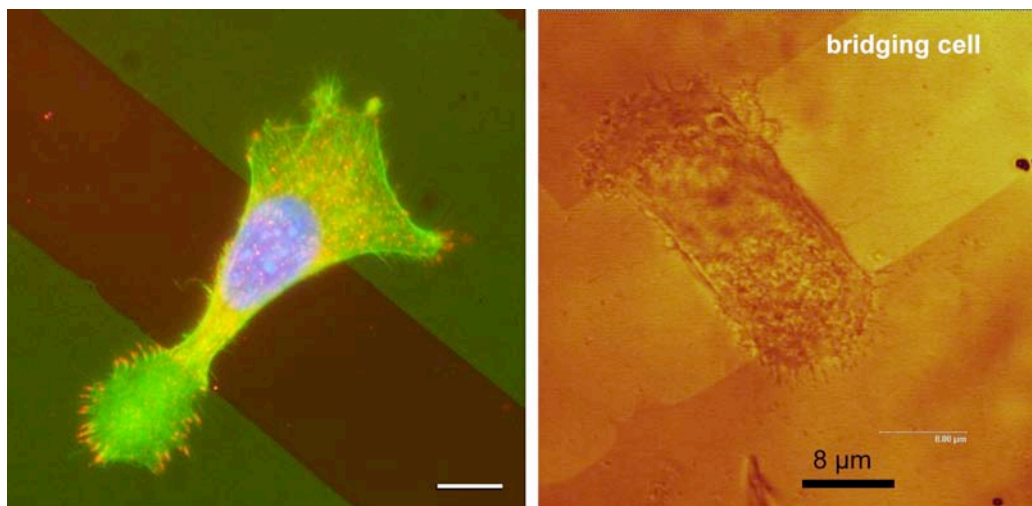


Fig. 61. Fibroblasts are able to span unfunctionalised areas. (A) Optical fluorescence microscopy image; the mouse 3T3 fibroblast was visualised by actin cytoskeleton staining (green), paxillin staining (red) and DAPI (blue). (B) AFM image shows *Xenopus* fibroblast spanning between two functionalised areas.

4.9.8 Cell adhesion on RGD-functionalised structured surfaces

Four RGD-containing isothiocyanate terminated peptides – GRGDS, GRGDSP, c(RGDfKG-), and c(-RGDfK-) – were used for biofunctionalisation of Au-ODT patterned surfaces by coupling in presence of Pluronic®. Fig. 62 illustrates behaviour of Swiss 3T3 fibroblasts on the produced samples. In the case of both linear peptides and cyclo(-RGDfKG-) the cells spread mainly on the functionalised stripes avoiding Au-ODT areas. Few Au-ODT attached fibroblasts are round or “bridged” between two functionalised areas. In the case of cyclo(-RGDfK-) the patterning distribution of the fibroblasts is not obvious; the cells spread even on Au-ODT stripes.

For statistical evaluation spread cells and attached round cells were counted on both areas – Au-ODT and biofunctionalised stripes – for all four peptides. Linear GRGDS and GRGDSP showed similar abilities to induce cell spreading on functionalised areas (Fig. 62). Less than 10% cells attached to Au-ODT stripes showing high selectivity of the patterning distribution. On cyclo(-RGDfKG-) the fibroblasts mainly adhered on the biofunctionalised areas but 20% of the cells were round. In contrast, less than 10% of cells attached to GRGDS- and GRGDSP-functionalised areas demonstrated round shape (Fig. 63).

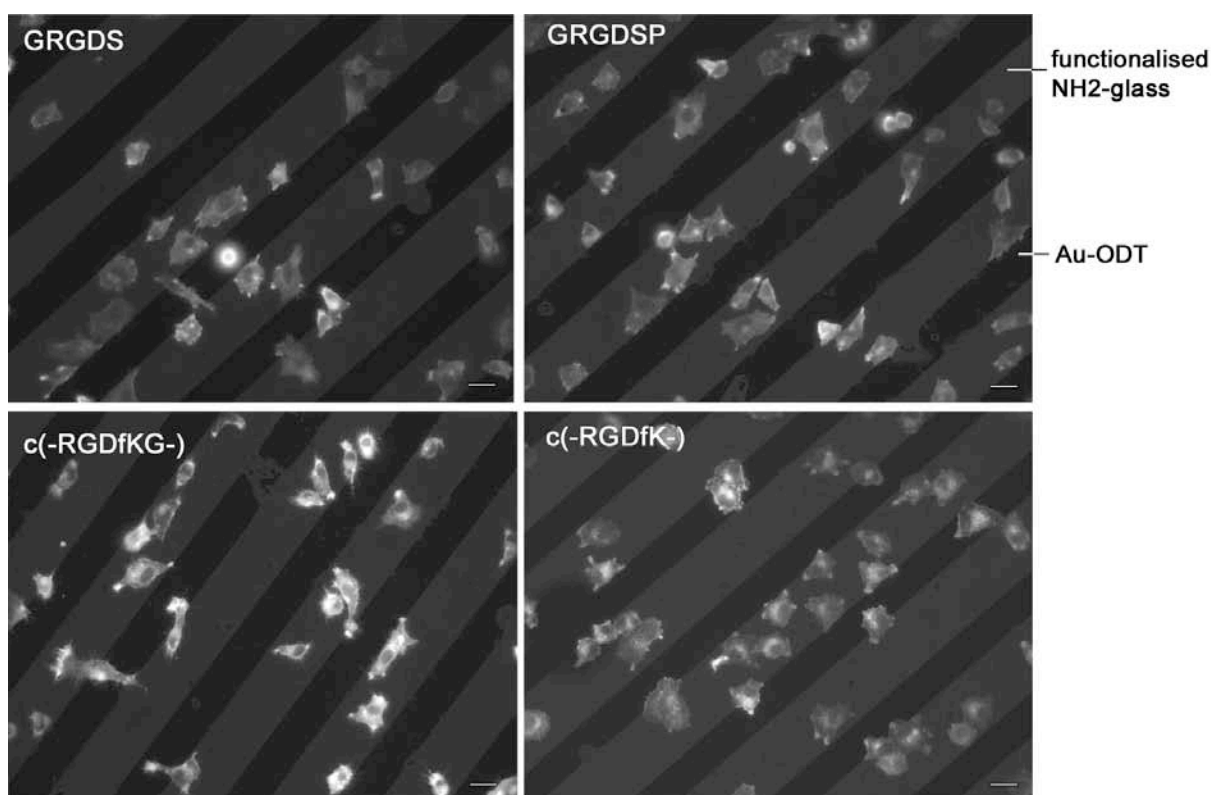


Fig. 62. Cell spreading behaviour on the patterned Au-ODT surfaces functionalised with different RGD-containing peptides. Linear peptides: GRGDS and GRGDSP; cyclic peptides: c(-RGDfKG-) and c(-RGDfK-). Mouse 3T3 Swiss fibroblasts are visualised with Oregon Green®-phalloidin staining. Scale bars 10 µm.

Cyclo(-RGDfK-) -functionalised surface showed low selectivity of cell distribution; the number of adhered on Au-ODT fibroblasts was twice lower then on peptide-functionalised areas, but more then 30% of the cells spread without any preference.

Paxillin staining revealed mature FAs in the lamellipodia of 3T3 Swiss fibroblasts spread on GRGDS- and GRGDSP-functionalised areas (Fig. 64). On both these linear peptides the cells demonstrated full spreading; well formed actin stress fibres spanned to FAs in lamellipodia. Thin filopodia were found extending from the cell body. Long filopodia extending over the Au-ODT layers that were not terminated by FAs were observed.

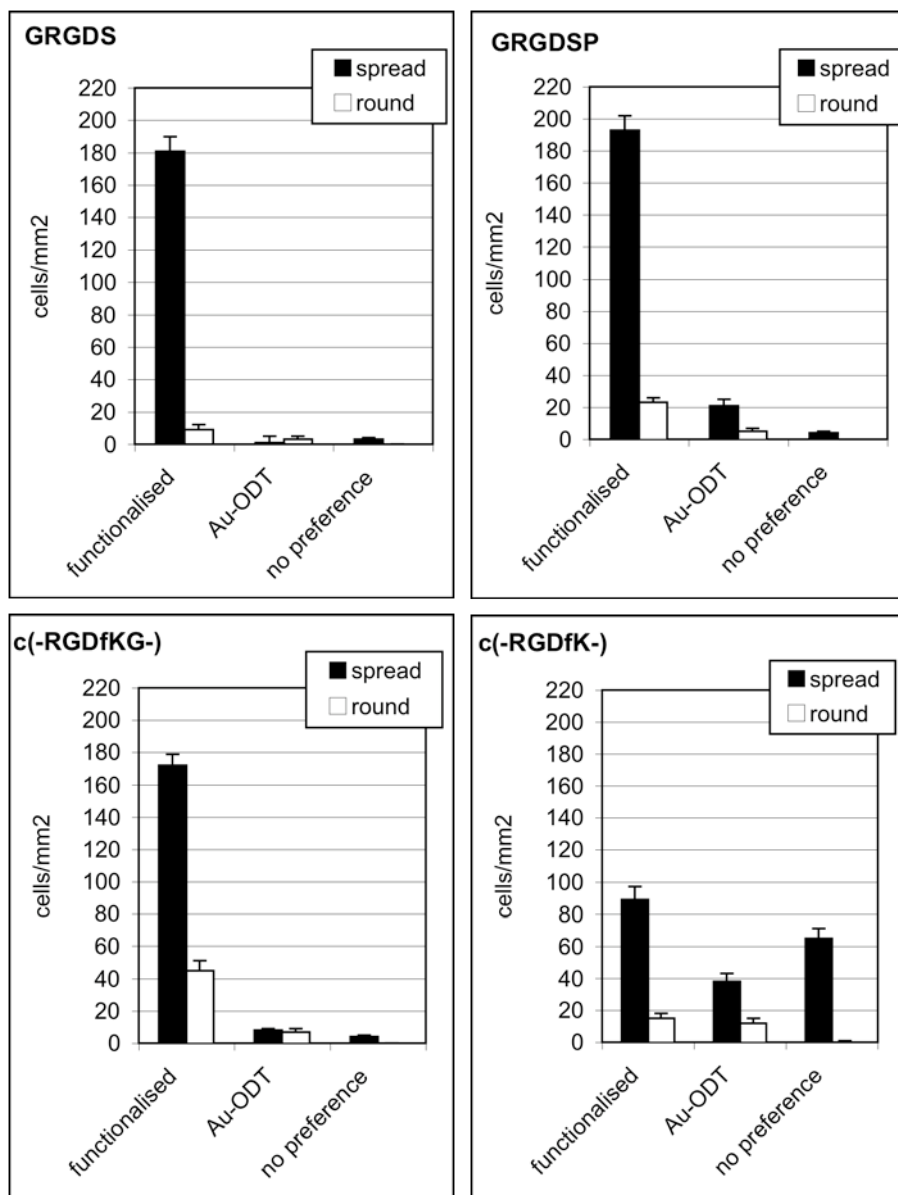


Fig. 63. Distribution of 3T3 Swiss fibroblasts on biofunctionalised patterned Au-ODT surfaces. For functionalisation linear - GRGDS and GRGDSP - and cyclic - c(-RGDfKG-) and c(-RGDfK-) - peptides were used.

In contrast, on both cyclic peptides the fibroblasts did not form obvious actin stress fibres. While on c(-RGDfKG-) the small FAs were revealed, on c(-RGDfK-) paxillin staining was negative for most cells.

Vinculin staining proved results of paxillin visualisation showing well formed FAs in the lamellipodia of mouse fibroblast spread on GRGDS-functionalised areas between Au-ODT stripes (Fig. 65).

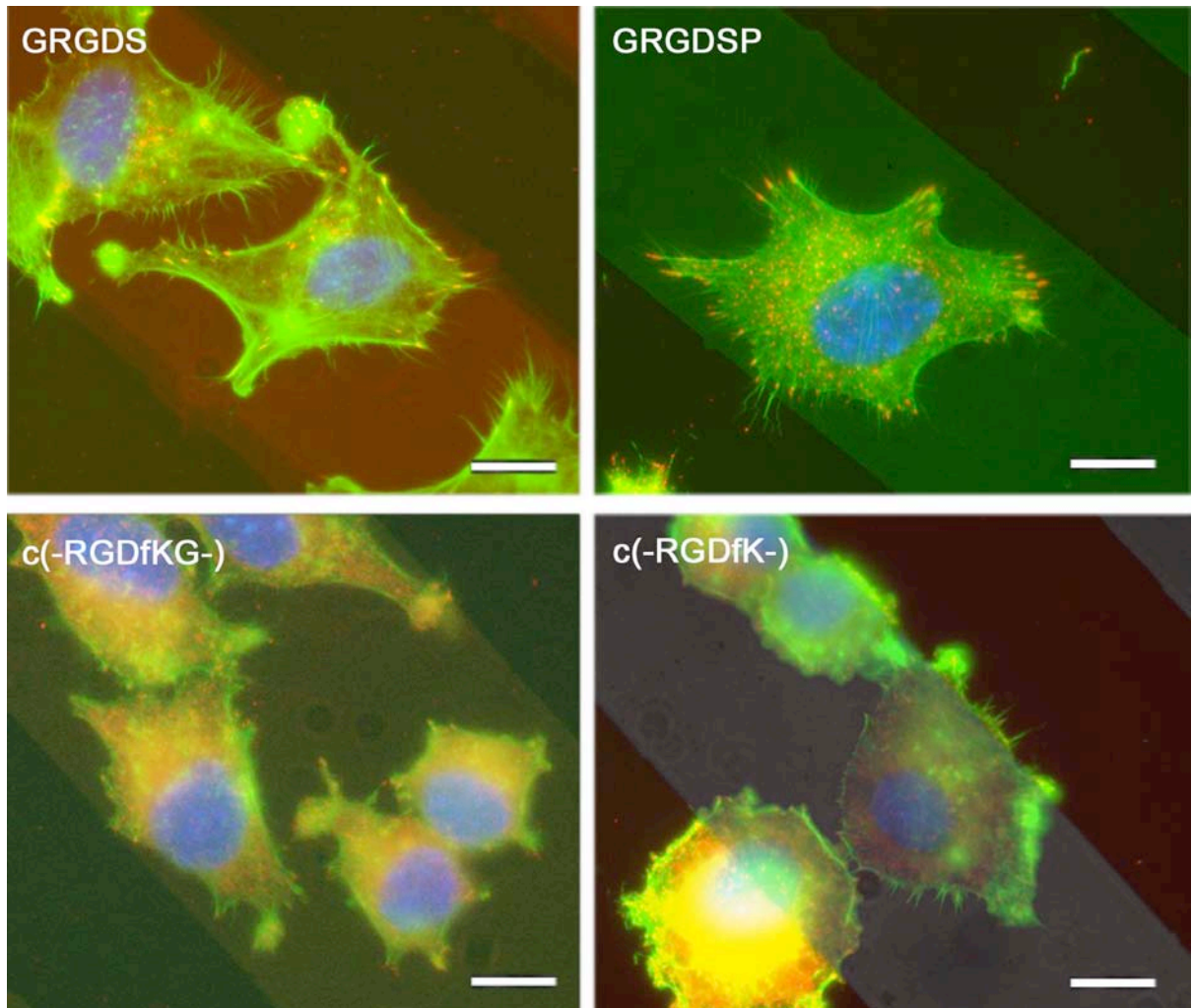


Fig. 64. Spreading behaviour of mouse fibroblasts on different RGD-containing peptides. Paxillin staining for focal adhesions in red, actin filament labelling with Oregon Green®-phalloidin in green, staining of nuclei with DAPI in blue. Scale bars: 10 μm.

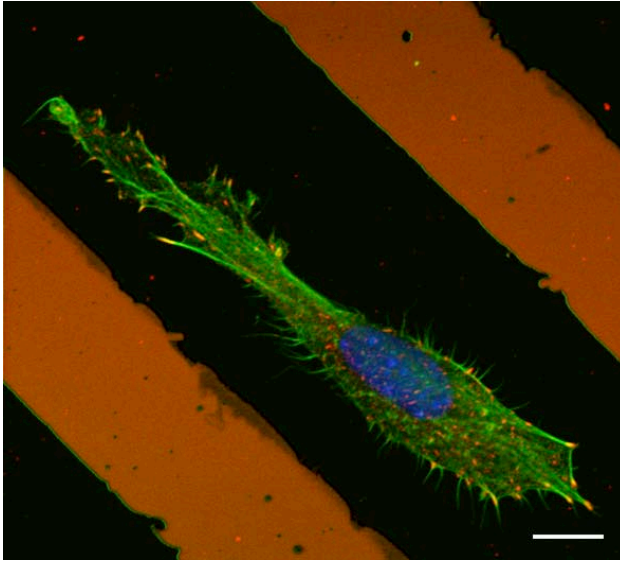


Fig. 65. Focal adhesion formation in mouse fibroblast on GRGDS-functionalised structured Au-ODT surface visualized by vinculin staining. Confocal laser microscope. Vinculin staining for focal adhesions in red, actin filament labelling with Oregon Green®-phalloidin in green, staining of nuclei with DAPI in blue. Scale bar 10µm.

4.9.9 Control of the surface biocompatibility

4.9.9.1 Control peptides

Behaviour of 3T3 Swiss fibroblasts on the structured Au-ODT surfaces functionalised with control RβAD-peptides was tested. The exchange of Glycine to beta Alanine in the RGD recognition motif should prevent cell spreading. The cell adhesion assays showed no spread cells on both linear – GRβADS and GRβADSP – and on cyclo(-RβADfKG-) (Fig. 66A). However, spread and flattened cells on the c(-RβADfK-) were found (Fig. 66B).

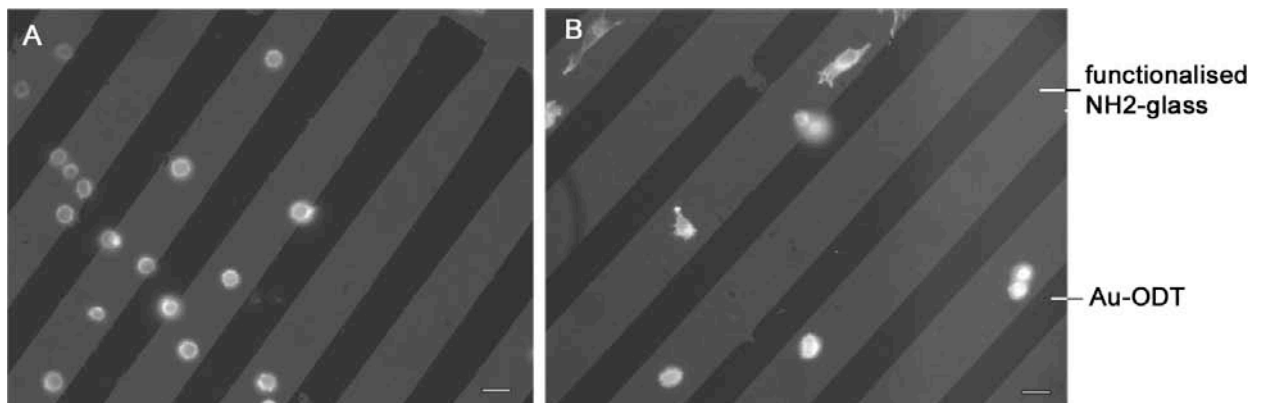


Fig. 66. Cells attached to the patterned Au-ODT surfaces functionalised with different control RβAD-peptides. (A) Mouse 3T3 Swiss fibroblasts on the GRβADS, GRβADSP and c(-RβADfKG-) were round. (B) Some spread and flattened cells on c(-RβADfK-) were found. The cells were visualised with Oregon Green®-phalloidin staining. Scale bars 10 µm.

Statistical evaluation showed a three times higher number of attached on cyclo(-R β ADfKG-) –functionalised samples cells in comparison with linear GR β ADS and 20 times higher in comparison with GR β ADSP. All cells attached on GR β ADS, GR β ADSP, and c(-R β ADfKG-) were round. Linear GR β ADSP demonstrated the lowest ability to induce the cell adhesion. Spread and flattened cells were found only on c(-R β ADfK-) functionalised samples; the cells avoided Au-ODT stripes and attached to peptide-covered surface (Fig. 67).

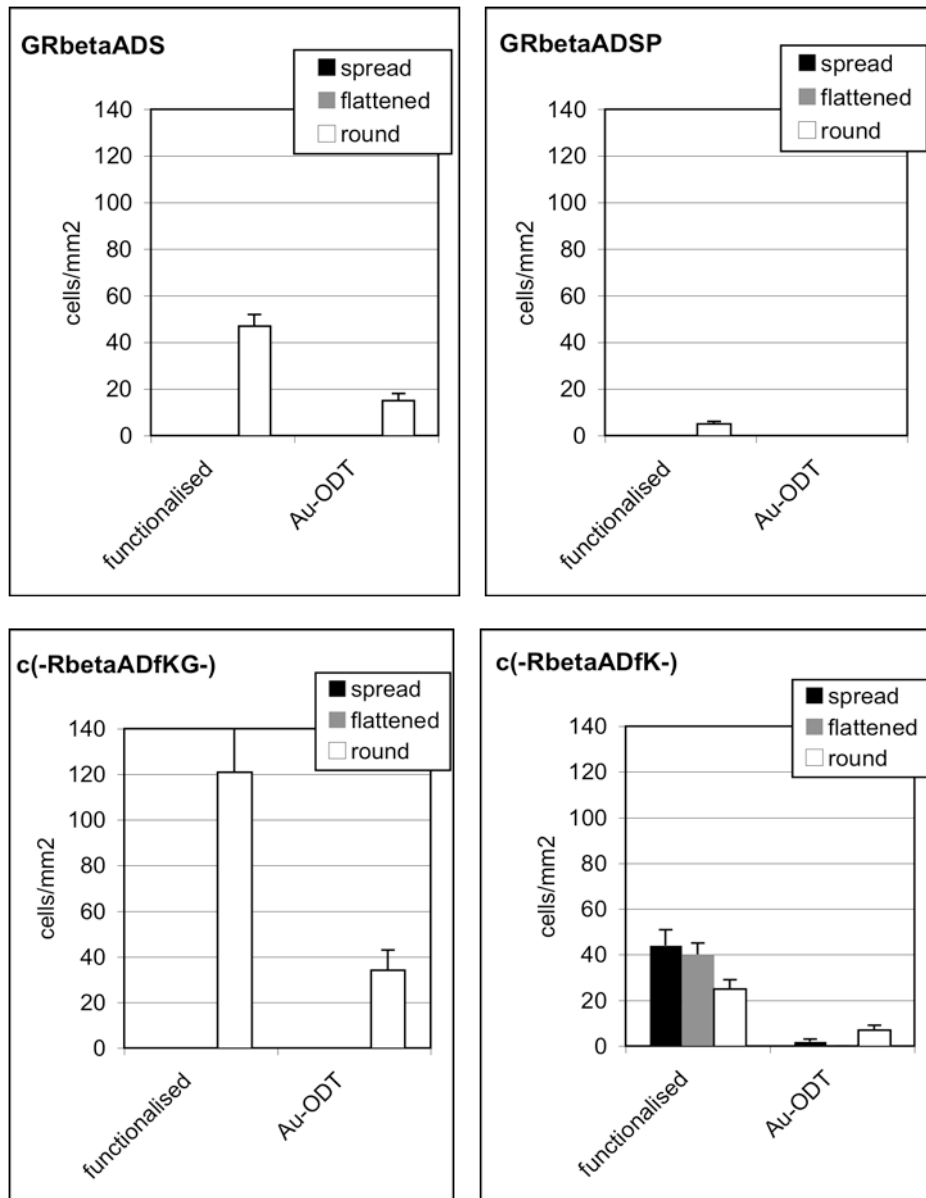


Fig. 67. Statistical evaluation of cell attachment to negative control peptides on structured Au-ODT surfaces.

Morphology of the cells on c(-R β ADfK-) were obviously different from completely round fibroblasts on GR β ADS, GR β ADSP, and c(-R β ADfKG-) peptides. However paxillin staining

did not revealed FAs in lamellipodia of spread and flattened fibroblasts on c(-R β ADfK-) (Fig. 68).

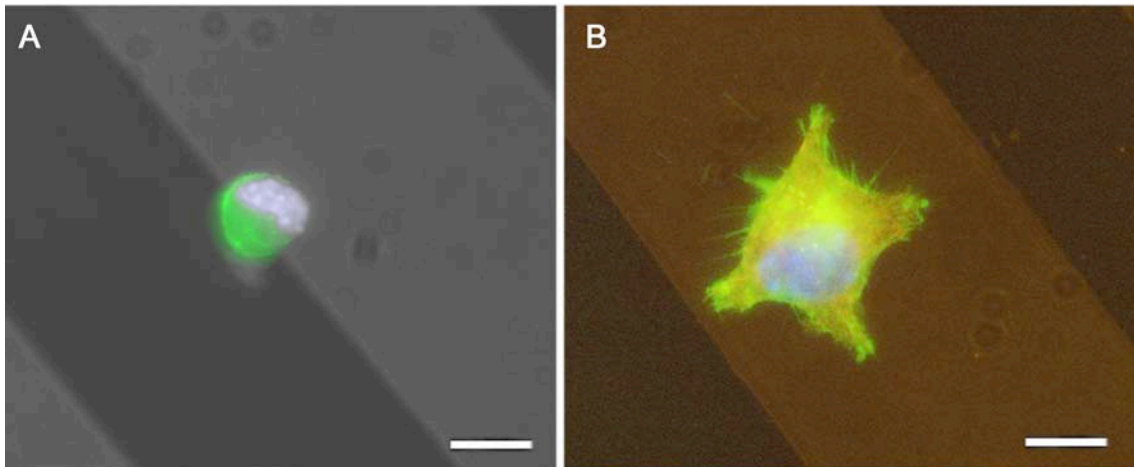


Fig. 68. Cell behaviour with negative control peptides. The surfaces were functionalized with GR β ADS (A) and c(R β ADfK-) (B). Paxillin staining for focal adhesions in red, actin filament labelling with phalloidin in green, staining of nuclei with DAPI in blue. Bars: 10 μ m

4.9.9.2 Proliferation assays

To estimate the cell ability to proliferate on the structured Au-ODT surfaces functionalised with RGD-peptide an enumeration of cells in mitotic stage was performed. Immunostaining of phosphorylated histone H3 revealed mitotic cells; comparison of their number with total number of surface adhered cells allowed to calculation of the proliferation index. The diagram in Fig. 69 shows an increasing with time in the number of mitotic cells cultivated on the Au-ODT/GRGDS surface at 4, 24 and 48 hours, that corresponds to an increase in the of total number of surface adhered cells.

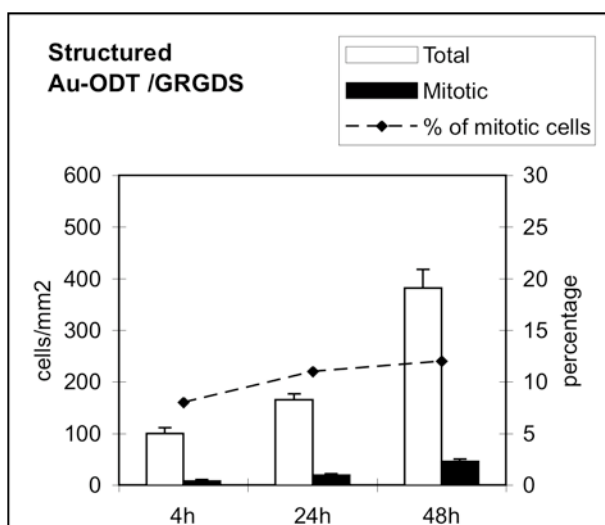


Fig. 69. 3T3 Swiss fibroblasts proliferate on the structured Au-ODT surface functionalised with GRGDS-peptide.

General dynamics of cell growth and proliferation revealed by counting of patterned surface attached fibroblasts correlated well with the results of a proliferation assay for uniform GRGDS-surfaces (see section 4.7.3). The low percentage of mitotic cells at first 4 hours after cell seeding correlated with cultivation of cell in a serum free medium. At 24 and 48 hours this parameter has increased to 11% and 12%, respectively.

4.9.9.3 Long-term stability of the structured distribution of cells

To test biocompatibility of structured Au-ODT/RGD surfaces the mouse 3T3 Swiss fibroblasts were cultivated on patterned samples for two days. Fig. 70 shows cell behaviour on the surface at 48 hours after seeding. The cells were polarised and spanned along pattern lines. They mainly avoided Au-ODT stripes spreading on RGDS-functionalised areas.

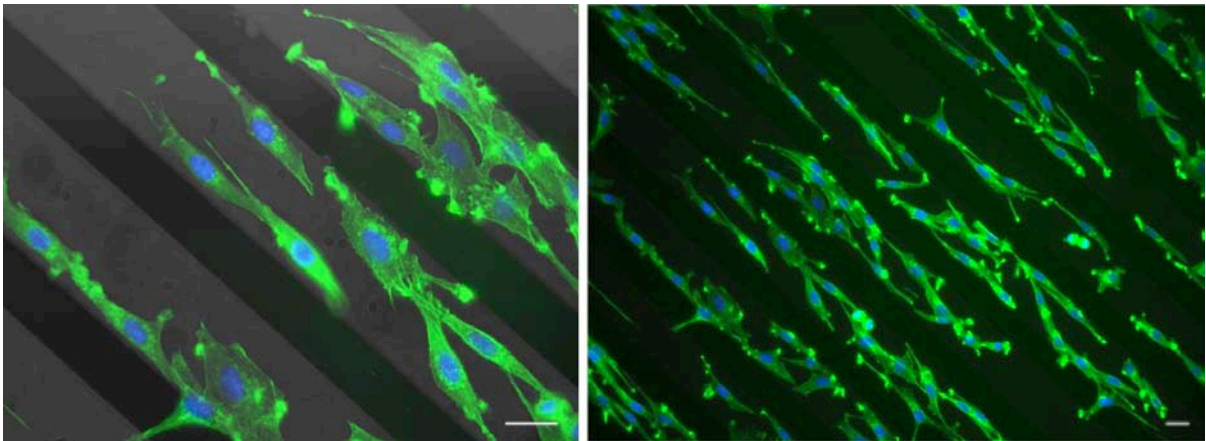


Fig. 70. 3T3 Swiss fibroblasts 48h incubated on the structured Au-ODT/GRGDS. Oregon Green®-phalloidin staining in green, staining of nuclei with DAPI in blue. Scale bars: 20 μm .

5 DISCUSSION

With this work a fast one-step method of surface biofunctionalisation via covalent binding of RGD-peptides has been developed. Different isothiocyanate terminated RGD-containing peptides including two molecules aminohexanoic acid molecules as a spacer were provided by Dr. Horst Kessler (TU, Munich). These were coupled to aminogroups on surfaces. Optimal aminofunctionalisation techniques, peptide coupling conditions and passivation processes had to be established which led to reproducible bioactivated surfaces of high quality and specificity. The method presented here can be applied to homogenous as well as structured surfaces. Cell-biological and medical applications require biocompatibility and non-toxicity of the designed surfaces, and this has been proven by different sets of experiments including focal contact and stress fibre formation, cell proliferation or long term cultivation. In the following, experimental results concerning biocompatibility and specificity of the coupling procedure, including tailoring and biofunctionalisation of structured surfaces as well as the adhesion behaviour of different cell types are discussed in detail.

5.1 Biocompatibility of different compounds required for RGD- surface functionalisation

The developed method of the surface RGD-functionalisation involved covalent binding of the peptides via an isothiocyanate linker and aminosilanisation of surfaces. When structured surfaces were created with μC printing and etching compounds like gold, titanium or chromium for gold adsorption and ODT for masking gold areas during the etching process were applied. All materials were monitored for how they influence cell adhesion and viability.

Highly reactive isothiocyanate groups could have a toxic effect in the case of incomplete or incorrect coupling of the molecules to the surface. To prove whether isothiocyanate terminated peptides are permissible for cell-biological applications they were adsorbed onto plastic slides and used as a substrate for cell adhesion. Mouse fibroblasts recognised the adsorbed isothiocyanate terminated peptides which were treated with BSA to block unspecific binding. Cells spread forming focal adhesions that proving biocompatibility of the material. Cells did not spread on BSA covered plastic alone thus proving specificity of peptide and/or isothiocyanate recognition. Substrates created by adsorption to the plastic using 1 mg/ml isothiocyanate terminated GRGDS solution showed higher cell adhesiveness than those adsorbed with the same concentration of commercially available GRGDS (Bachem, Germany) lacking the isothiocyanate group and the aminohexanoic acid spacer.

These experiments revealed that the isothiocyanate peptide itself seems to be non-toxic. The improved cell adhesion could be explained by higher absorption properties of isothiocyanate linked peptide, however, it cannot be excluded that the isothiocyanate promotes cell attachment. Nevertheless, in comparison to the chemical coupling procedure, discussed later, very high doses of the peptide need to be applied.

Aminosilanised glass did not by itself promote adhesion of 3T3 Swiss mouse fibroblasts according to cell adhesion assays performed in a serum-depleted medium. After 1 hour incubation of suspended cells to aminated glass no spread cells were found on the surface, however adhesion assays performed in serum-supplemented medium showed fibroblasts adhered to the surface. This indicates that compounds of the serum can adsorb to the aminated surface thereby indirectly mediating cell adhesion or alternatively, growth factors of the serum might change the responsiveness of these fibroblasts to amino groups. Long-term experiments lasting over at least 2 days showed that cells are able to spread and grow on aminosilanised surfaces in the presence of serum. Thus, 3T3 Swiss fibroblasts are not able to recognise aminated glass surfaces in the absence of serum, which is a prerequisite when specific RGD-peptide recognition has to be investigated.

Acidic protein bovine serum albumin is widely used in blocking unspecific protein binding based on electrical charges between amino acids side chains, due to configurational adaptability of the BSA molecule (Shirahama et al., 1989). In comparison to a single amino acid solution like 0.3 mg/ml aspartate solution and a mixture of 1 mg/ml arginine plus aspartate (data not shown) absorption of 1% pure BSA was found sufficient to prevent unspecific adhesion of 3T3 Swiss fibroblasts. I also tried 4-methoxyphenylisothiocyanate to block residual free amino groups mimicking the coupling reaction, but this resulted in complete loss of adhesion of 3T3 fibroblasts. Most likely the secondary aminogroup in the arginine (of the RGD peptide) was coupled to 4-methoxyphenylisothiocyanate and the peptide was no longer functional.

Gold and titanium used in procedures of surface patterning are widely used as metals in medical applications. However, the etching of titanium was found uncontrollable with the available laboratory equipment. Therefore chromium was used as adapter metal instead of titanium. Both Chromium (VI) and Chromium (III) are toxic (Gavin et al., 2007; Gardea-Torresdey et al., 1999) and the biocompatibility of chromium as well as other materials used in the patterning procedure – ODT and Pluronic® – had to be investigated. As criteria for biocompatibility cell shape, focal adhesion formation and proliferation rate in long term cultivation are often used (Saldana et al., 2005; Altankov et al., 1996). In this study proliferation rate over two days cultivation was monitored by phosphohistone staining. This staining showed that cells divide with a stable rate comparable to cells cultivated under normal conditions (Serrano et al., 2004). The cells remained adhered and spread on RGD-

functionalised surface areas avoiding settlement on Au-ODT stripes. Instead, they are able to form bridges, by spanning through Au-ODT stripes that indicates the cell non-toxicity of Au-ODT. Thus, all components used in the procedure of patterning are compatible and permissible for cell-adhesion applications.

For structured surface fabrication two different procedures were applied – performing aminosilanisation before or after metal layer evaporation. Both methods showed their compatibility and applicability for cell adhesion assays. However, technology of “Au-through-mask” evaporation on previously aminated surfaces led to “shadows” along the Au-stripes visualised by electron microscopy. Although not chemically characterized these shadows point to a residual adapter metal or gold layers of different thickness and might cause decrease in pattern stability. In contrast, the method of aminosilanisation after Au evaporation formed distinct borders between functionalised and unfunctionalised areas and therefore this technique was further developed.

Both mentioned methods of patterned surface design were shown to be insufficient to promote patterned cell distribution without any additional passivation step. For Au-ODT surfaces a method of Pluronic® treatment was found providing further selective cell attachment mainly on aminosilanised areas. In contrast, for the application of “Au-through-mask” an additional gold specific passivation technique that does not affect the amino groups on the glass needs to be developed.

5.2 Cells bind RGD-peptides specifically

The specificity of RGD-motif recognition on designed surfaces is critical for cell-adhesion applications because RGD recognition induces outside-in signalling of the integrin receptor complex and thereby influences survival, growth, differentiation and migration of cells (Giancotti and Ruoslahti, 1999). In this study the use of serum and cell cultivation longer than 2 hours was found to give false results.

Comparison of the cell behaviour showed that adhesion assays in serum-supplemented medium did not provide specific recognition of the substrate. In presence of foetal calf serum the mouse fibroblasts attached and spread, even on unfunctionalised aminated or non-aminated untreated glass. In contrast, the cells showed obvious RGD-dependent spreading in a serum-free medium; in absence of serum the fibroblasts spread neither on aminosilanised glass nor on control peptides with a scrambled RGD-motif. Thus, in the application of serum free medium in cell adhesion assay it is required in the read-out system to test the quality of surface RGD-functionalisation.

To prove substrate specificity of cell adhesion in classical cell substrate adhesion assays cells are allowed to adhere only for 1-2 hours depending on the cell type (Saldana et al., 2006). Longer cultivation covers the risk that cells synthesize their own extracellular matrix. Furthermore, the work Cohen et al. (Cohen et al., 2006) has shown that cells attach to surface within 2-10 minutes and form focal contacts after an additional two minutes. Taking both critical variables, serum and time-course of adhesion, many studies of cells on structured and functionalised surfaces are questionable and difficult to compare with the results presented in this work. Cells have been tested in presence of serum (Anderson et al., 2004; Kato and Mrksich, 2004; Behravesch et al., 2003) and after 4 and more hours of adhesion (Kato and Mrksich, 2004).

Additional control for recognition specificity is the use of scrambled RGD motifs, by exchanging the Glycine to β Alanine which prevents integrin binding and to compete ligand receptor interaction by competition with soluble RGDs-peptide. Furthermore, modification of the RGD peptide by addition of further amino acids or cyclization of the peptide itself allows one to distinguish between integrin receptors to some extent as they differ in their binding affinities to certain RGD-peptide modifications (Meyer et al., 2006). Thus, testing a set of modified RGD-peptides should further confirm recognition specificity.

The successful blocking of cell adhesion by soluble GRGDS-peptides in the medium confirmed the specific recognition of GRGDS, GRGDSP, and c(-RGDfKG-) motifs by the 3T3 fibroblasts. Specificity was confirmed as no cell adhesion was observed on the corresponding scrambled RGD-peptides containing the β Alanine. However, incomplete prevention of fibroblast adhesion to c(-RGDfK-) in the presence of the soluble peptide revealed unspecific mechanism of the cell binding to this cyclic peptide. Furthermore, the high background signal in the immunostainings (Fig. 30 and 31) point to an unspecific adsorption of proteins such as antibodies even in presence of the blocking reagent BSA. Unspecific surface adhesion was also visible by the failure in focal contact formation and atypical cell shapes. A relatively high amount of fibroblasts adhered to the corresponding scrambled peptide c(-R β AGfK-). Although cells were found only flattened rather than spread this cell behaviour also pointed to an unspecific binding of incorrectly synthesised molecules and showed necessity of change in the synthesis procedure for cyclic peptides. These extreme differences in comparison to the other linear and cyclic peptides led to a change in cyclic peptide synthesis. The synthesis of the functionalised cyclic peptides was modified in order to be able to do the cyclization step and the coupling of the spacer and the isothiocyanate anchor on solid phase. This allowed to avoid possible undesirable reactions and produce functional and specific cell recognisable peptide Nc(-RGDfK-). Fibroblasts spreading behaviour on Nc(-RGDfK-) was similar to c(-RGDfKG-) which was confirmed by competition with the soluble peptide and monitored by immunostaining for focal contacts

including statistical evaluations. Presence of soluble RGD-peptide in medium completely prevented attachment to Nc(-RGDfK-) surface, confirming RGD-dependence of substrate binding.

Though the cells recognised all tested RGD-containing peptides, differences in spreading behaviour of fibroblasts on linear in comparison to cyclic ones were observed. Counting of adhered cells to a 1 mm² area of the functionalised surface did not reveal statistically significant differences between peptides. However, the cell shape of fibroblasts spread on both linear peptides was found to be elongated exhibiting thick stress fibres of actin cytoskeleton. In contrast, on cyclic peptides the cell shape was more rounded. The amount of vinculin and paxillin positive FAs was similar for both linear peptides and nearly twice higher than for cells on c(-RGDfKG-) and Nc(-RGDfKG-). Importantly, the numbers of FAs formed by the fibroblasts on linear peptides perfectly matched to those formed on adsorbed fibronectin; there is no significant difference found between them.

Affinity to distinct integrin receptors depends on ligand conformation and amino acids flanking RGD-motif in the molecule (Hersel et al., 2003; Ruoslahti and Pierschbacher, 1987). Linear GRGDS and GRGDSP were published to promote $\alpha 5\beta 1$ and $\alpha v\beta 3$ integrin binding, while cyclo(-RGDfK-) and cyclo(-RGDfKG-) are known to have a higher affinity to $\alpha v\beta 3$, $\alpha v\beta 5$, and $\alpha IIb\beta 3$ (Auernheimer, 2005; Bin et al., 2000; Garanger et al.; 2006, Hersel et al., 2003). A higher ability of linear RGD-peptides in comparison to cyclic ones to block cell binding to a fibronectin layer promoted by $\alpha 5\beta 1$ was also reported (Takahashi et al., 2007). RT-PCR analyses showed that 3T3 Swiss fibroblasts used in this work express all integrin receptors mentioned above. Slight differences in the amount of transcripts were detected indicating that at least more $\alpha 5$ than αv and more $\beta 6$ compared $\beta 3$ and $\beta 1$ integrin is synthesised. The higher amount of $\alpha 5$ integrin might explain the preference of 3T3 Swiss fibroblasts to adhere to linear peptides. However, expression levels of integrin RNA cannot completely explain the differences since protein turnover or stability as well as integrin activation by inside-out signaling has also to be considered. Nevertheless, the observed differences in cell shape and FAs formation between linear and cyclic peptides could be induced by stimulation of distinct integrin receptors. A similar dependence on different integrin receptors in altering cell morphology has been reported by Danen (Danen et al., 2002); fibroblastoid and epithelioid cells were found more elongated in the case of $\alpha 5\beta 1$ -integrin mediated adhesion and more round when $\alpha v\beta 3$ -integrin was responsible for spreading. In agreement with this report it is allowed to speculate that the 3T3 Swiss fibroblasts respond to linear peptides by predominant use of the $\alpha 5\beta 1$ receptor and therefore are of elongated shape. However, when plated onto cyclic peptides $\alpha v\beta 3$ integrin is preferentially activated and cells take a more round shape. The differences in the numbers of

FAs per cell could be then limited by the amount of alpha subunits synthesised in these cells, so that less FAs can be formed by αv .

Immunostaining investigations together with statistical evaluation proved similarity of fibroblast behaviour on linear peptides and on absorbed fibronectin layers in terms of cytoskeleton organisation and focal adhesion formation. This correlation suggests a high level of similarity to the native substrate of the tested inanimate model designed by linear RGD-peptides covalently bound to surfaces. On surfaces fabricated with cyclic peptides, the fibroblasts demonstrated full spreading but decreased numbers of vinculin- and paxillin-positive focal adhesions. From other studies it is known, that the ability of cells to spread and form focal adhesion contacts depends on the distribution of ligands on the surface. Research group of Spatz (Arnold et al., 2004) showed that separation of adhesive dots on 73 nm and more led to aberrant cell adhesion and spreading as well as formation of focal adhesions, whereas distances up to 58 nm promoted effective cell adhesion. The group of Textor proved that increasing of the distance between RGD peptides reduced cell attachment to the surface, and reported that the density of RGD peptides also influenced the cell shape (Schuler et al., 2006).

In this work, the presence of RGD-peptides on the functionalised surface was shown with XPS, contact angle measurements and by changing in fluorescence intensity after surface treatment with rhodamin-RGD. The density of RGD-molecules could not be measured. In various approaches for designing optimal adhesive surfaces the functional molecules are used in a mixture with nonfunctional, "blank" ones to promote a certain distance between cell-recognisable ligands (Holzl et al., 2007; Kato and Mrksich, 2004; Romanova et al., 2006). Decreased numbers of observed FAs in lamellipodia of fibroblasts on cyclic RGD-peptides could be explained by non-optimal spacing of high affinity ligands. Low affinity ligands, like linear peptides, play a negligible role, since a decrease of linear peptide concentration in the coupling solution was shown to lead to a reduction of cell-adhesive properties of the functionalised surface. However, in the case of cyclic peptides additional experiments are required to find the optimal concentration in order to rule out that the observed differences are due to a combined effect of high affinity and high density RGD-peptides. Since the new synthesis pathway of the cyclic peptides has been started only two months ago only initial experiments with the Nc(-RGDfK-) could be included in this thesis.

5.3 Designed Au-ODT/RGD pattern promoted selective cell distribution

When the peptide coupling procedure was applied to surfaces structured by the microcontact printing method cell adhesion specificity to RGD was lost. Cell adhesion assays showed uniform cell distribution on both substrates of patterned surfaces – Au-ODT and aminosilanised RGD coupled stripes. Such cell adhesion behaviour with no preference indicated that during the coupling procedure RGD-peptides might also adsorb or were coupled to Au-ODT areas by unknown mechanisms. To achieve selective RGD-peptide distribution between the two different substrates a triblock copolymer Pluronic® F68 based on ethylene oxide and propylene oxide and PEG was tested for passivation. Adsorption of PEG and Pluronic® onto hydrophilic surfaces is used for preventing covering of such surface by other molecules, including proteins (DeFife et al. 1999; Prasad et al., 1979; Tan et al., 2004). Nontoxicity together with cell repellence caused these both polymers is applicable for design of patterned substrates (Arnold et al., 2004; Lee et al., 2005; Welle et al., 2005). Dependence of PEG and Pluronic adsorption on wettability of the surfaces made possible of their application to passivation of the hydrophobic ODT-SAMs.

Pluronic® F68 as well as PEG3350 were both found suitable to generate the desired alternating pattern of RGD functionalised aminosilanised glass stripes and inert Au-ODT bars. TOF-SIMS analysis performed by Physical Electronics (Chanhassen, USA) confirmed that Pluronic® specifically blocked the RGD functionalisation of the Au-ODT lines (unpublished data). The success in selected biofunctionalisation of the aminated glass stripes became obvious in cell adhesion assays when fibroblasts no longer attached and spread on the Au-ODT, but spread on RGD-coupled glass stripes. Pluronic® and PEG were shown to have a similar effect of to Au-ODT passivation. As the optimal method the coupling buffer was supplemented with 2 mM Pluronic® so that no further washing step is required.

Statistical evaluation proved that application of PEG or Pluronic® promoted high selective distribution of 3T3 fibroblasts on structured Au-ODT surfaces functionalised with GRGDS, GRGDSP, and c(-RGDfKG-). Cells preferred to adhere on areas of RGD-functionalised aminosilanised glass, and spread on it forming FAs; very few Au-ODT attached cells mainly stayed round. On c(-RGDfK-) cell distribution was not highly selective, correlating with other evidence of untypical behaviour of this peptide in comparison with other tested RGDs. This observation confirmed the sense of the adhesion used.

Since the structured surface also exhibited some topography, because etching after μC printing results in 60 nm deep and 21 μm wide channels, the capacity of cells to adhere to non-functionalised patterns was tested. However, this topography by itself is not able to promote patterned cell distribution; this was shown by adhesion experiments for the surfaces

without PEG and Pluronic® treatment. Therefore, such treatment is a necessary step for patterned RGD-functionalisation. To prove that topography of the surface is not able to promote cell adhesion by itself, cell assays with the two following types of structured Au-ODT surfaces were performed: (1) aminosilanised Au-ODT slides that were not treated with RGD peptide and (2) non-aminated Au-ODT slides that were incubated with RGDS for 2 hours. In both causes, in serum-free medium mouse fibroblasts adhered neither on Au-ODT nor glass or NH₂-glass demonstrating no adhesive effect of the surface topography.

A key question addressed in tissue regeneration using inanimate patterned cell-adhesive surfaces is the long-term stability of the pattern under cell culture conditions. Covalent immobilisation of RGD-peptides should guarantee a high stability of the pattern. However, in addition to the stability of RGD-molecules on the surface the question arises whether the cells will change the pattern by producing their own extracellular matrix molecules. A patterned substrate is able to effect cell orientation and cell movement that was shown e.g. for mouse dermal fibroblasts on two-dimensional collagen surfaces (Poole et al., 2005). The fibroblasts cultured on the structured Au-ODT/GRGDS slides for 2 days were found to be polarised along the stripes. The cells showed a constant proliferation index quite similar to cells cultivated on uniform GRGDS-surface, but the cell shape was obviously different as they were more elongated and uniformly orientated. The alignment of fibroblasts along the stripes suggests that the initial orientation of the cells according to the structure of the inanimate surface defines the later ECM network produced by the cells and thus results in the maintenance of the pattern.

5.4 Cell behaviour on RGD-surfaces is cell type dependent

As well as 3T3 Swiss fibroblast adhesion and spreading of other cell lines on the RGD-functionalised surfaces were also examined. *Xenopus* fibroblast, a cell line established from tadpoles, B16 melanoma cells expressing β 3-GFP-integrin and rat fibroblast stably transfected with YFP-paxillin were compared. The last two were chosen by promising in vivo imaging of focal adhesion formation due to the fluorescent labelled proteins. All cell types tested so far recognised and spread on substrates designed by covalent binding of isothiocyanate terminated RGD-peptides to aminosilanised glass. The cells showed a spreading behaviour similar to that on fibronectin, forming numerous focal adhesions. Phosphopaxillin staining revealed FAs at leading edge of lamellipodia; in REF52 rat fibroblasts phosphopaxillin clusters arranged in a ring like structure but not overlapping with the clusters of YFP-paxillin were observed. Cell adhesion assay with melanoma B16 β 3-

GFP-integrin exhibited GFP-integrin clusters formed on GRGDS, GRGDSP and c(-RGDfKG-).

Importantly, cell behaviour on aminosilanised glass was different, strongly depending on the tested cell line. Mouse Swiss 3T3 fibroblasts as well as *Xenopus* fibroblasts showed high selectivity in RGD-dependent adhesion. On aminosilanised glass – treated or untreated with BSA – *Xenopus* fibroblasts did not spread; statistical evaluations showed only few round attached cells. In contrast, human melanoma cells and MC3T3-E1 pre-osteoblasts showed full spreading on aminosilanised glass as well as on surfaces functionalised with R β AGD control peptides. The morphology of these cells was maintained whether they spread on RGD-functionalised surface, aminosilanised glass or on control peptides. Immunostaining revealed that focal adhesions were present. The melanoma cells transfected with GFP- β 3-integrin showed clusters of the labelled integrin in lamellipodia. Taken together, the comparison of the spreading behaviour between different cell lines demonstrated that only XTC and mouse 3T3 fibroblast selectively recognised RGD-peptides for adhesion while all other analysed cells showed a similar behaviour when plated on aminated or untreated glass surfaces which has been treated with BSA to avoid unspecific binding.

Cell binding to the substrate via RGD-peptides is not only controlled by ligand availability but also by “inside-out” signalling. Intracellular proteins are able to alter integrin receptor conformation and thereby make them responsive to the ligand and activate their clustering (Ginsberg et al., 1992). Overexpression e.g. talin, which binds to the β integrin cytoplasmic tail, can result in the receptor activation (Eigentaler et al., 1997). The observed RGD independent spreading and FAs formation of melanoma and pre-osteoblasts on aminosilanised and R β AD-surfaces might result from activation of integrin signalling by intracellular factors. Constitutively active β integrins are found in some tumours, they change the ability of cells to interact with their environment, and such loss in control can result in tumour progression (Brandsma et al., 2006). Activation of integrin receptors by clustering through overexpression or mutations in melanoma cells leading to a constitutive active inside-out-signalling may explain the RGD-independent spreading in these cell lines.

Overall, the application of the standard conditions for cell adhesion assays developed here revealed differences in selectiveness and specificity of ligand recognition among different cell lines. This strengthens the idea that the specific commitment of the selected cell line has to be investigated parallel to the design and fabrication of the suitable biofunctionalisation of an inanimate surface.

6 SUMMARY

Immobilisation of cell adhesive ligands on surfaces is applied to fabricate bioactive materials for different purposes, e.g. stem cell differentiation and tissue regeneration. Peptides containing the RGD (Arg-Gly-Asp) motif mimic binding sites of many ECM proteins that are recognised by integrin receptors. In this work, a novel method for immobilization of RGD-peptides to surfaces was developed. For this purpose different isothiocyanate terminated RGD peptides which include two molecules aminohexanoic acid as spacer were provided by Prof. Dr. Horst Kessler (TU, Munich). Covalent binding of these peptides to aminosilane self-assembled monolayers on glass as well as on silica dioxide surfaces resulted in the formation of adhesive surfaces proved by physical and biological methods.

Cells recognise and spread on RGD-functionalised surfaces, rearranged their actin cytoskeleton and formed stress fibres and active focal contacts. Absence of serum in the medium was found to be essential for specific recognition of the RGD-motif. The specificity of RGD mediated cell-adhesion was proved in competition assays with soluble GRGDS-peptides. As an additional control non-functional scrambled RGD motifs, containing beta-Alanine instead of Glycine were used.

Equal numbers of 3T3 fibroblasts adhered on linear and cyclic RGD peptides; however, actin cytoskeleton organisation and focal adhesion formation slightly differed between these peptides. When ligand recognition and spreading behaviour of various cell lines were compared, cell type specific differences were found.

The new method of RGD-functionalisation was improved for application to 2D structured surfaces. The latter were designed by soft-lithography-based microcontact printing producing alternating areas of aminosilanised glass and octadecylthiol self-assembled monolayers. Selective RGD-functionalisation of the aminosilanised glass areas resulted in a patterned distribution of adhered cells. The biocompatibility of different compounds required for RGD-surface functionalisation and the long-term stability of the pattern was demonstrated by cell adhesion and cell proliferation assays.

7 ZUSAMMENFASSUNG

Die Immobilisierung von zelladhäsiven Faktoren an Oberflächen findet in der Herstellung von bioaktiven Materialien zum Zweck der Stammzellendifferenzierung, Geweberegeneration und Organersatzbildung Anwendung. Peptide mit der RGD (Arg-Gly-Asp) Sequenz imitieren die Bindungsstellen vieler ECM Proteine, die von Integrinrezeptoren erkannt werden. In der vorliegenden Arbeit wurde eine neue Methode zur Immobilisierung von RGD Peptiden an Oberflächen entwickelt. Unterschiedliche RGD Peptide, die über zwei Amino-hexansäure-Einheiten mit einer endständigen Isothiocyanat-Gruppe verknüpft sind, wurden in der Arbeitsgruppe Prof. Dr. Horst Kessler (TU, München) synthetisiert und zur Verfügung gestellt. Die kovalente Bindung der Isothiocyanat-terminierten Peptide an aminosilanisierten selbst organisierte Monolagen (SAM: self assembly layer) auf Glass und auf Siliziumdioxid ergab die Ausbildung adhäsiver Oberflächen. Dies wurde mittels physikalischen und biologischen Methoden bestätigt.

Maus Fibroblasten (Swiss 3T3) erkannten RGD funktionalisierte Oberflächen und breiteten sich auf diesen Oberflächen aus. Dabei fand eine Umordnung des Actinzytoskeletts und die Bildung von Stressfasern und aktiven Fokalkontakten statt. Es wurde gezeigt, dass eine spezifische Erkennung der RGD Sequenz nur in serumfreien Medium nachweisbar ist. Die RGD Motiv vermittelte spezifische Zelladhäsion wurde durch Konkurrenz mit löslichem GRGDS Peptiden bewiesen. Als zusätzliche Negativ-Kontrolle wurden nicht funktionale RGD Motive, die beta-Arginin statt Arginin enthalten, eingesetzt.

Auf linearem und zyklischem RGD Peptid ist die Anzahl der adhären Zellen gleich groß. Allerdings unterscheiden sich die Zellen geringfügig in der Anzahl der gebildeten Fokalkontakte. Beim Vergleich unterschiedlicher Zelllinien, u.a. Osteoblasten, Melanomzellen, u wurden Zelltyp spezifische Unterschiede deutlich.

Die neue Methode zur RGD Funktionalisierung wurde für die Anwendung von 2D strukturierten Oberflächen verbessert. Letzteres wurde mittels auf Soft-Lithographie basierendem „microcontact printing“ gestaltet, aus der alternierend Flächen aus aminosilanisiertem Glass und selbst organisierende Monolagen von Octadecanthal hervor gingen. Selektive RGD Funktionalisierung der aminosilanisierten Glassflächen resultierten in einer musterabhängigen Verteilung der anwachsenden Zellen. Die Biokompatibilität der für die RGD Funktionalisierung benötigten Komponenten und die langzeitige Stabilität der Muster wurde mittels Zelladhäsions- und Zellproliferationstests bewiesen.

8 REFERENCES

- Abercrombie, M., Heaysman, J. E., and Pegrum, S. M. (1971). The locomotion of fibroblasts in culture. IV. Electron microscopy of the leading lamella. *Exp Cell Res* 67, 359-367.
- Adair, B. D., and Yeager, M. (2002). Three-dimensional model of the human platelet integrin alpha IIb beta 3 based on electron cryomicroscopy and x-ray crystallography. *Proc Natl Acad Sci U S A* 99, 14059-14064.
- Akagi, T., Murata, K., Shishido, T., and Hanafusa, H. (2002). v-Crk activates the phosphoinositide 3-kinase/AKT pathway by utilizing focal adhesion kinase and H-Ras. *Mol Cell Biol* 22, 7015-7023.
- Altankov, G., Grinnell, F., and Groth, T. (1996). Studies on the biocompatibility of materials: fibroblast reorganization of substratum-bound fibronectin on surfaces varying in wettability. *J Biomed Mater Res* 30, 385-391.
- Anderson, E. H., Ruegsegger, M. A., Murugesan, G., Kottke-Marchant, K., and Marchant, R. E. (2004). Extracellular matrix-like surfactant polymers containing arginine-glycine-aspartic acid (RGD) peptides. *Macromol Biosci* 4, 766-775.
- Arnold, M., Cavalcanti-Adam, E. A., Glass, R., Blummel, J., Eck, W., Kantlehner, M., Kessler, H., and Spatz, J. P. (2004). Activation of integrin function by nanopatterned adhesive interfaces. *Chemphyschem* 5, 383-388.
- Auernheimer, J. (2005). Funktionalisierung künstlicher Oberflächen mit Integrinliganden zur Stimulierung integrinvermittelter Zelladhäsion. Dissertation, TU München.
- Bacakova, L., Filova, E., Kubies, D., Machova, L., Proks, V., Malinova, V., Lisa, V., and Rypacek, F. (2007). Adhesion and growth of vascular smooth muscle cells in cultures on bioactive RGD peptide-carrying polylactides. *J Mater Sci Mater Med* 18, 1317-1323.
- Ballestrem C, Hinz B, Imhof BA, Wehrle-Haller B, (2001) Marching at the front and dragging behind: differential alphaVbeta3-integrin turnover regulates focal adhesion behavior. *The Journal of cell biology*. 155(7): 1319-32.
- Barbucci, R., Magnani, A., Chiumiento, A., Pasqui, D., Cangioni, I., and Lamponi, S. (2005). Fibroblast cell behavior on bound and adsorbed fibronectin onto hyaluronan and sulfated hyaluronan substrates. *Biomacromolecules* 6, 638-645.
- Barlos, K., Gatos, D., Kallitsis, J., Papaphotiu, G., Sotiriu, P., Weqing, Y., and Schaeffer, W. (1989a). Darstellung geschuetzter peptid fragmente unter einatz substituierter triphenylmethyl-harze. *Tetrahedron Lett* 30, 3943-3946.
- Barlos, K., Gatos, D., Kapalosa, S., Papaphotiu, G., Schaeffer, W., and Weqing, Y. (1989b). Veresterung von partiell geschuetzten peptid fragmenten mit harzen. Einsatz von 2-chlortritylchlorid zur Synthese von Leu15-gastrin I. *Tetrahedron Lett* 30, 3947-3950.
- Becker, J., Kirsch, A., Schwarz, F., Chatzinikolaidou, M., Rothamel, D., Lekovic, V., Laub, M., and Jennissen, H. P. (2006). Bone apposition to titanium implants biocoated with recombinant human bone morphogenetic protein-2 (rhBMP-2). A pilot study in dogs. *Clin Oral Investig* 10, 217-224.
- Beglova, N., Blacklow, S. C., Takagi, J., and Springer, T. A. (2002). Cysteine-rich module structure reveals a fulcrum for integrin rearrangement upon activation. *Nat Struct Biol* 9, 282-287.
- Behraves, E., Zygourakis, K., and Mikos, A. G. (2003). Adhesion and migration of marrow-derived osteoblasts on injectable in situ crosslinkable poly(propylene fumarate-co-ethylene glycol)-based hydrogels with a covalently linked RGDS peptide. *J Biomed Mater Res A* 65, 260-270.

- Bin, H., Senfang, S., Guttenberg, Z., and Baermann, M. (2000). The binding ability of immobilized biotinylated cyclic hexapeptide [cyclo(-Arg-Gly-Asp-D-Phe-Lys-Gly-)] containing RGD to integrin α IIb β 3 was tested by the methods of ELISA and SPR. *Chinese Science Bulletin* **45**, 2148-2152.
- Blancher, C., Omri, B., Bidou, L., Pessac, B., and Crisanti, P. (1996). Nectinepsin: a new extracellular matrix protein of the pexin family. Characterization of a novel cDNA encoding a protein with an RGD cell binding motif. *J Biol Chem* **271**, 26220-26226.
- Bono, P., Rubin, K., Higgins, J. M., and Hynes, R. O. (2001). Layilin, a novel integral membrane protein, is a hyaluronan receptor. *Mol Biol Cell* **12**, 891-900.
- Borowsky, M. L., and Hynes, R. O. (1998). Layilin, a novel talin-binding transmembrane protein homologous with C-type lectins, is localized in membrane ruffles. *J Cell Biol* **143**, 429-442.
- Brown, M. C., West, K. A., and Turner, C. E. (2002). Paxillin-dependent paxillin kinase linker and p21-activated kinase localization to focal adhesions involves a multistep activation pathway. *Mol Biol Cell* **13**, 1550-1565.
- Brandsma, D., Ulfman, L., Reijneveld, J. C., Bracke, M., Taphoorn, M. J., Zwaginga, J. J., Gebbink, M. F., de Boer, H., Koenderman, L., and Voest, E. E. (2006). Constitutive integrin activation on tumor cells contributes to progression of leptomeningeal metastases. *Neuro Oncol* **8**, 127-136.
- Brugnera, E., Haney, L., Grimsley, C., Lu, M., Walk, S. F., Tosello-Tramont, A. C., Macara, I. G., Madhani, H., Fink, G. R., and Ravichandran, K. S. (2002). Unconventional Rac-GEF activity is mediated through the Dock180-ELMO complex. *Nat Cell Biol* **4**, 574-582.
- Calalb, M. B., Polte, T. R., and Hanks, S. K. (1995). Tyrosine phosphorylation of focal adhesion kinase at sites in the catalytic domain regulates kinase activity: a role for Src family kinases. *Mol Cell Biol* **15**, 954-963.
- Carlsson, J., Gabel, D., Larsson, E., Ponten, J., and Westermark, B. (1979). Protein-coated agarose surfaces for attachment of cells. *In Vitro* **15**, 844-850.
- Cary, L. A., Han, D. C., Polte, T. R., Hanks, S. K., and Guan, J. L. (1998). Identification of p130Cas as a mediator of focal adhesion kinase-promoted cell migration. *J Cell Biol* **140**, 211-221.
- Cattelino, A., Cairo, S., Malanchini, B., and de Curtis, I. (1997). Preferential localization of tyrosine-phosphorylated paxillin in focal adhesions. *Cell Adhes Commun* **4**, 457-467.
- Chaki, N. K., and Vijayamohan, K. (2002). Self-assembled monolayers as a tunable platform for biosensor applications. *Biosens Bioelectron* **17**, 1-12.
- Claasen, B., Axmann, M., Meinecke, R., and Meyer, B. (2005). Direct observation of ligand binding to membrane proteins in living cells by a saturation transfer double difference (STDD) NMR spectroscopy method shows a significantly higher affinity of integrin α (IIb) β 3 in native platelets than in liposomes. *J Am Chem Soc* **127**, 916-919.
- Clark, R. A., Lin, F., Greiling, D., An, J., and Couchman, J. R. (2004). Fibroblast invasive migration into fibronectin/fibrin gels requires a previously uncharacterized dermatan sulfate-CD44 proteoglycan. *J Invest Dermatol* **122**, 266-277.
- Cohen, M., Kam, Z., Addadi, L., and Geiger, B. (2006). Dynamic study of the transition from hyaluronan- to integrin-mediated adhesion in chondrocytes. *Embo J* **25**, 302-311.
- Cook, A. D., Hrkach, J. S., Gao, N. N., Johnson, I. M., Pajvani, U. B., Cannizzaro, S. M., and Langer, R. (1997). Characterization and development of RGD-peptide-modified poly(lactic acid-co-lysine) as an interactive, resorbable biomaterial. *J Biomed Mater Res* **35**, 513-523.
- Danen, E. H., Sonneveld, P., Brakebusch, C., Fassler, R., and Sonnenberg, A. (2002). The fibronectin-binding integrins α 5 β 1 and α 5 β 3 differentially modulate RhoA-GTP

- loading, organization of cell matrix adhesions, and fibronectin fibrillogenesis. *J Cell Biol* **159**, 1071-1086.
- DeFife, K. M., Shive, M. S., Hagen, K. M., Clapper, D. L., and Anderson, J. M. (1999). Effects of photochemically immobilized polymer coatings on protein adsorption, cell adhesion, and the foreign body reaction to silicone rubber. *J Biomed Mater Res* **44**, 298-307.
- DeMali, K. A., Barlow, C. A., and Burridge, K. (2002). Recruitment of the Arp2/3 complex to vinculin: coupling membrane protrusion to matrix adhesion. *J Cell Biol* **159**, 881-891.
- DeMali, K. A., and Burridge, K. (2003). Coupling membrane protrusion and cell adhesion. *J Cell Sci* **116**, 2389-2397.
- DeMali, K. A., Wennerberg, K., and Burridge, K. (2003). Integrin signaling to the actin cytoskeleton. *Curr Opin Cell Biol* **15**, 572-582.
- Deng, C., Tian, H., Zhang, P., Sun, J., Chen, X., and Jing, X. (2006). Synthesis and characterization of RGD peptide grafted poly(ethylene glycol)-b-poly(L-lactide)-b-poly(L-glutamic acid) triblock copolymer. *Biomacromolecules* **7**, 590-596.
- Eigenthaler, M., Hofferer, L., Shattil, S. J., and Ginsberg, M. H. (1997). A conserved sequence motif in the integrin beta3 cytoplasmic domain is required for its specific interaction with beta3-endonexin. *J Biol Chem* **272**, 7693-7698.
- Elwing, H., Ivarsson, B., and Lundstrom, I. (1986). Complement deposition from human sera on silicon surfaces studied in situ by ellipsometry. The influence of surface wettability. *Eur J Biochem* **156**, 359-365.
- Emsley, J., Knight, C. G., Farndale, R. W., Barnes, M. J., and Liddington, R. C. (2000). Structural basis of collagen recognition by integrin alpha2beta1. *Cell* **101**, 47-56.
- Falconnet, D., Csucs, G., Grandin, H. M., and Textor, M. (2006). Surface engineering approaches to micropattern surfaces for cell-based assays. *Biomaterials* **27**, 3044-3063.
- Feuston, B. P., Culberson, J. C., and Hartman, G. D. (2003). Molecular model of the alpha(IIb)beta(3) integrin. *J Med Chem* **46**, 5316-5325.
- Fuchs, E., Dowling, J., Segre, J., Lo, S. H., and Yu, Q. C. (1997). Integrators of epidermal growth and differentiation: distinct functions for beta 1 and beta 4 integrins. *Curr Opin Genet Dev* **7**, 672-682.
- Gailit, J., Xu, J., Bueller, H., and Clark, R. A. (1996). Platelet-derived growth factor and inflammatory cytokines have differential effects on the expression of integrins alpha 1 beta 1 and alpha 5 beta 1 by human dermal fibroblasts in vitro. *J Cell Physiol* **169**, 281-289.
- Garanger, E., Boturyn, D., Coll, J. L., Favrot, M. C., and Dumy, P. (2006). Multivalent RGD synthetic peptides as potent alphaVbeta3 integrin ligands. *Org Biomol Chem* **4**, 1958-1965.
- Gardea-Torresdey, J. L., Tiemann, K. J., Gamez, G., and Dokken, K. (1999). Effects of chemical competition for multi-metal binding by *Medicago sativa* (alfalfa). *J Hazard Mater* **69**, 41-51.
- Gavin, I. M., Gillis, B., Arbieva, Z., and Prabhakar, B. S. (2007). Identification of human cell responses to hexavalent chromium. *Environ Mol Mutagen*.
- Gervais, M., Douy, A., and Erre, R. (1988). Surface analysis of lipopeptides using X-ray photoelectron spectroscopy. *J Colloid Interface Sci* **125**, 146-154.
- Giancotti, F. G., and Ruoslahti, E. (1999). Integrin signaling. *Science* **285**, 1028-1032.
- Gilmore, A. P., and Burridge, K. (1996). Regulation of vinculin binding to talin and actin by phosphatidylinositol-4-5-bisphosphate. *Nature* **381**, 531-535.
- Ginsberg, M. H., Du, X., and Plow, E. F. (1992). Inside-out integrin signalling. *Curr Opin Cell Biol* **4**, 766-771.

- Gottschalk, K. E., and Kessler, H. (2004). A computational model of transmembrane integrin clustering. *Structure* 12, 1109-1116.
- Hannigan, G. E., Leung-Hagesteijn, C., Fitz-Gibbon, L., Coppolino, M. G., Radeva, G., Filmus, J., Bell, J. C., and Dedhar, S. (1996). Regulation of cell adhesion and anchorage-dependent growth by a new beta 1-integrin-linked protein kinase. *Nature* 379, 91-96.
- Hashimoto, J., Kariya, Y., and Miyazaki, K. (2006). Regulation of proliferation and chondrogenic differentiation of human mesenchymal stem cells by laminin-5 (laminin-332). *Stem Cells* 24, 2346-2354.
- Hautanen, A., Gailit, J., Mann, D. M., and Ruoslahti, E. (1989). Effects of modifications of the RGD sequence and its context on recognition by the fibronectin receptor. *J Biol Chem* 264, 1437-1442.
- Hersel, U., Dahmen, C., and Kessler, H. (2003). RGD modified polymers: biomaterials for stimulated cell adhesion and beyond. *Biomaterials* 24, 4385-4415.
- Higgs, H. N., and Pollard, T. D. (2001). Regulation of actin filament network formation through ARP2/3 complex: activation by a diverse array of proteins. *Annu Rev Biochem* 70, 649-676.
- Hildebrand, J. D., Schaller, M. D., and Parsons, J. T. (1993). Identification of sequences required for the efficient localization of the focal adhesion kinase, pp125FAK, to cellular focal adhesions. *J Cell Biol* 123, 993-1005.
- Holden, M. A., Jung, S. Y., and Cremer, P. S. (2004). Patterning enzymes inside microfluidic channels via photoattachment chemistry. *Anal Chem* 76, 1838-1843.
- Holz, M., Tinazli, A., Leitner, C., Hahn, C. D., Lackner, B., Tampe, R., and Gruber, H. J. (2007). Protein-resistant self-assembled monolayers on gold with latent aldehyde functions. *Langmuir* 23, 5571-5577.
- Humphries, J. D., Askari, J. A., Zhang, X. P., Takada, Y., Humphries, M. J., and Mould, A. P. (2000). Molecular basis of ligand recognition by integrin alpha5beta 1. II. Specificity of arg-gly-Asp binding is determined by Trp157 of the alpha subunit. *J Biol Chem* 275, 20337-20345.
- Humphries, J. D., Byron, A., and Humphries, M. J. (2006). Integrin ligands at a glance. *J Cell Sci* 119, 3901-3903.
- Humphries, M. J. (1990). The molecular basis and specificity of integrin-ligand interactions. *J Cell Sci* 97 (Pt 4), 585-592.
- Humphries, M. J., McEwan, P. A., Barton, S. J., Buckley, P. A., Bella, J., and Mould, A. P. (2003). Integrin structure: heady advances in ligand binding, but activation still makes the knees wobble. *Trends Biochem Sci* 28, 313-320.
- Hynes, R. O. (1992). Integrins: versatility, modulation, and signaling in cell adhesion. *Cell* 69, 11-25.
- Hynes, R. O. (2002). Integrins: bidirectional, allosteric signaling machines. *Cell* 110, 673-687.
- Iuliano, D. J., Saavedra, S. S., and Truskey, G. A. (1993). Effect of the conformation and orientation of adsorbed fibronectin on endothelial cell spreading and the strength of adhesion. *J Biomed Mater Res* 27, 1103-1113.
- Kantlehner, M., Finsinger, D., et al. (1999). Selektive RGD-vermittelte Adhaesion von Osteoblasten an Implantat Oberflaechen. *Angew. Chem.* 111(4): 587-590.
- Kato, M., and Mrksich, M. (2004). Using model substrates to study the dependence of focal adhesion formation on the affinity of integrin-ligand complexes. *Biochemistry* 43, 2699-2707.

- Katz, B. Z., Zamir, E., Bershadsky, A., Kam, Z., Yamada, K. M., and Geiger, B. (2000). Physical state of the extracellular matrix regulates the structure and molecular composition of cell-matrix adhesions. *Mol Biol Cell* *11*, 1047-1060.
- Khor, E. (1997). Methods for the treatment of collagenous tissues for bioprostheses. *Biomaterials* *18*, 95-105.
- Klemke, R. L., Leng, J., Molander, R., Brooks, P. C., Vuori, K., and Cheresch, D. A. (1998). CAS/Crk coupling serves as a "molecular switch" for induction of cell migration. *J Cell Biol* *140*, 961-972.
- Krijgsman, B., Seifalian, A. M., Salacinski, H. J., Tai, N. R., Punshon, G., Fuller, B. J., and Hamilton, G. (2002). An assessment of covalent grafting of RGD peptides to the surface of a compliant poly(carbonate-urea)urethane vascular conduit versus conventional biological coatings: its role in enhancing cellular retention. *Tissue Eng* *8*, 673-680.
- Kroemker, M., Rudiger, A. H., Jockusch, B. M., and Rudiger, M. (1994). Intramolecular interactions in vinculin control alpha-actinin binding to the vinculin head. *FEBS Lett* *355*, 259-262.
- LaFlamme, S. E., Akiyama, S. K., and Yamada, K. M. (1992). Regulation of fibronectin receptor distribution. *J Cell Biol* *117*, 437-447.
- Laplantine, E., Maurer, P., Vallar, L., Eble, J., Paulsson, M., Bruckner, P., Kieffer, N., and Aumailley, M. (2002). The integrin beta1 subunit cytoplasmic tail forms oligomers: a potential role in beta1 integrin clustering. *Biol Cell* *94*, 375-387.
- Lee, J. O., Bankston, L. A., Arnaout, M. A., and Liddington, R. C. (1995a). Two conformations of the integrin A-domain (I-domain): a pathway for activation? *Structure* *3*, 1333-1340.
- Lee, J. O., Rieu, P., Arnaout, M. A., and Liddington, R. (1995b). Crystal structure of the A domain from the alpha subunit of integrin CR3 (CD11b/CD18). *Cell* *80*, 631-638.
- Lee, J. H., Go, A. K., Oh, S. H., Lee, K. E., and Yuk, S. H. (2005). Tissue anti-adhesion potential of ibuprofen-loaded PLLA-PEG diblock copolymer films. *Biomaterials* *26*, 671-678.
- Li, R., Babu, C. R., Lear, J. D., Wand, A. J., Bennett, J. S., and DeGrado, W. F. (2001). Oligomerization of the integrin alphaIIb beta3: roles of the transmembrane and cytoplasmic domains. *Proc Natl Acad Sci U S A* *98*, 12462-12467.
- Li, R., Mitra, N., Gratkowski, H., Vilaire, G., Litvinov, R., Nagasami, C., Weisel, J. W., Lear, J. D., DeGrado, W. F., and Bennett, J. S. (2003). Activation of integrin alphaIIb beta3 by modulation of transmembrane helix associations. *Science* *300*, 795-798.
- Lin, H. B., Garcia-Echeverria, C., Asakura, S., Sun, W., Mosher, D. F., and Cooper, S. L. (1992). Endothelial cell adhesion on polyurethanes containing covalently attached RGD-peptides. *Biomaterials* *13*, 905-914.
- Lin, H. B., Lewis, K. B., Leach-Scampavia, D., Ratner, B. D., and Cooper, S. L. (1993). Surface properties of RGD-peptide grafted polyurethane block copolymers: variable take-off angle and cold-stage ESCA studies. *J Biomater Sci Polym Ed* *4*, 183-198.
- Liu, S., Thomas, S. M., Woodside, D. G., Rose, D. M., Kiosses, W. B., Pfaff, M., and Ginsberg, M. H. (1999). Binding of paxillin to alpha4 integrins modifies integrin-dependent biological responses. *Nature* *402*, 676-681.
- Liu, Y., Loijens, J. C., Martin, K. H., Karginov, A. V., and Parsons, J. T. (2002). The association of ASAP1, an ADP ribosylation factor-GTPase activating protein, with focal adhesion kinase contributes to the process of focal adhesion assembly. *Mol Biol Cell* *13*, 2147-2156.
- Lo, S. H. (2006). Focal adhesions: what's new inside. *Dev Biol* *294*, 280-291.

- Luo, B. H., Carman, C. V., and Springer, T. A. (2007). Structural basis of integrin regulation and signaling. *Annu Rev Immunol* 25, 619-647.
- Marinelli, L., Lavecchia, A., Gottschalk, K. E., Novellino, E., and Kessler, H. (2003). Docking studies on alphavbeta3 integrin ligands: pharmacophore refinement and implications for drug design. *J Med Chem* 46, 4393-4404.
- Massia, S. P., Stark, J., and Letbetter, D. S. (2000). Surface-immobilized dextran limits cell adhesion and spreading. *Biomaterials* 21, 2253-2261.
- McCarthy, J. B., Chelberg, M. K., Mickelson, D. J., and Furcht, L. T. (1988). Localization and chemical synthesis of fibronectin peptides with melanoma adhesion and heparin binding activities. *Biochemistry* 27, 1380-1388.
- McClain, S. A., Simon, M., Jones, E., Nandi, A., Gailit, J. O., Tonnesen, M. G., Newman, D., and Clark, R. A. (1996). Mesenchymal cell activation is the rate-limiting step of granulation tissue induction. *Am J Pathol* 149, 1257-1270.
- Mecheri, G., Piras, Ciotti, Cocco and Caminati (2002). Immobilization of electroactive molecules in organized thin films *Materials Science and Engineering* 22, Pages 307-312.
- Meucci, G. a. C. (1999). *Mater Sci Eng*, 135.
- Meuer, S., Wittwer, C. Nakagawara K.. (2001). *Rapid Cycle real-time PCR*. Springer-Verlag, Berlin.
- Meyer, A., Auernheimer, J., Modlinger, A., and Kessler, H. (2006). Targeting RGD recognizing integrins: drug development, biomaterial research, tumor imaging and targeting. *Curr Pharm Des* 12, 2723-2747.
- Michishita, M., Videm, V., and Arnaout, M. A. (1993). A novel divalent cation-binding site in the A domain of the beta 2 integrin CR3 (CD11b/CD18) is essential for ligand binding. *Cell* 72, 857-867.
- Miyamoto, S., Teramoto, H., Coso, O. A., Gutkind, J. S., Burbelo, P. D., Akiyama, S. K., and Yamada, K. M. (1995). Integrin function: molecular hierarchies of cytoskeletal and signaling molecules. *J Cell Biol* 131, 791-805.
- Mould, A. P., Askari, J. A., and Humphries, M. J. (2000). Molecular basis of ligand recognition by integrin alpha 5beta 1. I. Specificity of ligand binding is determined by amino acid sequences in the second and third NH2-terminal repeats of the alpha subunit. *J Biol Chem* 275, 20324-20336.
- Mould, A. P., Komoriya, A., Yamada, K. M., and Humphries, M. J. (1991). The CS5 peptide is a second site in the IIICS region of fibronectin recognized by the integrin alpha 4 beta 1. Inhibition of alpha 4 beta 1 function by RGD peptide homologues. *J Biol Chem* 266, 3579-3585.
- Mould, A. P., Symonds, E. J., Buckley, P. A., Grossmann, J. G., McEwan, P. A., Barton, S. J., Askari, J. A., Craig, S. E., Bella, J., and Humphries, M. J. (2003). Structure of an integrin-ligand complex deduced from solution x-ray scattering and site-directed mutagenesis. *J Biol Chem* 278, 39993-39999.
- Muller, R., Abke, J., Schnell, E., Macionczyk, F., Gbureck, U., Mehrl, R., Ruszczak, Z., Kujat, R., Englert, C., Nerlich, M., and Angele, P. (2005). Surface engineering of stainless steel materials by covalent collagen immobilization to improve implant biocompatibility. *Biomaterials* 26, 6962-6972.
- Myohanen, H. T., Stephens, R. W., Hedman, K., Tapiovaara, H., Ronne, E., Hoyer-Hansen, G., Dano, K., and Vaheri, A. (1993). Distribution and lateral mobility of the urokinase-receptor complex at the cell surface. *J Histochem Cytochem* 41, 1291-1301.

- Na, K., Choi, H. K., Akaike, T., and Park, K. H. (2001). Conjugation of Arg-Gly-Asp (RGD) sequence in copolymer bearing sugar moiety for insulinoma cell line (MIN6) culture. *Biosci Biotechnol Biochem* 65, 1284-1289.
- Na, K., Jung, J., Shin, B., and Hyun, J. (2006). Micropatterning of cell-repellent polymer on a glass substrate for the highly resolved virus microarray. *Langmuir* 22, 10889-10892.
- Nalayanda, D. D., Kalukanimuttam, M., and Schmidtke, D. W. (2007). Micropatterned surfaces for controlling cell adhesion and rolling under flow. *Biomed Microdevices* 9, 207-214.
- Nanci, A., Wuest, J. D., Peru, L., Brunet, P., Sharma, V., Zalzal, S., and McKee, M. D. (1998). Chemical modification of titanium surfaces for covalent attachment of biological molecules. *J Biomed Mater Res* 40, 324-335.
- Nony, P. A., and Schnellmann, R. G. (2001). Interactions between collagen IV and collagen-binding integrins in renal cell repair after sublethal injury. *Mol Pharmacol* 60, 1226-1234.
- Nuzzo, A. (1983). Adsorption of bifunctional organic disulfides on gold surfaces. *J Am Chem Soc* 105, 4481 - 4483.
- Oliva, A. A., Jr., James, C. D., Kingman, C. E., Craighead, H. G., and Banker, G. A. (2003). Patterning axonal guidance molecules using a novel strategy for microcontact printing. *Neurochem Res* 28, 1639-1648.
- Olski, T. M., Noegel, A. A., and Korenbaum, E. (2001). Parvin, a 42 kDa focal adhesion protein, related to the alpha-actinin superfamily. *J Cell Sci* 114, 525-538.
- Park, K. H., Na, K., and Lee, K. C. (2004). Immobilization of Arg-Gly-Asp (RGD) sequence in sugar containing copolymer for culturing of pheochromocytoma (PC12) cells. *J Biosci Bioeng* 97, 207-211.
- Parsons, J. T. (2003). Focal adhesion kinase: the first ten years. *J Cell Sci* 116, 1409-1416.
- Pearson, D. A., Blanchette, M., Baker, M. L., Guidon, C. A. (1989). Trialkyl silanes as scavengers for the trifluoroacetic acid deblocking of protecting groups in peptide synthesis. *tetrahedron Lett.* 30: 2739-2742.
- Perepichka, D. F., Kondratenko, M., and Bryce, M. R. (2005). Self-assembly and multistage redox chemistry of strong electron acceptors on metal surfaces: polynitrofluorenes on gold and platinum. *Langmuir* 21, 8824-8831.
- Pierschbacher, M. D., and Ruoslahti, E. (1984). Cell attachment activity of fibronectin can be duplicated by small synthetic fragments of the molecule. *Nature* 309, 30-33.
- Pierschbacher, M. D., and Ruoslahti, E. (1987). Influence of stereochemistry of the sequence Arg-Gly-Asp-Xaa on binding specificity in cell adhesion. *J Biol Chem* 262, 17294-17298.
- Plow, E. F., Haas, T. A., Zhang, L., Loftus, J., and Smith, J. W. (2000). Ligand binding to integrins. *J Biol Chem* 275, 21785-21788.
- Poole, K., Khairy, K., Friedrichs, J., Franz, C., Cisneros, D. A., Howard, J., and Mueller, D. (2005). Molecular-scale topographic cues induce the orientation and directional movement of fibroblasts on two-dimensional collagen surfaces. *J Mol Biol* 349, 380-386.
- Prasad, K. N., Luong, T. T., Florence, A. T., Paris, J., Vaution, C., Seiller, M., and Puisieux, F. (1979). Surface activity and association of ABA polyoxyethylene-polyoxypropylene block copolymers in aqueous solution. *J Colloid Interface Sci* 69, 225.
- Price, L. S., Leng, J., Schwartz, M. A., and Bokoch, G. M. (1998). Activation of Rac and Cdc42 by integrins mediates cell spreading. *Mol Biol Cell* 9, 1863-1871.
- Pudney, M., Varma, M.G., and Leake, C.J. (1973). Establishment of a cell line (XTC 2) from the South African clawed toad, *Xenopus laevis*. *Experientia* 29, 466-467.

- Puleo, D. A., Kissling, R. A., and Sheu, M. S. (2002). A technique to immobilize bioactive proteins, including bone morphogenetic protein-4 (BMP-4), on titanium alloy. *Biomaterials* 23, 2079-2087.
- Quirk, R. A., Chan, W. C., Davies, M. C., Tendler, S. J., and Shakesheff, K. M. (2001). Poly(L-lysine)-GRGDS as a biomimetic surface modifier for poly(lactic acid). *Biomaterials* 22, 865-872.
- Randazzo, P. A., Andrade, J., Miura, K., Brown, M. T., Long, Y. Q., Stauffer, S., Roller, P., and Cooper, J. A. (2000). The Arp GTPase-activating protein ASAP1 regulates the actin cytoskeleton. *Proc Natl Acad Sci U S A* 97, 4011-4016.
- Ren, X. D., Kiosses, W. B., and Schwartz, M. A. (1999). Regulation of the small GTP-binding protein Rho by cell adhesion and the cytoskeleton. *Embo J* 18, 578-585.
- Robey, P. G. (1996). Vertebrate mineralized matrix proteins: structure and function. *Connect Tissue Res* 35, 131-136.
- Rohatgi, R., Nollau, P., Ho, H. Y., Kirschner, M. W., and Mayer, B. J. (2001). Nck and phosphatidylinositol 4,5-bisphosphate synergistically activate actin polymerization through the N-WASP-Arp2/3 pathway. *J Biol Chem* 276, 26448-26452.
- Romanova, E. V., Oxley, S. P., Rubakhin, S. S., Bohn, P. W., and Sweedler, J. V. (2006). Self-assembled monolayers of alkanethiols on gold modulate electrophysiological parameters and cellular morphology of cultured neurons. *Biomaterials* 27, 1665-1669.
- Rowley, J. A., Madlambayan, G., and Mooney, D. J. (1999). Alginate hydrogels as synthetic extracellular matrix materials. *Biomaterials* 20, 45-53.
- Ruoslahti, E. (1996). RGD and other recognition sequences for integrins. *Annu Rev Cell Dev Biol* 12, 697-715.
- Ruoslahti, E., and Pierschbacher, M. D. (1987). New perspectives in cell adhesion: RGD and integrins. *Science* 238, 491-497.
- Sagiv (1980). Organized monolayers by adsorption. 1. Formation and structure of oleophobic mixed monolayers on solid surfaces. *J Am Chem Soc* 102, 92 - 98.
- Saldana, L., Gonzalez-Carrasco, J. L., Rodriguez, M., Munuera, L., and Vilaboa, N. (2006). Osteoblast response to plasma-spray porous Ti6Al4V coating on substrates of identical alloy. *J Biomed Mater Res A* 77, 608-617.
- Saldana, L., Vilaboa, N., Valles, G., Gonzalez-Cabrero, J., and Munuera, L. (2005). Osteoblast response to thermally oxidized Ti6Al4V alloy. *J Biomed Mater Res A* 73, 97-107.
- Schaller, M. D., Hildebrand, J. D., and Parsons, J. T. (1999). Complex formation with focal adhesion kinase: A mechanism to regulate activity and subcellular localization of Src kinases. *Mol Biol Cell* 10, 3489-3505.
- Schaller, M. D., Otey, C. A., Hildebrand, J. D., and Parsons, J. T. (1995). Focal adhesion kinase and paxillin bind to peptides mimicking beta integrin cytoplasmic domains. *J Cell Biol* 130, 1181-1187.
- Schuler, M., Trentin, D., Textor, M., and Tosatti, S. G. (2006). Biomedical interfaces: titanium surface technology for implants and cell carriers. *Nanomed* 1, 449-463.
- Shaporenko, A., Ulman, A., Terfort, A., and Zharnikov, M. (2005). Self-assembled monolayers of alkaneselenolates on (111) gold and silver. *J Phys Chem B* 109, 3898-3906.
- Schneider, D., and Engelman, D. M. (2004). Involvement of transmembrane domain interactions in signal transduction by alpha/beta integrins. *J Biol Chem* 279, 9840-9846.
- Scotchford, C. A., Ball, M., Winkelmann, M., Voros, J., Csucs, C., Brunette, D. M., Danuser, G., and Textor, M. (2003). Chemically patterned, metal-oxide-based surfaces produced by

photolithographic techniques for studying protein- and cell-interactions. II: Protein adsorption and early cell interactions. *Biomaterials* 24, 1147-1158.

Serrano, M. C., Pagani, R., Vallet-Regi, M., Pena, J., Ramila, A., Izquierdo, I., and Portoles, M. T. (2004). In vitro biocompatibility assessment of poly(epsilon-caprolactone) films using L929 mouse fibroblasts. *Biomaterials* 25, 5603-5611.

Shaporenko, A., Ulman, A., Terfort, A., and Zharnikov, M. (2005). Self-assembled monolayers of alkaneselenolates on (111) gold and silver. *J Phys Chem B* 109, 3898-3906.

Shimaoka, M., Xiao, T., Liu, J. H., Yang, Y., Dong, Y., Jun, C. D., McCormack, A., Zhang, R., Joachimiak, A., Takagi, J., *et al.* (2003). Structures of the alpha L I domain and its complex with ICAM-1 reveal a shape-shifting pathway for integrin regulation. *Cell* 112, 99-111.

Shirahama, H., Shikuma, T., and Suzawa, T. (1989). Participation of electrolyte cations in albumin adsorption onto negatively charged polymer latices *Colloid & Polymer Science* 267, 1435-1536.

Situma, C., Wang, Y., Hupert, M., Barany, F., McCarley, R. L., and Soper, S. A. (2005). Fabrication of DNA microarrays onto poly(methyl methacrylate) with ultraviolet patterning and microfluidics for the detection of low-abundant point mutations. *Anal Biochem* 340, 123-135.

Stephansson, S. N., Byers, B. A., and Garcia, A. J. (2002). Enhanced expression of the osteoblastic phenotype on substrates that modulate fibronectin conformation and integrin receptor binding. *Biomaterials* 23, 2527-2534.

Takagi, J. (2004). Structural basis for ligand recognition by RGD (Arg-Gly-Asp)-dependent integrins. *Biochem Soc Trans* 32, 403-406.

Takagi, J., Petre, B. M., Walz, T., and Springer, T. A. (2002). Global conformational rearrangements in integrin extracellular domains in outside-in and inside-out signaling. *Cell* 110, 599-511.

Takagi, J., Strokovich, K., Springer, T. A., and Walz, T. (2003). Structure of integrin alpha5beta1 in complex with fibronectin. *Embo J* 22, 4607-4615.

Takahashi, S., Leiss, M., Moser, M., Ohashi, T., Kitao, T., Heckmann, D., Pfeifer, A., Kessler, H., Takagi, J., Erickson, H. P., and Fassler, R. (2007). The RGD motif in fibronectin is essential for development but dispensable for fibril assembly. *J Cell Biol* 178, 167-178.

Tamura, T., Hato, T., Yamanouchi, J., and Fujita, S. (2004). Critical residues for ligand binding in blade 2 of the propeller domain of the integrin alphaIIb subunit. *Thromb Haemost* 91, 111-118.

Tan, J. L., Liu, W., Nelson, C. M., Raghavan, S., and Chen, C. S. (2004). Simple approach to micropattern cells on common culture substrates by tuning substrate wettability. *Tissue Eng* 10, 865-872.

Tang, H., Kerins, D. M., Hao, Q., Inagami, T., and Vaughan, D. E. (1998). The urokinase-type plasminogen activator receptor mediates tyrosine phosphorylation of focal adhesion proteins and activation of mitogen-activated protein kinase in cultured endothelial cells. *J Biol Chem* 273, 18268-18272.

Tselepis, V. H., Green, L. J., and Humphries, M. J. (1997). An RGD to LDV motif conversion within the disintegrin kistrin generates an integrin antagonist that retains potency but exhibits altered receptor specificity. Evidence for a functional equivalence of acidic integrin-binding motifs. *J Biol Chem* 272, 21341-21348.

Tsubouchi, A., Sakakura, J., Yagi, R., Mazaki, Y., Schaefer, E., Yano, H., and Sabe, H. (2002). Localized suppression of RhoA activity by Tyr31/118-phosphorylated paxillin in cell adhesion and migration. *J Cell Biol* 159, 673-683.

Turner, C. E. (2000). Paxillin interactions. *J Cell Sci* 113 Pt 23, 4139-4140.

- Ulman, E., Tillman (1989). The Packing and Molecular Orientation of Alkyl Thiol Monolayers on Gold Surfaces. *Langmuir* 5, 1147, 1147.
- van der Flier, A., and Sonnenberg, A. (2001). Function and interactions of integrins. *Cell Tissue Res* 305, 285-298.
- Vansant, v. D. V. a. V. (1995). Characterization and Chemical Modification of The Silica Surface.
- Vaughan, F., Swart and Yarwood (1992). *Thin Solid Films*, 574.
- Vinogradova, O., Velyvis, A., Velyviene, A., Hu, B., Haas, T., Plow, E., and Qin, J. (2002). A structural mechanism of integrin alpha(IIb)beta(3) "inside-out" activation as regulated by its cytoplasmic face. *Cell* 110, 587-597.
- Vuori, K., Hirai, H., Aizawa, S., and Ruoslahti, E. (1996). Introduction of p130cas signaling complex formation upon integrin-mediated cell adhesion: a role for Src family kinases. *Mol Cell Biol* 16, 2606-2613.
- Wei, Y., Yang, X., Liu, Q., Wilkins, J. A., and Chapman, H. A. (1999). A role for caveolin and the urokinase receptor in integrin-mediated adhesion and signaling. *J Cell Biol* 144, 1285-1294.
- Welle, A., Horn, S., Schimmelpfeng, J., and Kalka, D. (2005). Photo-chemically patterned polymer surfaces for controlled PC-12 adhesion and neurite guidance. *J Neurosci Methods* 142, 243-250.
- Wilbur, K., Biebuyck, Kim, Whitesides (1996). Microcontact printing of self-assembled monolayers: applications in microfabrication. *Nanotechnology*, 452-457.
- Winkler, J., Lunsdorf, H., and Jockusch, B. M. (1996). The ultrastructure of chicken gizzard vinculin as visualized by high-resolution electron microscopy. *J Struct Biol* 116, 270-277.
- Woods, A., Longley, R. L., Tumova, S., and Couchman, J. R. (2000). Syndecan-4 binding to the high affinity heparin-binding domain of fibronectin drives focal adhesion formation in fibroblasts. *Arch Biochem Biophys* 374, 66-72.
- Woods, A., Oh, E. S., and Couchman, J. R. (1998). Syndecan proteoglycans and cell adhesion. *Matrix Biol* 17, 477-483.
- Xiong, J. P., Stehle, T., Diefenbach, B., Zhang, R., Dunker, R., Scott, D. L., Joachimiak, A., Goodman, S. L., and Arnaout, M. A. (2001). Crystal structure of the extracellular segment of integrin alpha Vbeta3. *Science* 294, 339-345.
- Xiong, J. P., Stehle, T., Zhang, R., Joachimiak, A., Frech, M., Goodman, S. L., and Arnaout, M. A. (2002). Crystal structure of the extracellular segment of integrin alpha Vbeta3 in complex with an Arg-Gly-Asp ligand. *Science* 296, 151-155.
- Yang, X. B., Roach, H. I., Clarke, N. M., Howdle, S. M., Quirk, R., Shakesheff, K. M., and Oreffo, R. O. (2001). Human osteoprogenitor growth and differentiation on synthetic biodegradable structures after surface modification. *Bone* 29, 523-531.
- Yauch, R. L., Felsenfeld, D. P., Kraeft, S. K., Chen, L. B., Sheetz, M. P., and Hemler, M. E. (1997). Mutational evidence for control of cell adhesion through integrin diffusion/clustering, independent of ligand binding. *J Exp Med* 186, 1347-1355.
- Yokosaki, Y., Matsuura, N., Higashiyama, S., Murakami, I., Obara, M., Yamakido, M., Shigeto, N., Chen, J., and Sheppard, D. (1998). Identification of the ligand binding site for the integrin alpha9 beta1 in the third fibronectin type III repeat of tenascin-C. *J Biol Chem* 273, 11423-11428.
- You, M., Kogan, Chen, Li, Kassir, Holland, and Dixon (2002). A 3D Structure Model of Integrin 41 Complex: I. Construction of a Homology Model of 1 and Ligand Binding Analysis. *Biophys J Vol.* 82, p. 447-457.

-
- Zaidel-Bar, R., Kam, Z., and Geiger, B. (2005). Polarized downregulation of the paxillin-p130CAS-Rac1 pathway induced by shear flow. *J Cell Sci* *118*, 3997-4007.
- Zaidel-Bar, R., Milo, R., Kam, Z., and Geiger, B. (2007). A paxillin tyrosine phosphorylation switch regulates the assembly and form of cell-matrix adhesions. *J Cell Sci* *120*, 137-148.
- Zamir, E., and Geiger, B. (2001a). Components of cell-matrix adhesions. *J Cell Sci* *114*, 3577-3579.
- Zamir, E., and Geiger, B. (2001b). Molecular complexity and dynamics of cell-matrix adhesions. *J Cell Sci* *114*, 3583-3590.
- Zimmerman, B., Volberg T., Geiger, B. (2004). Early molecular events in the assembly of the focal adhesion-stress fiber complex during fibroblast spreading. *Cell Motil Cytoskeleton*. Jul;58(3):143-59.
- Zimmermann, P., and David, G. (1999). The syndecans, tuners of transmembrane signaling. *Faseb J* *13 Suppl*, S91-S100.

9 MISCELLENOUS

List of abbreviations

4MOPIT	4-methoxyphenylisothiocyanate
ADMIDAS	Adjacent to the MIDAS site
APS	Aminopropylsilane
APTES	(3-Aminopropyl)-triethoxysilane
Arp 2/3	Actin-related protein 2/3
BMP	Bone morphogenetic protein
BT	Butanethiol
DMEM	Dulbecco's modified Eagle medium
DMSO	Dimethylsulfoxide
DTT	Dithiotritol
ECM	Extracellular matrix
EGF	Epidermal growth factor
FA	Focal adhesion
FAK	Focal adhesion kinase
HT	Hexylthiol
ILK	Integrin-linked kinase
LIMBS	Ligand-associated metal binding site
MIDAS	Metal ion-dependent adhesion site
ODT	Octadecylthiol
OTS	Octadecyltrichlorosilane
PDMF	Phenylmethanesulfonyl fluoride
PDMS	Polydimethylsiloxane
PEG	Polyethelenglicol
PI3-kinase	Phosphoinositide 3-kinase
PSI	Aminoterminal plexin/semaphorin/integrin
REF	Rat embryonic fibroblasts
SAM	Self-assembled monolayer
SPPS	Solid phase peptide synthesis
STI	Trypsin inhibitor from soybean
TCP	Tritylchloride polystyrene
WASP	Wiskott-Aldrich syndrome protein
XTC	Xenopus tadpole fibroblasts
β TD	β -tail domain
μ CP	Microcontact printing
μ FLP	Microfluidic patterning

Curriculum vitae

Personal details:

Name: Sviatlana Kalinina

Born: 22.04.1972

Place of birth: Minsk, Belarus

Education:

1989 – 1992 B.S. course, Department of Physics, Belarus State University.

1992 – 1995 M.S. course, Department of Physics, Belarus State University.
Specialization in Biophysics.

M.S. Thesis: *Oxygen-activating abilities of immune system's cells
at cardio cerebral injuries.*

1995 – 1997 Post-graduate student, Department of Physics, Belarus State University.
Specialization in Biophysics.

Professional experience:

1995 – 1997 Junior Researcher
Laboratory of Biophysics of Complex System,
Chair of Biophysics, Department of Physics, Belarus State University.

1998 – 2001 Research assistant
Association of Professional Ecologists,
Minsk, Belarus.

List of publications

Talks at conferences:

Biofunctionalisation of micropatterned surfaces

S. Kalinina, J. Auernheimer, H. Gliemann, T. Schimmel, D. Wedlich, H. Kessler, A. Schambony

FRONTIERS Young Scientists Meeting 2006, Karlsruhe, 28. – 31. March 2006.

Poster presentations:

Design of micropatterned cell adhesive surfaces

J. Auernheimer, S. Kalinina, H. Gliemann, T. Schimmel, A. Schambony, D. Wedlich, H. Kessler

28th Annual Meeting of the German Society for Cell Biology, Heidelberg, 16. – 19 March 2005.

Design of micropatterned cell adhesive surfaces

J. Auernheimer, S. Kalinina, H. Gliemann, T. Schimmel, A. Schambony, D. Wedlich, H. Kessler

CFN Summer School on Nano-Biology, Bad Herrenalb 5. – 8. September 2005.

Patterned adhesive surfaces

S. Kalinina, J. Auernheimer, H. Gliemann, T. Schimmel, D. Wedlich, H. Kessler, A. Schambony

FRONTIERS Annual Meeting 2005, Karlsruhe, 18 – 21. September 2005.

Design of micropatterned cell adhesive surfaces

S. Kalinina, J. Auernheimer, H. Gliemann, T. Schimmel, D. Wedlich, H. Kessler, A. Schambony

2nd International Symposium „Interface Biology of Implants“, Rostock-Warnemünde, 17. – 19. May 2006.

Nanostructures templates with specific adhesive properties

S. Kalinina, S. Engin, H. Gliemann, T. Schimmel, M. López-García, H. Kessler, D. Wedlich

CFN Summer School on Nano-Biology, Bad Herrenalb 20. – 23. August 2007.

Characterisation of RGD-functionalised surface by ToF-SIMS

A. Petershans, A. Lyapin, S. Reichlmaier, S. Kalinina, D. Wedlich, H. Gliemann

CFN Summer School on Nano-Biology, Bad Herrenalb 20. – 23. August 2007.